8-2007

Optimization of Interfacial Interactions to Achieve the Nanoscale Dispersion of Clay in Polymer/Clay Nanocomposites

Deepali Kumar
University of Tennessee - Knoxville

Follow this and additional works at: https://trace.tennessee.edu/utk_graddiss

Part of the Chemistry Commons

To the Graduate Council:

I am submitting herewith a dissertation written by Deepali Kumar entitled "Optimization of Interfacial Interactions to Achieve the Nanoscale Dispersion of Clay in Polymer/Clay Nanocomposites." I have examined the final electronic copy of this dissertation for form and content and recommend that it be accepted in partial fulfillment of the requirements for the degree of Doctor of Philosophy, with a major in Chemistry.

Mark D. Dadmun, Major Professor

We have read this dissertation and recommend its acceptance:

Charles Feigerle, Roberto Benson, Jimmy Mays

Accepted for the Council:

Carolyn R. Hodges

Vice Provost and Dean of the Graduate School

(Original signatures are on file with official student records.)

To the Graduate Council:

I am submitting herewith a dissertation written by Deepali Kumar entitled "Optimization of Interfacial Interactions to Achieve the Nanoscale Dispersion of Clay in Polymer/Clay Nanocomposites". I have examined the final electronic copy of this dissertation for form and content and recommend that it be accepted in partial fulfillment of the requirements for the Degree of Doctor of Philosophy, with a major in Chemistry.

_____

Mark D. Dadmun, Major Professor

We have read this dissertation

and recommend its acceptance:

Charles Feigerle

_____

Roberto Benson

_____

Jimmy Mays

_____

Accepted for Council:

Carolyn R. Hodges

_____

Vice Provost and Dean of the
Graduate School

(Original Signatures are on file with official student records)

Optimization of Interfacial Interactions to Achieve Nanoscale Dispersion of Clay in Polymer/Clay Nanocomposites

A Dissertation

Presented for the

Doctor of Philosophy

Degree

The University of Tennessee, Knoxville

Deepali Kumar

August 2007

ACKNOWLEDGEMENTS

ABSTRACT

Polymer clay nanocomposites are a promising class of multicomponent systems where incorporation of small amount of clay results in dramatic improvement of mechanical, thermal and barrier properties. However, accomplishment of these properties necessitates molecular level dispersion of the clay platelets in the polymer matrix. This thesis presents the guidelines for obtaining thermodynamically stable nanocomposites where strong specific interactions such as hydrogen bonding between the polymer and the clay can be utilized to achieve the desired goal of nanoscale dispersion of clay sheets.

In first part of the dissertation, optimization of intermolecular hydrogen bonding between the polymer and clay is carried out by controlling the distribution of hydroxyl groups on the copolymer of styrene and 4-vinyl phenol. Copolymers ranging from 0-100% vinyl phenol are synthesized by free radical polymerization. Nanocomposites containing 50 % poly(vinyl phenol) and 40 % poly(vinyl phenol) show optimum dispersion due to large extent of intermolecular hydrogen bonding with drastic improvement in glass transition temperature.

Furthermore, the effect of the nature of clay surfactant on the dispersion of clay sheets in the polymer matrix is also studied. Nanomer I.24 TL and Cloisite 25A show similar trends in dispersion for all the copolymer compositions. Increase in vinyl phenol content from 0-50% enhances the dispersion of clay platelets. However, Nanomer I.24 TL and Cloisite 25A show different morphological behavior than Cloisite Na^+ towards the polymer containing 100% vinyl phenol. This behavior arises due to the fact that hydrophobic surfactants of Nanomer I.24 TL and Cloisite 25A do not find themselves

very compatible with hydrophilic polymer, poly(vinyl phenol) thus giving rise to intercalated morphology in opposition to exfoliation observed for Cloisite Na$^+$ nanocomposite with the same polymer. Cloisite Na$^+$ is highly hydrophilic and therefore very miscible with 100% vinyl phenol, consequently a nanocomposite with improved dispersion is obtained.

Next, clay loading is also optimized in the nanocomposites to obtain the best morphological and thermal improvements. Clay loadings of 1, 3, 5 and 8 wt % are mixed with copolymers ranging from 0-100 % vinyl phenol. 3 and 5 % clay loadings with PVPh40 and PVPh50 nanocomposites exhibit optimum dispersion of clay platelets with drastic improvement in glass transition temperature.

.

TABLE OF CONTENTS

LIST OF TABLES

LIST OF FIGURES

CHAPTER 1 INTRODUCTION

1.1   Introduction

Polymers have revolutionized the field of material science replacing metals, ceramics, glass and wood in various applications including structural applications, packaging, clothing, electronics, the automotive industry, electrical applications and medical devices due to the tailor-ability of properties, high strength to weight ratio, low production costs, ease of handling and low transportation costs. Although properties can be tailored by changing the monomer structure, synthesizing new polymers for target applications can be expensive and time consuming. Developing polymer blends and composites is an alternative approach to tailor the properties for various applications. Desired properties in such multi-component systems can be attained by judicious choice of proper components without having to synthesize new polymers. Blending of two or more polymers can be used to produce materials that span a wide spectrum of properties. Various examples of commercially successful blends can be found in the industry. Noryl^{TM} is an example of a commercial polymer blend of Polyphenylene oxide (PPO) and high impact polystyrene. PPO is a heat resistant material but very tough to process due to its high glass transition temperature (T_g) of 210°C. Blending PPO with polystyrene lowers the T_g of the resulting blend and makes it more processable than pure PPO.

Polymer composites can also be used to produce a better material with improved properties without the need of synthesizing new polymers. Polymer composites involve the reinforcement of the thermoplastic or a thermoset polymer matrix by fillers such as talc, silica, calcium carbonate, carbon black, carbon fiber, mica or glass to obtain better

thermal, mechanical and barrier properties with improved toughness and stiffness compared to a neat polymer. Effective reinforcement depends on the filler aspect ratio, the filler mechanical properties, filler loading, dispersion of the filler, surface area of the filler and the adhesion between the matrix and the filler. Although enhancement in properties can mostly be achieved by the incorporation of these fillers, it usually comes with some penalties such as loss of transparency, brittleness and large filler loadings (30-40%). These disadvantages are observed due to the poor adhesion of the matrix and the filler and aggregation of the filler in the matrix. Consequentially, the need for materials which are transparent and light weight led to the exploration of fillers with nanoscale dimensions. Composites where the reinforcement phase has one of its dimensions on the order of a nanometer are called "nanocomposites". Some of the nanofillers in use are spherical silica nanoparticles, carbon nanotubes, cellulose whiskers and layered silicates/ clays.

1.2   Properties and Applications of Polymer/Clay nanocomposites

Single clay layers were proposed to be an ideal reinforcing agent in 1974 due to their extremely high aspect ratio and also due to the nanometer filler thickness being comparable to the scale of the polymer chain structure.[1] Moreover, clay is abundantly available and is an inexpensive resource suitable for the production of nanocomposites. But it was the introduction of a nylon-6/clay hybrid by Toyota researchers in the 1990's that brought attention to the enormous potential of polymer/clay nanocomposites. They were able to achieve drastic improvement in the performance of the nylon-6 with the addition of as little as 4.2 wt % montmorillonite clay. The strength in the resulting hybrid

increased by 50% and heat distortion temperature increased by 80°C.[2] Polymer clay nanocomposites since then have become a promising class of muticomponent systems. Complete dispersion of clay sheets at the nanoscale level strongly impacts the macroscopic properties of the nanocomposites. Such nanocomposites exhibit exceptional improvement in such properties as high modulus[3-7], increased thermal stability[8-10], high mechanical strength[11-12], improved flame resistance[13-14] and outstanding barrier property[15-19] relative to neat polymers or traditionally filled composites. The complete dispersion of clay nanolayers in a polymer nanocomposite optimizes the number of available reinforcing elements for carrying an applied load and deflecting cracks. The coupling between the tremendous surface area of the clay ($\sim760m^2$/g) and the polymer matrix facilitates stress transfer to the reinforcement phase, allowing for tensile and toughening improvements.[20] Enhancement in other properties such as barrier characteristics, reduced solvent uptake, and flame retardance arise from hindered diffusion pathways observed in polymer-clay nanocomposites. The high aspect ratio of clay platelets increases the tortuosity or the path of gas or water molecules as they diffuse into the nanocomposites increasing the barrier characteristics.[21]

All these properties can be attained in the resulting nanocomposite while maintaining high optical clarity without inducing brittleness. The nanocomposites maintain transparency due to the nanometer length scale of the dispersed clay platelets, thus they undergo minimum scattering of light. Optical clarity and excellent barrier properties make nanocomposites highly suitable for food packaging applications. They also exhibit better recyclability without the need of multipolymer layered design otherwise required for obtaining improved barrier properties e.g Aegis® HFX Nylon

resin made by Honeywell is a high oxygen barrier Nylon for juice, tea and condiment bottles. These bottles provide excellent oxygen protection, glass like clarity and recyclability. [22]

Additionally, nanocomposites are light materials in comparison to the conventional micron-level composites as the addition of a small amount of clay ($\leq 5\%$) provides considerable improvement in the properties of polymers. Production of light weight materials is highly advantageous as it cuts down the transportation costs. Weight saving is an important factor for automotive applications to improve fuel economy which has resulted in the replacement of metal parts with plastics.[23] To obtain much better performance, polymer composites reinforced with particulate fillers are utilized.[24] Polymer nanocomposites are slowly replacing the conventional microcomposites in the automobile industry, as very low filler loading can lead to exceptional improvement in properties as opposed to 30-40 wt % loading required in traditionally filled composites. This leads to enormous weight reduction. Toyota, in year 2001, introduced bumpers made out of nanocomposites which are 60% lighter and twice as resistant to denting and scratching.[25] Nanocomposites are also being used in GM safari and Astro vans as "step-assists". Polyolefin nanocomposites used in this application are scratch resistant, light weight, rust-proof, with significant improvement in strength and reduction in weight leading to improved fuel efficiency and increased longevity.[26]

Another advantage of nanocomposites is that they are amenable to the major processing techniques such as extrusion, injection molding and compression molding, making their commercial implementation more feasible. These methods are applicable for all kinds of polymers ranging from commodity polymers such as polystyrene and

polyethylene to engineering plastics like poly(ethylene terephthalate) and nylon.

Polymer clay nanocomposites are a green alternative for the production of flame resistant polymers, unlike chemicals usually utilized to prepare flame retardant materials that can produce poisonous gases on combustion, for instance bromine containing chemicals. The dispersal of nanofiller clay in a polymer matrix is an inexpensive and environmentally benign method of producing flame retardant plastics. High flame retardancy is exhibited by nanocomposites due to the formation of a carbonaceous char layer which develops on the outer surface during combustion. This surface-char has a high concentration of clay layers and acts as an excellent insulator and and a mass transport barrier (slowing the oxygen supply as well as the escape of the combustion products generated during decomposition).[21]

A wide variety of polymer matrices can be utilized in the preparation of nanocomposites which has made them the materials of great choice to be studied academically and to be employed for commercial applications. Polymer matrices that have been investigated include polyamides[27-32], epoxy resins[27, 33-36], polypropylene[27, 37-39], polyethylene[27, 40], polyimides[41-43], poly (methyl methacrylate)[28, 44, 45], polycaprolactam[46], polyurethane.[47] The commercial significance of polymer clay nanocomposites can be seen in various applications ranging from thermoplastic polyolefin based exterior claddings, barrier beer bottles, nylon packaging films and in paper coating applications. Table 1.1 shows the types of polymers used in the preparation of nanocomposites, with their benefits and applications.

Table 1.1 Applications of Polymer Clay nanocomposites

Product	Characteristics	Applications	Producer
Nylon Nanocomposites	improved modulus, strength, heat distort temperature, barrier properties	automotive parts (e.g. timingbelt cover, engine cover, barrier, fuel line), packaging , barrier film	Bayer Honeywell Polymer RTP Company Toyota Motors Ube Unitika
Polyolefin nanocomposites	stiffer, stronger, less brittle, lighter, more easily recycled, improved flame retardancy	step-assist for GMC Safari and chevrolet Astro vans, heavy-duty electrical enclosure	Basell, Blackhawk Automotive, Plastics Inc, General Motors, Gitto Global Corporation, Southern Clay Products
M9	High barrier properties	Juice or beer bottles, multi-layer films, containers	Mitsubishi Gas Chemical Company
Durethan KU2-2601 (nylon 6)	Doubling of stiffness, high gloss and clarity, reduced oxygen transmission rate, improved barrier properties	Barrier films, paper coating	Bayer
Aegis NC (nylon 6/barrier nylon)	doubling of stiffness, higher heat distort temperature, improved clarity	medium barrier bottles and films	Honeywell Polymer
Aegis TM OX	Highly reduced oxygen transmission rate, improved clarity	High barrier beer bottles	Honeywell Polymer
Forte nanocomposite	improved temperature resistance and stiffness, very good impact properties	automotive furniture appliance	Nobel Polymer

Various methods have been utilized for the production of nanocomposites including in situ polymerization, solution and melt blending[48-57]. Melt blending is an environmentally benign and industrially appealing technique which does not require the use of any organic solvents but essentially needs favorable polymer-clay interaction and shear for obtaining delaminated composites. In this method, polymer and the inorganic component can be mixed by any processing technique, such as extrusion, with few difficulties due to the low filler loading utilized. In-situ polymerization is highly effective in producing exfoliated nanocomposites since the polymerization of monomers is carried out in the presence of clay. Monomers are small molecules which easily penetrate the clay galleries and as they polymerize in presence of an initiator, push the clay sheets apart resulting in exfoliation. In solution blending, polymer chains dissolved in the solvent diffuse in between the clay galleries and the removal of solvent often results in an intercalated/exfoliated structure. In this process, the entropy gained by desorption of the solvent molecules allows the polymer chains to diffuse between the clay layers, compensating for their decrease in conformational entropy[58].

1.3   Clay Types and Structure

Clay is a natural, fine grained ceramic material, composed mainly of silica, alumina and water. Clay minerals are classified in terms of structure as allophone, kaolinite, halloysite, smectite, illite, chlorite, vermiculite and mixed layer minerals.[58-59] Smectite clays are one of the predominantly used clays for the preparation of nanocomposites because of their swelling properties, high cation exchange capacities, high aspect ratio and large surface area.[60-63] Smectite are a family of clays primarily composed of hydrated

sodium calcium aluminium silicates. The crystal lattice of smectite clays is composed of units made up of two silica tetrahedral sheets with a central alumina or magnesia octahedral sheet. Montmorillonite and hectorite are one of the most common smectite clays.[62] Their chemical formulae are, respectively, $Al_4Si_8O_{20}(OH)_4 . nH_2O$ and

$Mg_6Si_8O_{20}(OH)_4 . nH_2O$.

Figure 1.1 represents the structure of montmorillonite clay. It is composed of aluminium octahedral sandwiched between two silica tetrahedral with the thickness of 1nm and lateral dimension ranging from 30 nm to several microns. An isomorphous substitution of Al^{+3} in the octahedral layer by Mg^{+2} or Fe^{+2}, or Mg^{+2} by Li^+ results in the negatively charged surface of montmorillonite clays. The amount of positive ions such as Na^+ or Ca^{+2} , which can be taken up by the clay to balance the negative charge in the interlayer is a property known as the cation exchange capacity (CEC) which is expressed as milliequivalents/100g of clay.

This clay is inherently hydrophilic due to its charged surface and exhibits high specific surface area (700-800 m^2/g). The layered morphology of these silicates with a Van der Waal gap between the sheets makes them an excellent choice as filler in a nanocomposite, as the organic molecules and polymeric chains can intercalate into this gap and enable the dispersion of the individual sheets.

1.4 Morphologies in Nanocomposites

Different morphologies in polymer clay composites are possible depending on the level of dispersion of clay sheets (refer Figure 1.2). The morphology depends on the method of synthesis, processing technique and clay-polymer interactions.
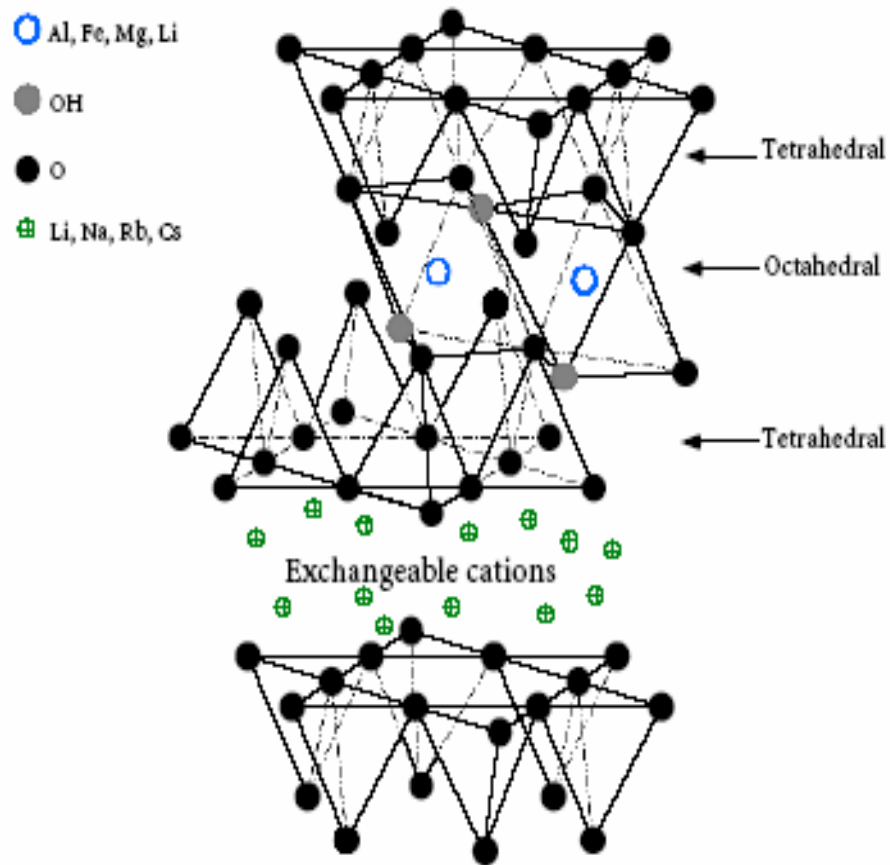
Figure 1.1 Structure of Montmorillonite Clay
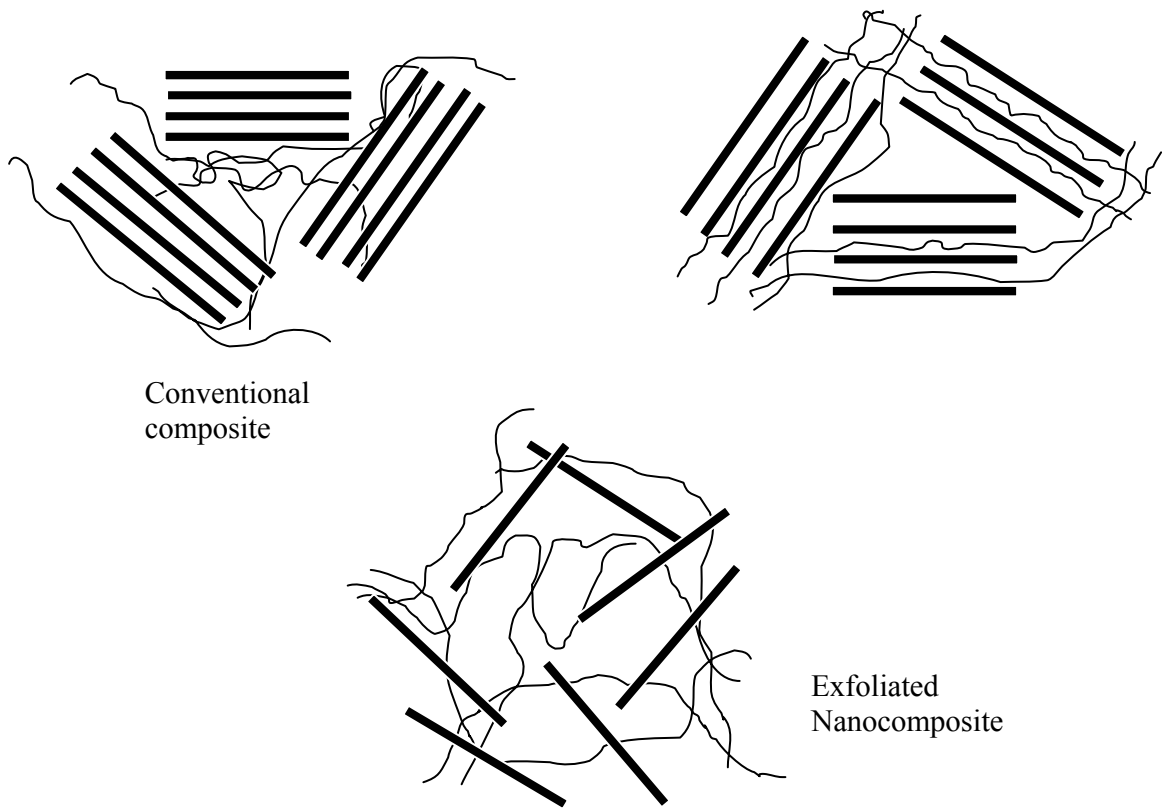
Conventional
composite

Exfoliated
Nanocomposite

Figure 1.2 Morphologies Exhibited by Nanocomposites

If polymer and clay are completely immiscible, phase-separated polymer/silicate nanocomposites with poor mechanical properties are usually obtained. This kind of a composite is a coarsely blended microcomposite with chemically distinct phases. There is poor physical attraction between organic and inorganic components leading to agglomeration and weak materials with inferior mechanical properties. In another scenario where polymer and clay are compatible, the mixing of a polymer with a layered silicate can result in the exfoliation or intercalation of the clay by the polymer. In the intercalated structure, ordering of the clay sheets is retained with a larger spacing (2-3 nm) due to insertion of a few extended polymeric chains between layers. In this state, the clay layers stay parallel to each other with alternate polymer silicate layers but are not able to provide optimum level of reinforcement. However, in an exfoliated system, the clay mineral particles are completely dispersed in the polymer. Here ordering of clay sheets is completely lost due to extensive polymer permeation. In this morphological state, there is high interfacial interaction between the clay sheets and the polymer matrix due to large surface area of dispersed clay. It is this exfoliated structure which provides optimal property improvement making these nanocomposites desired commercially.

1.5   Challenges

The homogeneous dispersion of clay sheets in a polymer matrix is very critical in attaining optimal enhancement of properties in nanocomposites. Most polymers do not exfoliate clays due to their incompatibility with hydrophilic clays. Polymers and clay tend to remain phase separated without mixing, forming chemically distinct phases. Additionally, the interlayer spacing between the clay sheets is on the order of 1 nm which

is much smaller than the radius of gyration of a polymer (5-10 nm). As a result, if a polymeric chain permeates inside the clay galleries, it cannot adopt as many conformations as in the bulk state, which leads to a loss of entropy. These factors inhibit the penetration of the polymer into the clay galleries and subsequent exfoliation of the clay sheets.

These difficulties have partially been mitigated by the replacement of the interlayer cations with non-polar long chain organic surfactants such as alkyl ammonium salts (for example dioctadecyl dimethyl ammonium bromide[64]) (Figure 1.3). Incorporation of these molecules with non-polar long chains results in an increased gallery space between individually stacked clay sheets, thus facilitating the penetration of polymer chains. Secondly, the strong interaction between the clay sheets is greatly reduced lowering the surface energy of the clay and improving the wetting characteristics of the clay with the polymer. An increase in the compatibility between the clay sheets and the polymer chains also enhances the diffusion of polymer chains into the clay galleries. Third, the nature of the organic modifier can be specifically adapted to the matrix material, e.g by introducing functional groups at the chain ends, thus fine tuning the interfacial interaction between the matrix and the reinforcement.

But the modification of clay by long chain surfactants is not usually sufficient to attain exfoliation. Giannellis and Vaia demonstrated both theoretically and experimentally in a series of studies[65, 66] that the entropy gain associated with the surfactant layer separation cannot compensate for the entropy loss associated with the confinement of a polymer melt. Therefore the outcome of the hybrid formation was dominated by the energetic factors which include the pair interactions of silicate

12
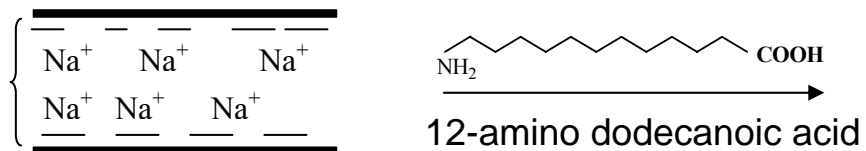
Hydrophilic clay

$d_{001} = 10.8A°$

12-amino dodecanoic acid
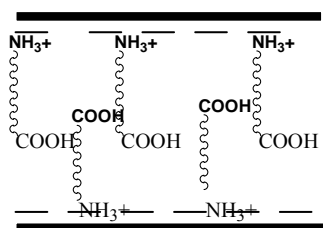
Nanomer I.24 TL

$d_{001} = 16.7A°$

Organophilic clay

Figure 1.3 Modification of Clay using exchange reaction of inter-gallery cations (Na+, Ca++) by organic cations.

surface/polymer, silicate surface/ surfactant and surfactant/polymer. To realize the intercalation of a polymer into the gallery of clay, the energy released by the change in these pair interactions must compensate the entropy loss as the polymer chains try to permeate inside the clay galleries as described by the equation:

$$\Delta H - T\Delta S = \Delta G < 0$$

The enthalpy change ΔH, summarizes the change in the interactions between members of the mixture such as polymer and surfactant, polymer and silicate surface, surfactant and silicate surface, upon mixing, while the entropy change ΔS results from the gain in releasing the constraint to the surfactant chains and by the loss in confinement of the polymer molecules upon forming the clay hybrid and ΔG represents the free energy of mixing the polymer and clay. [67]

1.6   Different Polymer-Clay Interactions

It is generally accepted that favorable interaction between the polymer and silicate surface is of substantial importance in overcoming the entropic losses on polymer permeation and are needed to obtain improved dispersion. These interactions determine the morphology of the nanocomposites. Strong specific interactions such as covalent bonding, ionic bonding and hydrogen bonding have been used to achieve this purpose. Toyota Researchers in the 1990's showed that the addition of 4.2 wt % montmorillonite clay to nylon-6 increases the strength by 50% and heat distortion temperature by 80°C. [68] The excellent mechanical properties in the hybrid were attributed to the high surface area of the dispersed clay and the formation of ionic bonds between the polymer and the silicate surface. Nylon-6 molecules have one –COOH and one –NH$_2$ end group. Titration

14

of nylon 6 with hydrochloric acid and sodium hydroxide shows that similar concentration of these functional groups coexists in the neat polymer. However, upon formation of a nylon clay hybrid, the concentration of $-NH_2$ end groups was found to decrease relative to the amount of $-COOH$ groups. The decreased $-NH_2$ concentration was attributed to the formation of NH_3^+ ionically bonded to the silicate surface. ^{15}N CP-MAS NMR spectroscopy was also carried out to study the formation of these ionic bonds. These results indicate that the $-NH_2$ group present in the neat polymer has a ^{15}N NMR chemical shift at 7.0 ppm but the nylon-6 clay hybrid exhibited a chemical shift at 11.2 ppm. This downfield chemical shift was attributed to the ionic interaction of NH_3^+ end-groups of the nylon-6 bonded to the negatively charged silicate surface. Thus, by tuning the structure at molecular level, they observed drastic improvement in the macroscopic properties of the nanocomposite.

Barber and coworkers[69] found that the random incorporation of ionic functionalities along a poly(ethylene terephthalate) (PET) chain improved the interactions between the polymer and clay resulting in predominantly exfoliated morphology. The random ionomers used were sulfonate functionalized PET ranging from 1.8-5.8 mole percent. An increase in the ionic content in the copolymer improved the dispersion of montmorillonite clay, resulting in the formation of an exfoliated structure as determined by X-ray diffraction and TEM. The enhancement in dispersion was obtained due to ionic interactions between the negatively charged sulfonate groups on the PET backbone and the positively charged edges of the clay platelets. Mechanical properties also showed an improvement with increasing ionic content of the copolymer in the nanocomposite.

Covalent interactions between the polymer and clay have also been utilized to

obtain exfoliation. Nanocomposites made of reactive silicate clays and thermoplastic urethanes (polyesterpolyol), exhibited a 125% increase in tensile strength, a 100% increase in elongation and a 78% increase in tensile modulus.[70] Polymer chains containing –NCO end groups reacted with the –CH$_2$CH$_2$OH groups on the clay particles. Nanocomposites created from polyesterpolyol with –NCO end groups showed exfoliated and well-dispersed clay sheets in TEM image, while the composite that was prepared using the pristine thermoplastic polyurethane without the –NCO end groups, showed a peak at the characteristic clay d-spacing and intercalation at 3.4 nm and TEM also showed that clay sheets were present as aggregated regions. The evidence of this tethering reaction was monitored by Fourier Transform Infrared spectroscopy (FTIR). In another study by Kung-Hwa Wei, [71] reactive organoclay was utilized in preparing polyimide nanocomposites. An ion-exchange reaction in sodium-montmorillonite clay with p-phenylene diamine created an organoclay capable of undergoing covalent bonding with the anhydride end group of poly (amic acid). Complete imidization after heating at 400⁰ C produced nanostructured materials with a 2.5 fold higher modulus than pure polyimide films.

Hydrogen bonding interactions have also been found effective at dispersing clay sheets in polymer matrices. Nanocomposites of functionalized diblock copolymer (Polystyrene-block-hydroxylated polyisoprene) were compared to those made with unmodified polystyrene-block-polyisoprene copolymer by Lee and improved dispersion was observed in the hydroxylated copolymer nanocomposite, which was attributed to hydrogen bonding between clay modified with methyl tallow bis (2-hydroxyethyl) quaternary ammonium chloride (Cloisite 30B) and the hydroxyl groups on the

copolymer.[72] The hydroxyl groups on the copolymer can form hydrogen bonds with the hydroxyl groups present on the aliphatic tail (2-hydroxy ethyl) of the surfactant as well as the silicate surface. Small Angle X-ray scattering showed no observable peak and Transmission Electron Microscopy confirmed the presence of well dispersed clay sheets. In the nanocomposite that is formed from the unmodified polystyrene-block-polyisoprene copolymer, the clay sheets did not effectively disperse in the matrix, as documented by the presence of clay aggregates as observed by transmission electron microscopy. The presence of strong hydrogen bonding interactions has been verified by comparing the linear dynamic viscoelastic properties of the nanocomposites containing hydroxylated and unhydroxylated copolymers. An unusual temperature dependence of dynamic storage modulus (G') and complex viscosity $|\eta^*|$ was found for the hydroxylated copolymer nanocomposites containing 5% clay where G' and $|\eta^*|$ increased as temperature was increased from 170 to 240° C, while the G' and $|\eta^*|$ decreased as the temperature was increased from 90 to 125 $^\circ$ C for the non-hydroxylated copolymer containing nanocomposite. In situ Fourier Transform infrared spectroscopy results indicate that hydrogen bonding persisted in the hydroxylated copolymer nanocomposite until 240 $^\circ$C, which was not observed for the neat copolymer. Much stronger hydrogen bonding interactions between the hydroxyl groups of the copolymer and hydroxyls of the clay modifier than between the copolymer chains is presented as the cause for this observation. Based on these results, they concluded that the unusual temperature dependence of G' and $|\eta^*|$ was due to these specific interactions resulting in enhanced dispersion of the clay sheets with high surface area of the dispersed clay.   Further

17

evidence of hydrogen bonding was observed by measuring the area under the absorption band 3330 cm^{-1} at 30 $^{\circ}$ C which was much higher for the nanocomposite containing hydroxylated copolymer than that of the neat copolymer.

It has also been shown that non-polar polymers such as polypropylene (PP) and polyethylene (PE) can produce a well dispersed nanocomposite when the PP or PE is modified with maleic anhydride. [73-75] Polypropylene oligomers modified by maleic anhydride (PP-MA) were mixed with clays that have octadecylammonium surfactants. TEM and XRD showed the presence of highly exfoliated nanocomposites for PP clay hybrids containing PP-MA oligomers whereas conventional composites with clay aggregates in the hundreds of microns were obtained for the polypropylene clay hybrid without the maleic anhydride modified oligomers. Also drastic improvement was observed in the mechanical properties of the nanocomposites with PP-MA oligomers. Hybrids containing the PP-MA oligomers showed an increase of 57% in storage modulus compared to the neat polymer and an increase of 32% with respect to polypropylene clay hybrids. This was attributed to better dispersion of clay sheets in the presence of the maleic anhydride modified oligomers. The authors believe that the improved dispersion is attainable in such nanocomposites due to strong hydrogen bonding interactions between the maleic anhydride group and the oxygen groups of silicates, although direct evidence of these specific interactions was not provided in the study.

1.7   Theoretical studies

Self consistent field (SCF) calculations have been completed by Balazs[76] to investigate the nanoscale interactions between the polymers and silicate sheets. In this treatment, the

18

phase behavior of polymer systems has been modeled by combining Markov chain statistics with a mean field approximation for the free energy. The results of the SCF calculations provide guidelines for the determination of the stability and morphology of polymer-clay mixtures. In these calculations, the characteristics of the surfactants, polymers and substrate were modified and thus the impact of these factors that drive the polymers to permeate the clay galleries was isolated.

As the polymer chains within the clay gallery come into contact with solid surfaces, they cannot assume as many conformations against the impenetrable interfaces as in the bulk state. Thus the intermixing of polymer and clay is unfavorable and the mixture usually phase-separates. It was predicted that if a polymer had a large degree of polymerisation and the Flory–Huggins interaction parameter between itself and clay was negative, the nanocomposites would only exhibit an intercalated morphology. For easy penetration into the gallery, the polymer must contain a segment that is highly attracted to the clay surface and a longer segment that is not attracted to the clay layers because having a long chain anchored to the clay surface promotes the stability of the exfoliated morphology. In the case of organically modified clay surfaces, favorable enthalpic interactions between the tethered surfactants and the polymers can overwhelm the entropic losses and lead to effective intermixing of the polymer and clay. Figure 1.4 shows the change in free energy of mixing, $\Delta F/A$ versus H (where H is the separation between plates) profiles for various values of the polymer-surfactant interaction parameter, χ with fixed surfactant length and grafting density. For $\chi > 0$, the free energy change of mixing is positive and so the polymer and clay are immiscible. For $\chi \approx 0$, the plots show a distinct local minimum for $\Delta F < 0$. Such local minimum indicates the

19

formation of an intercalated structure. The lowest free energy state is where the polymers penetrate the gallery and enhance the separation between the plates by a fixed amount. For $X < 0$, the plot indicates that there is a global minimum at large (infinite) separation. Such plots point to an exfoliated structure, where the sheets are effectively separated from each other and dispersed within the melt. Using thermodynamic consideration, it was shown that increasing the attraction between the polymers and surfactants promotes the formation of stable composites and could result in the creation of exfoliated structures.

Minisini and Tsobnang[77] performed a molecular dynamics study to analyze the interaction energy between an organo-modified clay surface and functionalized polypropylene. The interaction energies of polypropylene/montmorillonite nanocomposites with different functional groups (Figure 1.5) were analyzed. Comparison was also made with neat polypropylene nanocomposites. The energetic interactions between the polymer and silicate surface were found to improve with the presence of functional group present. Among the three functional groups examined, PPSMA (paramethylphenyl maleic anhydride) exhibited optimal interaction with the organically modified montmorilllonite. These results demonstrate the capacity of molecular dynamic simulations to classify the functional groups as a function of their interactions with organomodified clay surface.
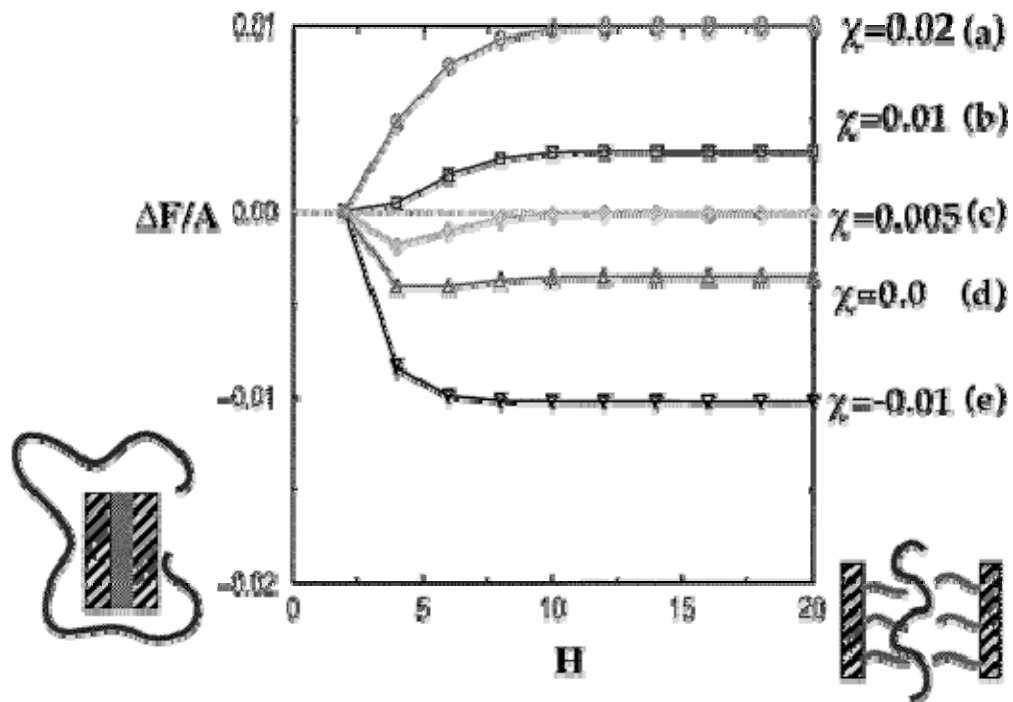
Figure 1.4   F/A versus H for various   values.

The parameters are N_{gr} = 25, ρ= 0.04, N = 100, and χ_{surf} = 0. The diagram on the left shows the reference state, where the grafted chains form a melt between the surfaces, and in the diagram on the right, the surfaces are separated by the intervening polymers.
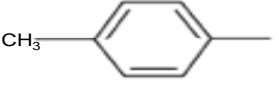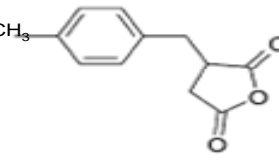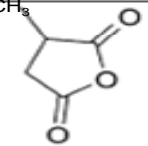
Models	Functionalized Groups	
PPMS	CH₃— (structure)	Paramethylphenyl
PPMSMA	CH₃— (structure)	Paramethylphenyl maleic anhydride
PPMA	CH₃ (structure)	Maleic anhydride

Figure 1.5 Chemical Structure of the groups grafted on polypropylene

Vaia and Giannelis[65, 66] developed a mean-field, lattice-based model of polymer melt intercalation into organically-modified silicates. They discussed that the interplay of the entropy and energetics of the mixing determines the free energy of the clay hybrid, suggesting three possible equilibrium states- immiscible, intercalated, and exfoliated. It was determined that the entropic penalty of polymer confinement may be compensated for by the increased conformational freedom of the surfactant chain as the layers separate.

Because of this small change in the total entropy, small changes in the system's internal energy determine whether intercalation is thermodynamically possible. Complete layer separation depends on the establishment of very favorable polymer-clay surface interactions to overcome the penalty of polymer confinement. In another study, Vaia and Giannelis combined experimental observations (effect of silicate functionalization, anneal temperature, polymer molecular weight, and constituent interactions on polymer melt intercalation of a variety of styrene-derivative polymers in alkylammonium-

functionalized silicates) with qualitative predictions of a mean-field lattice-based model of polymer melt intercalation to establish general guidelines for hybrid formation. They proposed that packing density and chain length of the organic modifier in the silicate must be optimized to maximize the configurational freedom of these modifer chains upon layer separation while maximizing potential interaction sites with the surface. To maximize the layer separation in silicates, favorable interactions between the polymer and clay surface are essential. With an increase in the polar / hydrophilic nature of the polymer, the chain length of the organic modifier in the silicate needs to be shortened to minimize unfavorable interactions between the polymer and the clay.

1.8   Goals and Strategy

The homogeneous dispersion of clay sheets is highly critical in achieving dramatic improvements in the properties of polymer nanocomposites. Various strategies such as varying the surfactant length of the clay, processing conditions and polymer-clay interaction have been utilized to achieve the desired results. Strong specific interactions such as covalent bonding, electrostatic interactions and hydrogen bonding between polymer and clay have been examined for their ability to obtain thermodynamically stable exfoliated systems. Understanding the role of molecular level interactions between the nanofiller and the polymer system on the properties and dispersion of a clay nanocomposite still poses a significant challenge. Therefore, this study entails the investigation of the effect of the extent of hydrogen bonding between the polymer and clay on the nanoscopic structure of polymer/clay nanocomposites and their properties. The extent of hydrogen bonding in the polymer-clay nanocomposites can be controlled

by changing the composition of the copolymer that is the matrix, poly(styrene-co-vinylphenol). Although hydrogen bonding interactions have been used to achieve miscibility between the polymer and clay, quantification of this interaction has not been completed. Quantification of hydrogen bonding between the polymer and clay using FT-IR spectroscopy provides direct evidence for the underlying physics which controls the morphology, which is observed by small angle x-ray scattering (SAXS) and transmission electron microscopy (TEM).

Studies from our group[78, 79, 80, 81] and others[82, 83] have shown that the use of strong specific interactions such as hydrogen bonding has the capability of enhancing the dispersion and miscibility of polymers mixed with anisotropic fillers, such as liquid crystalline polymers and carbon nanotubes. For instance, Dadmun et al. examined methods to control the extent of hydrogen bonding and optimize the dispersion of a rod like liquid crystalline polyurethane (LCPU) in an amorphous polymer, PS-co-VPh. Most polymers don't mix with each other due to the low entropy of mixing long polymer chains and the usual unfavorable enthalpy of mixing.[84] This tendency to phase separate is much more pronounced in the case of a mixture where one of the polymer is a rigid rod and the other is a random coil. [85] Flory showed that this occurs due to the structural dissimilarity between rigid and flexible polymers, which tends to segregate the rigid rod polymer into an anisotropic phase separating out the isotropic flexible polymer. Dadmun et al. further demonstrated that the optimization of the extent of intermolecular hydrogen bonding through control of polymer chain structure provides a mechanism to create a blend with large miscibility window. In this system, the amount of intermolecular hydrogen bonding determined by FTIR was correlated to the phase behavior of the

blends. It was determined that the intermolecular hydrogen bonding can be optimized by systematically varying the composition of the PS-co-VPh copolymer.

Based on these guidelines, we intend to investigate if a similar proptocol can be applied to our system. Our blend system consists of rigid montmorillonite clay and a flexible copolymer of styrene and vinyl phenol. The structures of the clay and the copolymer are dissimilar and don't readily mix. Clay sheets are crystalline in nature and prefer a stacked structure, therefore they tend to phase separate from the flexible polymer. Through this study, we will examine if the use of strong specific interactions such as hydrogen bonding can be utilized to enhance the dispersion of clay in a polymer matrix. The clay has oxide ions on its surface with the capability of undergoing hydrogen bonding with the hydroxyl groups of the copolymer. The extent of intermolecular hydrogen bonding will be controlled by varying the copolymer architecture where the copolymer consists of a hydrogen-bonding monomer, 4-vinyl phenol and a non-hydrogen bonding monomer, styrene. The mole percentage of these monomers will be varied ranging from 0-100% vinyl phenol and the extent of intermolecular hydrogen bonding between clay and the copolymer will be studied by FT-IR spectroscopy. The results are correlated to the dispersion obtained by SAXS and TEM and thermal properties.

The structure of the copolymer employed in the studies is shown in Figure 1.6 and expected interaction of clay with the copolymer is depicted in Figure 1.7.
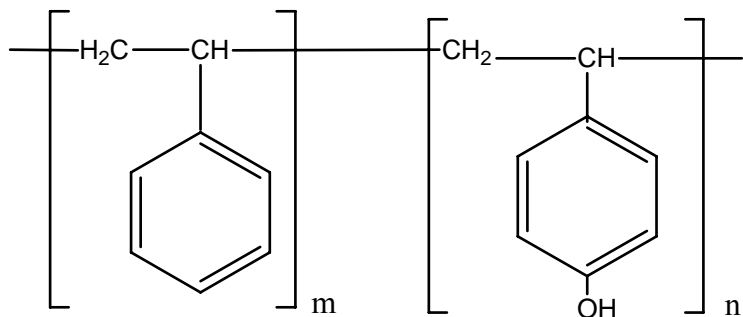
Figure 1.6   Structure of the Copolymer of Styrene and 4-vinyl phenol
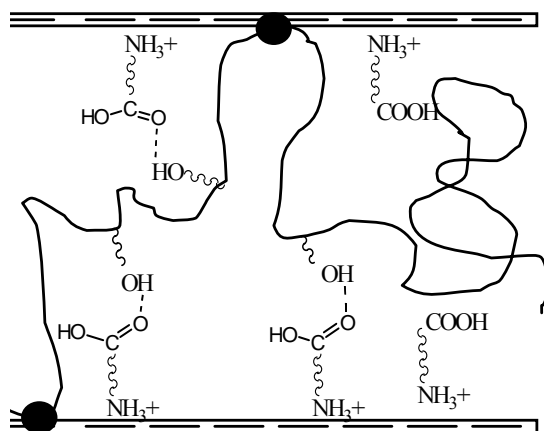
Figure 1.7 Schematic Showing Hydrogen Bonding between poly(styrene-co-vinyl phenol) and clay.● Represents Hydrogen Bonding of Hydroxyl Group of Copolymer with the Oxides of Silicate.

CHAPTER 2 EXPERIMENTAL TECHNIQUES

In this chapter, the experimental techniques are described in detail, including synthesis

and characterization of polymers and preparation and characterization of nanocomposites.

2.1   Synthesis of copolymers of styrene and vinyl phenol.

Copolymers with varying mole percentages of 4-vinyl phenol (0-50%) are synthesized by

free radical polymerization. Free radical polymerization is one of the most common

techniques of synthesizing polymers from vinyl monomers.[86]

Initiation: An azo compound, 2,2'-azobis(isobutyronitrile) (AIBN) is used as an

initiator, which decomposes at relatively low temperatures. The driving force for

decomposition is the formation of nitrogen and a resonance stabilized cyanopropyl

radical.
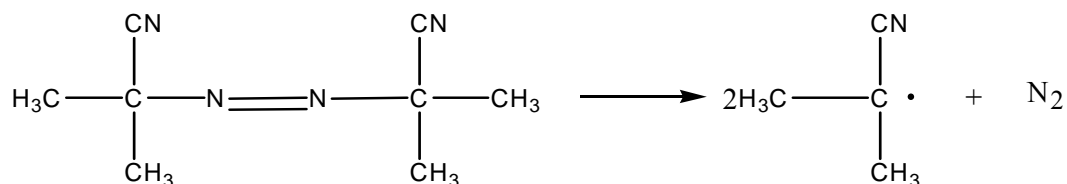
This cyanopropyl radical initiates the free radical polymerization of styrene where it adds

to the styrene monomer and generates another radical.
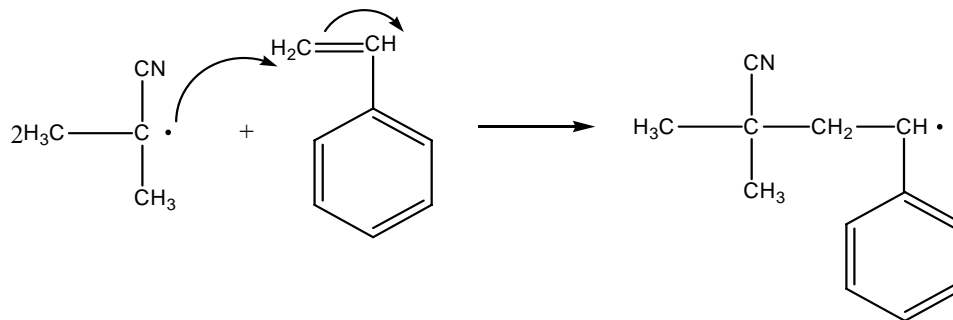
`**Propagation:** In the propagation step, the radical monomer adds to another monomer molecule to form a new radical and this process continues until a reaction occurs that terminates the chain growth.
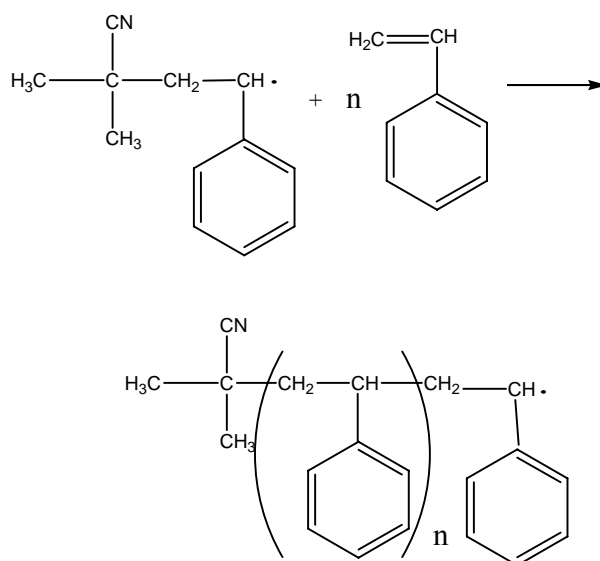
Termination: There are two principal methods to terminate a free radical polymerization- coupling or the combination of chain end radicals or disproportionation involving the transfer of an atom, usually hydrogen, from one chain end to another.[87] The route of termination depends on steric effects and the availability of alpha hydrogens for hydrogen transfer.

Coupling or Combination:

Disproportionation:

At low temperatures, polystyryl radicals primarily undergo termination by coupling but in general both the processes occur.

Free Radical Polymerization Procedure: Random copolymers of styrene and 4-vinyl

phenol were prepared by the free radical copolymerization of styrene and 4-acetoxystyrene using AIBN as the initiator, followed by the hydrolysis of the acetoxy groups using hydrazine hydrate. Copolymers containing 0, 10, 20, 30, 40, and 50 mol % vinyl phenol were synthesized.

As an example of the synthesis, for the preparation of 20 % vinyl phenol copolymer, styrene (27.593 mL, 0.240 mmol), 4-acetoxystyrene (7.33mL, 0.0480 mmol), and AIBN (0.080 g) were transferred into a three-neck round-bottom flask filled with dioxane (65 mL). Different compositions were synthesized by varying the ratio of 4-acetoxy styrene to styrene in the flask. Monomer to initiator weight ratio of (411:1) and monomer to solvent weight ratio of (1:2) was used to obtain target molecular weights. The mixture was freeze-pump-thawed once and kept in a pre-heated oil bath at 60°C for 20 h under a mild flow of argon. Precipitation was carried out in cold methanol. The polymer was dried in a vacuum oven for 2 days at 80°C. ^{1}H NMR peak assignments: 1.4 ppm (2H, d, CH$_2$); 1.7 ppm (1H, t, CH); 2.2 ppm (3H, s, -OCOCH$_3$); 6.2-7.2 ppm (9H, m, aromatic H). Acetoxy styrene groups are randomly distributed throughout the copolymer, since the reactivity ratios of styrene and 4-acetoxy styrene are 0.8 and 1.02, respectively.[88]

Next, the hydrolysis of the acetoxy groups to hydroxyl groups was carried out by the dissolution of 2 g of poly(styrene-*co*-4-acetoxystyrene) in dioxane (40 mL) in a round-bottom flask.[89] Hydrazine hydrate (6 mL) was then added to this solution and stirred for 40 h at room temperature. Copolymers with 20% poly(vinyl phenol) or less were precipitated into cold methanol and the copolymers with more than 20% poly(vinyl phenol) were precipitated into hexanes. They were then dried in a vacuum oven for 48 h.

The completion of the hydrolysis was verified by the disappearance of the methyl peak of acetoxy group at 2.2 ppm in the NMR spectrum. Figure 2.1 shows a schematic for the synthesis of the copolymers of styrene and 4-vinyl phenol. Fig 2.2 (a) and (b) show reperesentative NMR spectra of poly(styrene-co-4-acetoxystyrene) and the hydrolyzed copolymer poly(styrene-co-4-vinyl phenol) respectively. Table 1 lists the molecular weight characteristics and vinyl phenol content of the random copolymers used in this study.

2.2   Preparation of nanocomposites

Nanocomposites with constant clay loading of 5 wt % were prepared by solution blending. A suspension of clay in tetrahydrofuran was sonicated for one hour in a Branson BH1200 sonicator and the copolymer was then added to the solution, followed by sonication for one more hour. Sonication tends to break up the clay agglomerates and enhances the dispersion of the clay sheets in the polymer matrix. After sonication, the mixture was allowed to stir for seven days. The composite was then precipitated from the solution in cold methanol if it contained 0-20% vinyl phenol or in hexane if it contained 20% -100% poly(vinyl phenol). The presence of more than 20% poly(vinyl phenol) in the copolymer makes it significantly polar to require a non-polar solvent to precipitate it. The nanocomposites were then dried in a vacuum oven at 80° C for 48 hrs.

2.3   Characterization of copolymers and Nanocomposites

Determination of the percentage of 4-acetoxy styrene repeat units in the copolymer and to verify its hydrolysis to vinyl phenol were carried out by 300MHz ^{1}H-NMR with TMS as
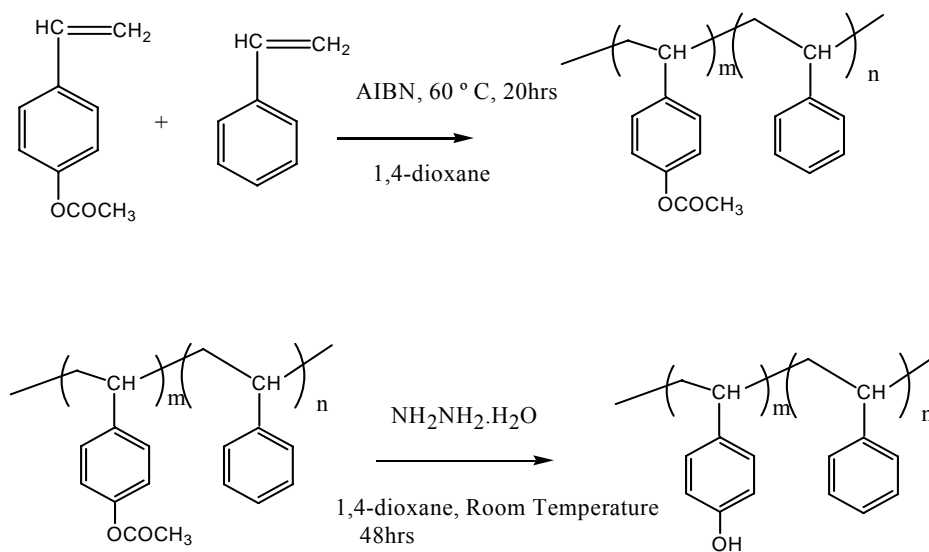
Figure 2.1 Schematic showing the synthesis of poly(styrene-co-4-vinyl phenol)

(a)

(b)
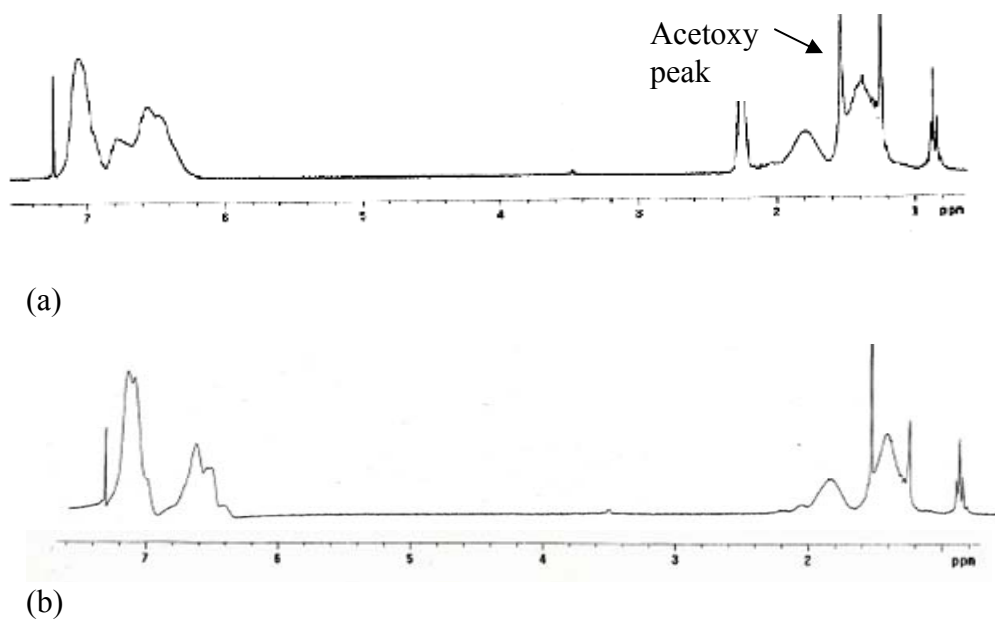
Figure 2.2 (a) 1H-NMR Spectrum of a random copolymer of poly(styrene-co-acetoxy styrene); (b) ^{1}H-NMR Spectrum of a random copolymer of poly(styrene-co-(4-vinyl phenol))

Table 2.1 Molecular weight properties of copolymers used in this study

Polymer	M_n	M_w	M_w/M_n	% Vinyl Phenol
Polystyrene	66000	97000	1.47	0
PSPVPh10	53700	79300	1.45	13.5
PSVPh 20	66000	135000	1.95	20
PSVPh30	59900	90000	1.50	30
PSVPh40	60700	88100	1.45	38
PSVPh50	57000	85500	1.50	47.5
Poly(vinyl phenol)	22000	—	—	100

an internal standard. Deuterated chloroform was used as a solvent for all poly(styrene-co-acetoxystyrene) compositions and deuterated dimethyl sulfoxide was used for the 30-50% poly(styrene-co-vinyl phenol) copolymers because of their higher polarity. A peak at 2.2 ppm showed the presence of acetoxy groups in the copolymer, due to the presence of the -OCOCH$_3$ protons. Integration of the peak area of the acetoxy groups at 2.2 ppm and the styrene aromatic peak area at 6.2-7.2 ppm was utilized to determine the percentage of 4-acetoxy styrene in the copolymer. The compositions of the copolymer (PS-co-4-vinyl phenol) were determined using the method of Radmard[90] and Coleman and Painter.[91]

The normalized area per proton corresponding to the acetoxy styrene repeating unit can be determined as:

$$A_{acetoxy} = \text{Area of 2.2 ppm peak} / 3$$

The broad peaks at 6.2-7.2 ppm correspond to the aromatic protons of styrene (5 hydrogens) and acetoxy styrene (4 hydrogens). Thus the normalized area per proton corresponding to the styrene repeating unit can be calculated as:

$$A_{styrene} = [(\text{Total area of region from 6.2-7.2}) - 4\,A_{acetoxy}] / 5$$

The percentage of acetoxy styrene repeating units can then be calculated from:

$$\% \text{ acetoxy styrene} = 100 * A_{acetoxy} / (A_{styrene} + A_{acetoxy})$$

2.3.1 *Small angle X-ray scattering*

Small angle x-ray scattering (SAXS) is an analytical technique for the structural characterization of solid and fluid materials in the nanometer range. In SAXS experiments, the sample is irradiated by a well-defined, monochromatic X-ray beam. When a non-homogeneous medium is irradiated, structural information of the

scattering particles can be derived from the intensity of the scattered beam as a function of scattering angle. Scattering occurs due to the spatial distribution of the electron densities of the components in the sample. This technique is fast and straightforward and does not require any special sample preparation. It can be utilized to analyze most samples under ambient conditions without any chemical or mechanical pre-treatment. Bragg's law states that the scattering from an ordered crystal is given by:

$$n\lambda = 2d\sin\theta \qquad\qquad (2.1)$$

Where d is the distance between the atomic layers in a crystal, λ is the wavelength of incident radiation, θ is half of the scattering angle measured from the incident beam and n is an integer. According to Bragg's law, the structural size is inversely proportional to the scattering angle, so high angle relates to smaller structure and low angle relates to larger structures.[92]

Small angle x-ray scattering can be used as a valuable tool to determine the dispersion of clay sheets in a polymer matrix. The interlayer spacing in the clays can be determined by plotting the scattering intensity as a function of q (scattering vector), where

$$q = 4\pi/\lambda \, \sin(\theta) \qquad\qquad (2.2)$$

combining equations 2.1 and 2.2, the relationship between the q-position of a peak in the scattering curve and d-spacing of the clay can be obtained as:

$$q = 2\pi/d \qquad\qquad (2.3)$$

The spacing between the clay sheets can thus be determined from a SAXS

pattern using equation 2.3. Clay sheets are crystalline in nature and have a stacking order, thus they exhibit a characteristic peak in the SAXS pattern at a q that corresponds to the van der Waal spacing (d-spacing). Therefore changes in the SAXS pattern can be monitored to discern changes in the clay stacking or its d-spacing. This d-spacing is affected by the permeation of polymer chains in the clay galleries. If there is no discernible change in d-spacing as exhibited in the SAXS pattern, a traditional composite with chemically distinct phases (polymer and clay) has been formed. However, a shift towards the higher d-spacing reflects the formation of an intercalated nanocomposite and the complete loss of a characteristic peak is indicative of an exfoliated morphology, which can also be verified using transmission electron microscopy (TEM).

The SAXS pattern shown in this work were recorded on a Molecular Metrology small angle x-ray using Cu K_{α} radiation (λ = 1.5418 A°) equipped with two dimensional position sensitive proportional detector of circular shape (diameter = 2.5cm). A monochromatic x-ray source from the x-ray sealed tube is focused by a pair of Kirkpatrick-Baez microfocusing mirrors. The sample-to-detector distance was 0.5m with the q range of $0.018A^{°-1}$-$0.50\ A^{°-1}$. The x-ray operating voltage was 45kV with the current of 0.66mA. The exposure time for measuring each sample was 1h.

2.3.2   *Transmission Electron Microscopy*

Transmission electron microscope is an excellent tool to directly investigate the morphology of polymer/clay nanocomposites. The instrument uses a focused beam of

electrons instead of light to "see through" a specimen. A "light source" at the top of the microscope emits the electrons that travel through vacuum in the column of the microscope. Instead of glass lenses focusing the light in the light microscope, the TEM uses electromagnetic lenses to focus the electrons into a very thin beam. The electron beam then travels through the specimen. Depending on the density of the material present, some of the electrons are scattered. At the bottom of the microscope the unscattered electrons hit a fluorescent screen, which gives rise to a "shadow image" of the specimen with its different parts displayed in varied darkness according to their electron density. The image can be studied directly by the operator or photographed with a camera.

TEM is based on the electron density differences in the sample and for our system contrast between the layered silicates and the polymer phase was sufficient for imaging of the nanocomposites and did not require any additional staining. Clay, due to its higher electron density, allows fewer electrons to be transmitted through and appears darker relative to the polymer and thus the dispersion in the nanocomposites can be viewed directly using this technique.

Transmission electron Micrographs were obtained on a Hitachi H800 using an accelerating voltage of 100 kV. The nanocomposite samples were sectioned into ultrathin slices (< 100nm) at room temperature using a Richert microtome equipped with a diamond knife and then mounted on 200 mesh carbon coated copper grids.

2.3.3   *Fourier Transform Infrared spectroscopy*

Electromagnetic (EM) radiation with frequencies between 4000 and 400 cm^{-1} (wavenumbers) is termed infrared (IR) radiation. IR spectroscopy is an invaluable tool in organic structure determination and verification. Radiation in the region (400-4000cm^{-1}) can be absorbed by interatomic bonds in organic compounds. Each chemical bond has specific frequencies at which it vibrates corresponding to energy levels. Also, the absorption of chemical bonds in different environments will vary transitions intensity between distinct frequency. This absorption information is collected and analysed to provide information on the state of the bonds within a given compound.

This technique will be used to examine the system of polymer and clay mixtures where the carboxylic acid groups and hydroxyl groups of the clay will be examined, as they can undergo hydrogen bonding with hydroxyl groups of the copolymer. Hydrogen bonding will affect the bond length of the C=O of carboxylic acid, which is reflected in the frequency shift to lower wavenumber of the C=O stretch. Similarly, the hydroxyl stretch bond in the FTIR spectra can be analysed through curve fitting and resolved into free, intermolecular and intramolecularly hydrogen bonded hydroxyls. The deconvolution of the IR peaks was carried out using Peakfit software version 4.11 with baseline correction. Infrared spectra were obtained on a Bio-Rad FTS 6000 Spectrometer using 4000 scans to obtain sufficient signal to noise ratio at a resolution of 2 cm^{-1}. Samples for FTIR studies were obtained by mixing solid polymer sample (10mg) with potassium bromide (90mg) which was ground to a fine powder and pressed using a die. Potassium bromide is used for sample preparation because it is transparent in the mid-IR region. Pressed pellets obtained using the dies were dried in vacuum at 60 ^{o}C for two days to

eliminate moisture.

2.3.4 Differential Scanning Calorimetry

The thermal properties of the nanocomposites were determined using a by Mettler DSC 821. Calibration of the DSC was completed using indium as a standard (m.p. 156.6°C and heat of fusion=28.45 J/g). Measurements were made from 25-160°C at a scanning rate of 20°C/min under argon. To eliminate the influence of thermal history, data from the first heating was discarded.

CHAPTER 3 OPTIMIZATION OF INTERFACIAL INTERACTIONS TO ACHIEVE NANOSCALE DISPERSION OF CLAY SHEETS IN THE POLYMER MATRIX

3.1   Introduction

In this chapter, the optimization of the extent of intermolecular hydrogen bonding in a polymer clay nanocomposite is investigated by controlling the distribution of hydroxyl groups in a copolymer. This is realized by synthesizing copolymers of styrene and 4-vinyl phenol where styrene is a non-hydrogen bonding monomer and 4-vinyl phenol can participate in hydrogen bonding via its hydroxyl group. It is expected that the extent of intermolecular hydrogen bonding between the polymer and clay can be manipulated by controlling the amount of vinyl phenol groups in the copolymers. Moreover, hydrogen bonding provides favorable enthalpic interactions between the polymer and clay, which in turn will affect the dispersion of the clay in the polymer matrix. Copolymers with varying mole percentages of 4-vinyl phenol (0-50%) are synthesized by free radical polymerization. The morphological behavior of the nanocomposites is observed using small angle x-ray scattering and transmission electron microscopy and correlated to the molecular level interaction, which is obtained through fourier transform infrared spectroscopy. The carbonyl stretching vibration has been used to quantify the extent of inter-molecular hydrogen bonding between the polymer and clay in the nanocomposite and further support has been provided by examination of the hydroxyl stretching vibration. The extent of this intermolecular hydrogen bonding between different clays and the polymer matrix can provide fundamental information on the underlying physics

that governs the ultimate morphology of polymer clay nanocomposites and provide guidelines to improve their dispersion for a wide range of polymer matrices.

3.2 Results and Discussion

3.2.1 Morphological Studies

Small angle x-ray scattering and transmission electron microscopy are used to determine the morphology and dispersion of clay sheets in the nanocomposites. Small angle x-ray scattering is a valuable tool to determine the dispersion of clay sheets in the polymer matrix. The interlayer spacing of the clays is related to the momentum transfer (q) of a peak in the SAXS curve, where q is defined as:

$$q = \frac{4\pi}{\lambda} \sin\left(\frac{\theta}{2}\right)$$

and λ is the wavelength of the radiation used and θ is the scattering angle.

The spacing between the clay sheets, d, is related to the q of the peak as $(d = 2\pi/q)$. A peak in the SAXS curve is expected because the clay sheets are crystalline and have a stacking order. This stacking order, however, maybe affected by permeation of polymer chains in the clay galleries which will alter the obtained SAXS curve. Upon mixing the clay with the polymer, characteristic clay peak may stay at the same value q value, indicating poor dispersion, or a shift in the peak towards higher d-spacing can take place indicating an intercalated morphology. In the case of the complete disappearance of the q peak, this indicates the disappearance of order in the clay sheets and an "exfoliated" structure is expected. However, these results must be supported by transmission electron microscopy experiments, which provide direct visualization of the nanocomposite morphology.

The clay modified by 12-amino dodecanoic acid (Nanomer I.24 TL) exhibits a peak in a small angle x-ray scattering experiment corresponding to a d-spacing of 16.7 Å. This is a larger d-spacing compared to sodium montmorillonite clay. Nanomer I.24 TL was selected as the nanofiller as its organic modifier has a carboxylic acid group capable of undergoing hydrogen bonding with the hydroxyl group of the copolymer that can be quantitatively examined with FTIR. The oxide ions present on the clay surface can also participate in inter-molecular hydrogen bonding with the polymer. Nanocomposites of Nanomer I.24 TL were made with 5 wt% clay mixed with copolymers that ranged in composition from 0-100 % vinyl phenol. More specifically, Polystyrene, PVPh10, PVPh20, PVPh30, PVPh40, PVPh50 and PVPh (100%) were used as polymer matrices. Fig. 3.1 shows the SAXS patterns for these nanocomposites.

Nanocomposites PS, PVPh10 and PVPh20 show a characteristic peak at 16.7 Å, the same position as the pure clay. Thus, no discernible change in the basal spacing of the clay in the composite was observed, indicating that the Nanomer I.24 TL has failed to imbibe the polymer chains resulting in a conventional composite with clay tactoids. This is further confirmed by Figs. 3.2(a), 3.2 (b) and 3.3 (a), which show their TEM micrographs that exhibit aggregated clay sheets suggesting poor dispersion in these nanocomposites. This is not unexpected as these polymers do not have sufficient hydrogen bonding to realize effective inter-molecular hydrogen bonding with the clay. It is known that polymer chains lose entropy as they intercalate inside a clay gallery thus enthalpic interactions between the polymer and clay are needed to obtain significant dispersion of the clay. Apparently the inter-molecular hydrogen bonding is insufficient in these composites to realize intercalation giving rise to poor dispersion.
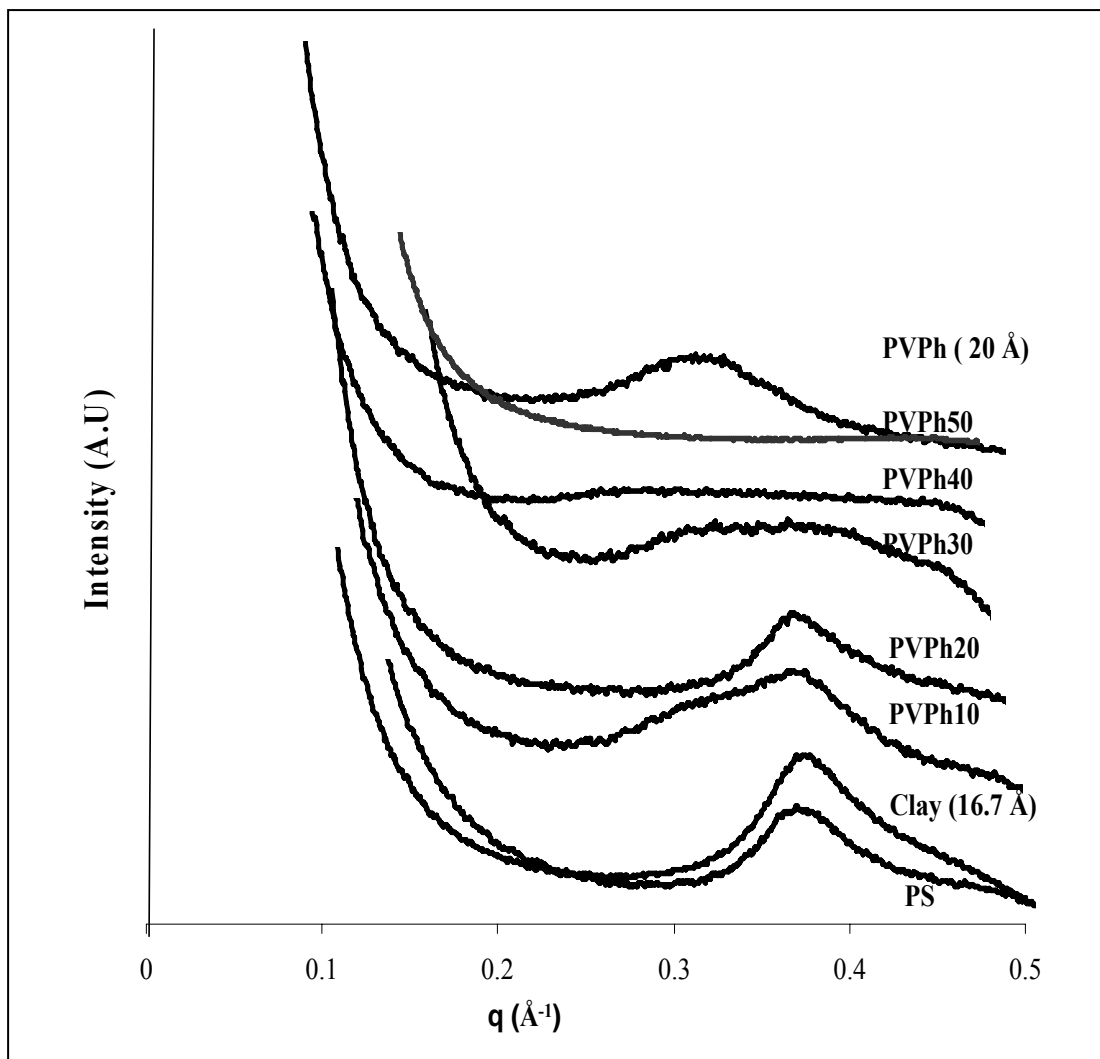
**Figure 3.1 SAXS patterns for the nanocomposites containing 5 wt%
Nanomer I.24 TL clay**
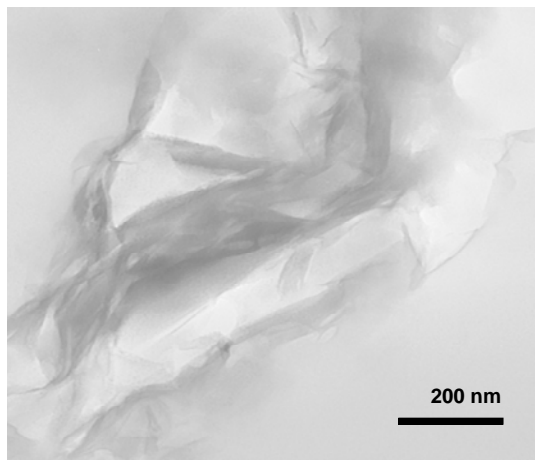
(a)
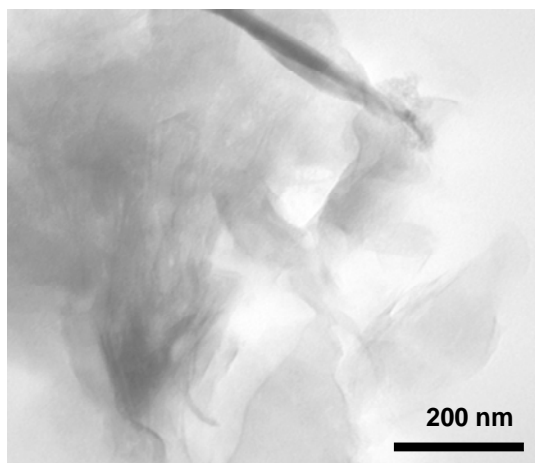
(b)

Figure 3.2Transmission Electron Micrographs of Nanocomposites containing 5 wt% Nanomer I.24 TL clay. (a) PS (b) PVPh10
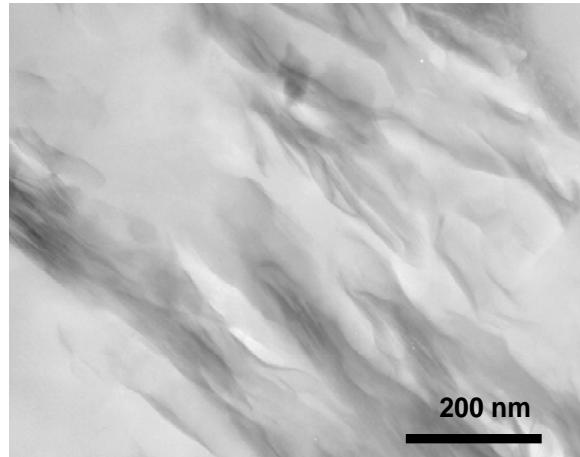
(a)
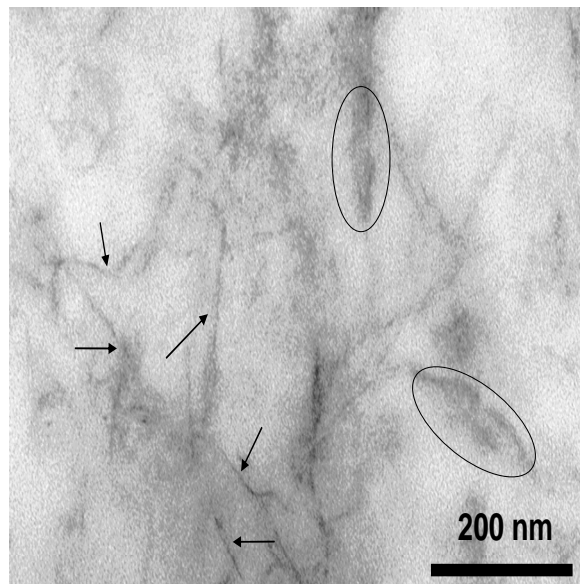
(b)

Figure 3.3Transmission Electron Micrographs of Nanocomposites containing 5 wt % Nanomer I.24 TL clay (a) PVPh20 (b) PVPh30

On increasing the vinyl phenol content to 30% in the copolymer, the SAXS curve of the nanocomposite shows a broad peak in the region of pure clay d-spacing suggesting an intermediate structure between intercalation and exfoliation.[93] This can be verified by referring to Fig. 3.3 (b) where both stacked and exfoliated sheets can be observed in the TEM of the sample. The improved dispersion of clay sheets in this sample can be attributed to enhanced inter-molecular hydrogen bonding between the polymer and the clay. PVPh30 has more hydroxyl groups which increases the propensity to engage in inter-molecular hydrogen bonding with the clay. Thus it appears that these enthalpic interactions in the form of hydrogen bonding are able to offset some of the entropic losses as the polymer chains try to permeate the clay interlayer space.

The SAXS curve of the nanocomposite containing the 40% poly(vinyl phenol) copolymer as the matrix in Fig. 3.1, exhibits no peak at $q = 0.376$ Å^{-1}, but a small shoulder is observed for this nanocomposite at $q = 0.26$ Å^{-1}. This corresponds to a d spacing of 24 Å. Thus some intercalation of the polymer into the clay gallery has occurred with a significant portion of the nanocomposite is exfoliated. According to the spectra, some intercalation has taken place but mostly the nanocomposite should be exfoliated. Additionally, Fig. 3.4 (a) is a TEM image of this PVPh40 nanocomposite, demonstrating that individual clay sheets are present, indicating that significant disruption of stacked clay sheets has taken place resulting in high delamination. Similarly, the SAXS curve of the PVPh50 nanocomposite displayed in Fig. 3.1, shows the complete disappearance of the peak in the region of clay d-spacing ($q = 0.376$ Å^{-1}). The absence of any peak suggests that ordering of clay sheets is completely lost and the clay sheets are homogeneously distributed in the polymer matrix. Since it is not possible

to detect periodicity beyond 8.8 nm using SAXS, we can expect that clay sheets are separated by more than 8.8 nm. At this separation, they are completely exfoliated.

Figure 3.4 (b) shows the TEM micrograph for the PSVPh50 nanocomposite where the clay sheets represented by the dark color are completely separated from each other confirming complete exfoliation. It is believed that PVPh40 and PVPh50 have sufficient hydroxyl groups, which results in efficient intermolecular hydrogen bonding with the clay. These strong specific interactions provide sufficient enthalpic gain to overcome entropic losses when penetrating the clay gallery, which in turn, gives rise to a mostly exfoliated structure in both nanocomposites.

As the vinyl phenol percentage in the copolymer is increased to 100% vinyl phenol (PVPh), a similar trend may be expected, where complete exfoliation should occur. However, an intercalated morphology is observed in the nanocomposite where clay sheets are separated by a d-spacing of 20 Å. The presence of long non-polar alkyl chains present as surfactants in the clay galleries in the Nanomer I.24 TL might provide some repulsive interaction for the very hydrophilic PVPh chains containing –OH groups as they try to diffuse inside the interlayer spacing. The TEM micrograph of this sample is shown in Figure 3.5, where the clay sheets maintain their ordered structure with the permeation of a few polymer chains. Further support for the observed morphological behavior of the nanocomposites will be provided by FTIR analysis of the intermolecular interactions of this system.

47
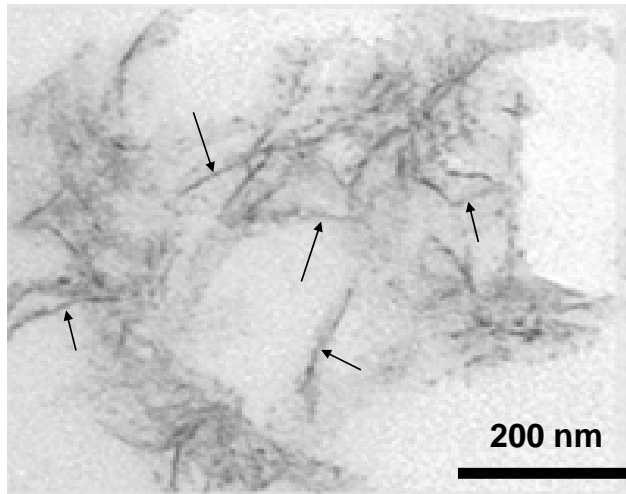
(a)
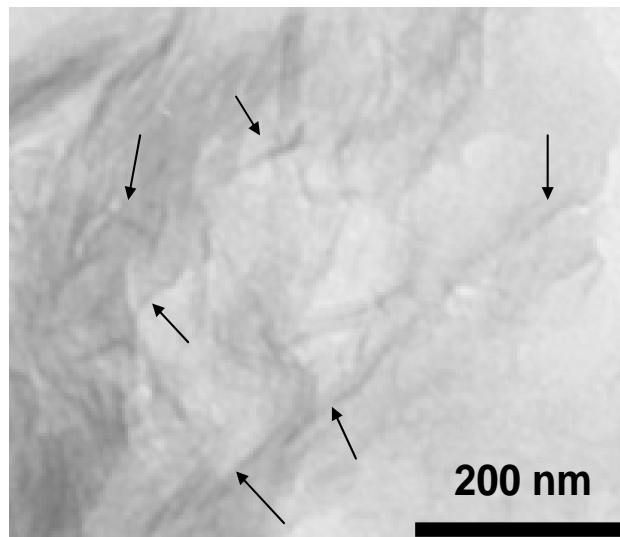
(b)

Figure 3.4 Transmission Electron Micrographs of Nanocomposites containing 5 wt% Nanomer I.24 TL clay (a) PVPh40 (b) PVPh50
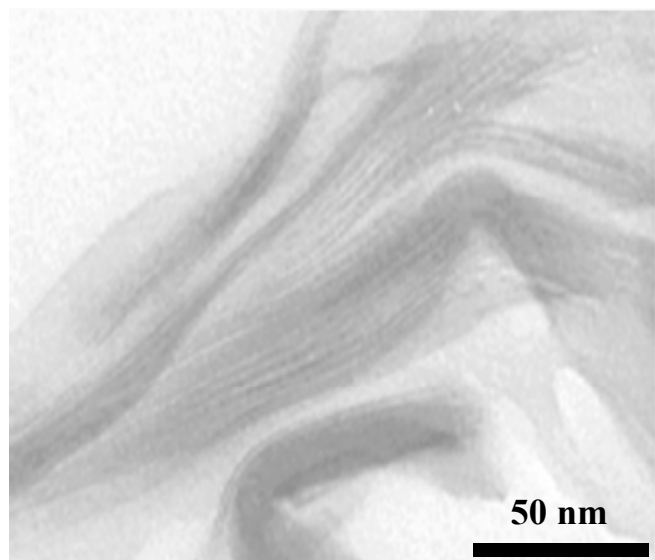
**Figure 3.5 Transmission electron Micrographs of Nanocomposite containing 5 wt %
Nanomer I.24 TL clay and PVPh**

3.2.2 *FTIR studies*

Infrared spectroscopy is a powerful technique to determine intermolecular hydrogen bonding between two polymer components in a mixture. This technique will be used for the polymer and clay mixtures in this study, where the carboxylic acid group of the clay can undergo hydrogen bonding with hydroxyl groups of the copolymer. Examination of the carbonyl stretching vibration of the clay surfactant and the hydroxyl group stretching of the copolymer can provide information on the extent of hydrogen bonding in these nanocomposites. However, quantitative evaluation of hydrogen bonding by examining the hydroxyl region is not possible due to vibration overlap of CH_2 asymmetric and symmetric vibrations and possible changes in absorption coefficients of intra- and inter-associated hydroxyl components.[94] This hydroxyl peak is also plagued by the overtone of

the fundamental carbonyl stretching vibration.[95] Based on these observations the carbonyl stretching vibrations is examined to quantitatively evaluate the extent of hydrogen bonding interactions in the nanocomposite, while qualitative analysis of hydroxyl stretching vibrations will provide information to aid in the interpretation of the carbonyl results.

The carbonyl group can be involved in three hydrogen bond interactions including intramolecular hydrogen bonding with another carboxylic acid moiety to form a dimer, intermolecular hydrogen bonding between the –COOH of the surfactant with the hydroxyl group of the copolymer or it can form an hydrogen bond with the –OH of another carboxylic acid group, denoted as a monomeric carbonyl. The carbonyls may also not participate in hydrogen bonding and be free. Figure 3.6 represents the hydrogen bonding interactions possible for the carbonyl present in the clay.

First, the infrared analysis of the pure clay (Nanomer I.24TL) was carried out to assign the peaks of the carbonyl stretching vibration in the samples. The deconvolution of the IR peaks was carried out by Peakfit software version 4.11 with baseline correction. After resolving the carbonyl peaks using the software, three peaks were revealed and assigned to the free C=O at 1805 cm^{-1}, the monomeric C=O hydrogen bonded to the hydroxyl of another carboxylic acid group at 1772 cm^{-1}, and the C=O hydrogen bonded to another carbonyl of clay in dimeric form at 1714 cm^{-1} (Figure 3.7). To confirm this assignment, a separate infrared study on dodecanoic acid was completed by dissolving in a non-polar solvent heptane (7 mg of dodecanoic acid in 2 mL of heptane) and the deconvolution of the C=O peak again showed three peaks at 1715 cm^{-1}, 1769 cm^{-1} and 1801 cm^{-1}, which were attributed to dimeric, monomeric and free carbonyls respectively (Figure 3.7).

50
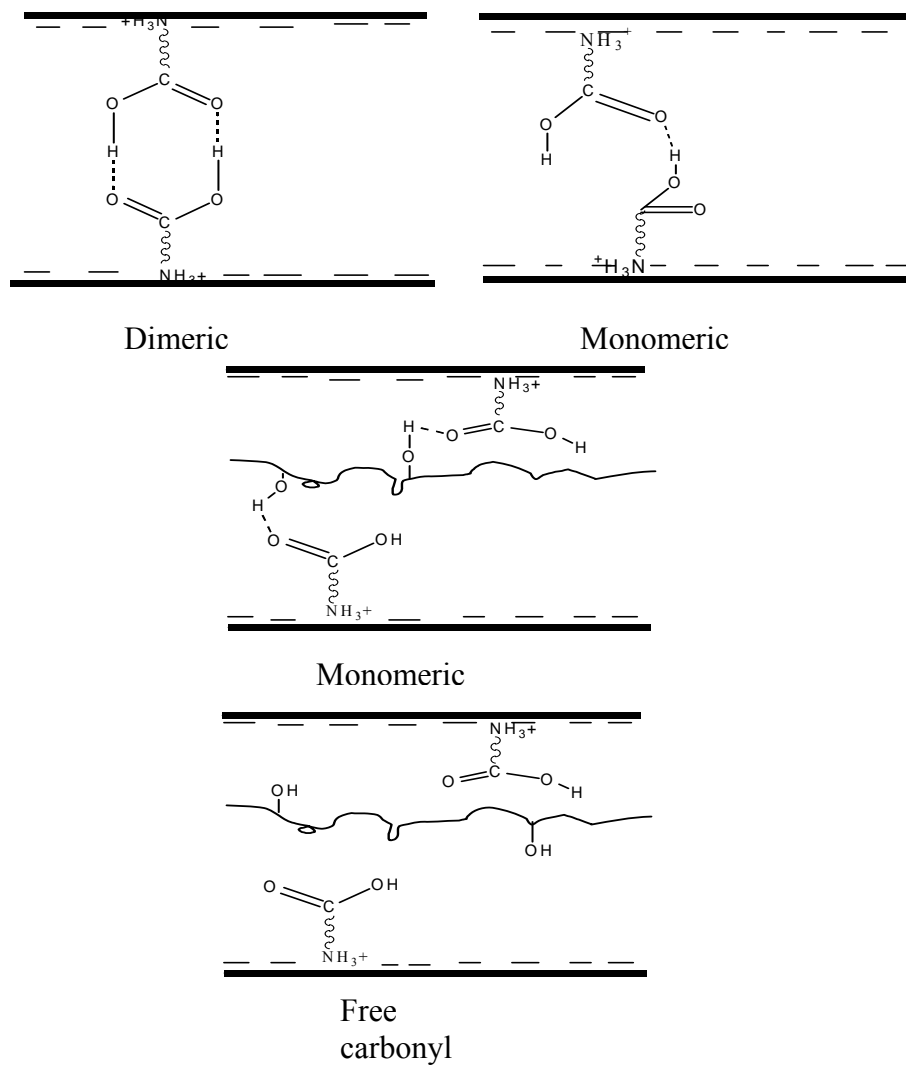
Figure 3.6 Possible hydrogen bonding interactions in the polymer/clay nanocomposites
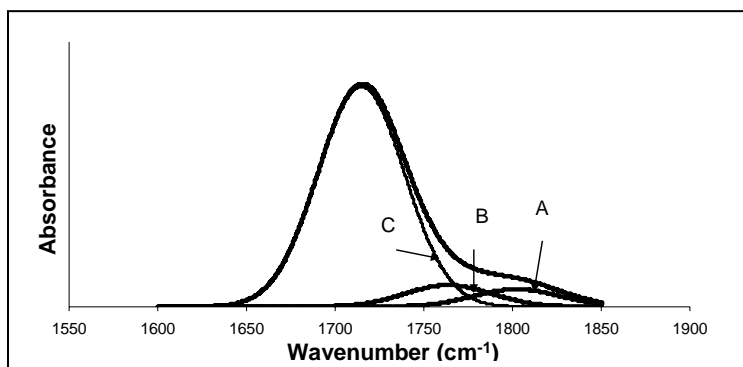
Pure clay (Nanomer I.24 TL)
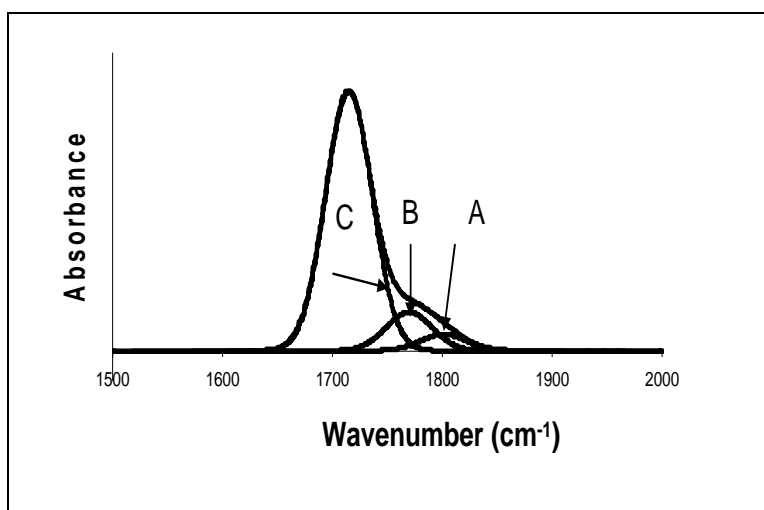
Dodecanoic acid

Figure 3.7 Deconvolution of carbonyl stretching region in the clay Nanomer I.24 TL and Dodecanoic acid where the peaks are assigned as: A) Free C=O; B) Monomeric H-bonded C=O; C) Dimeric C=O

The analysis of these peaks in the nanocomposites is required to determine the percentage of carbonyl groups in the clay participating in intermolecular hydrogen bonding with the copolymer. Infrared spectral data recorded for the nanocomposites containing 5 wt % clay and different copolymers with vinyl phenol content ranging from 0-100 % are depicted in Figure 3.8. The spectra shows that on increasing the vinyl phenol content of the copolymer in the nanocomposite, the peak observed around 1772 cm^{-1}, which has been attributed to monomeric hydrogen bonding, increases in intensity while the free C=O at 1805 cm^{-1} decreases, suggesting that with the availability of more of hydroxyl groups in the copolymer, more carbonyl functionalities of the clay participate in monomeric hydrogen bonding, thus increasing the extent of intermolecular hydrogen bonding. The quantitative analysis of these peaks to extract the % carbonyl that participate in the intermolecular interaction is also possible. It is known that the absorption coefficients and frequency of the free carbonyl vibrations do not change with blend composition.[94] However, for the hydrogen-bonded vibration, variations of 1-2 cm^{-1} have been observed and have been attributed to changes in hydrogen bond geometry distribution and strength as a function of composition in the blends. Based on this observation, in the data analysis, the frequency and the width of the free carbonyl vibration remain constant and the frequency and width of the hydrogen bonded carbonyl varies during the curve fitting. Moreover, since the absorption coefficient of hydrogen-bonded carbonyl is greater than that of the free carbonyl in polymer blends, [96, 97] a correction factor must be introduced to account for these differences.
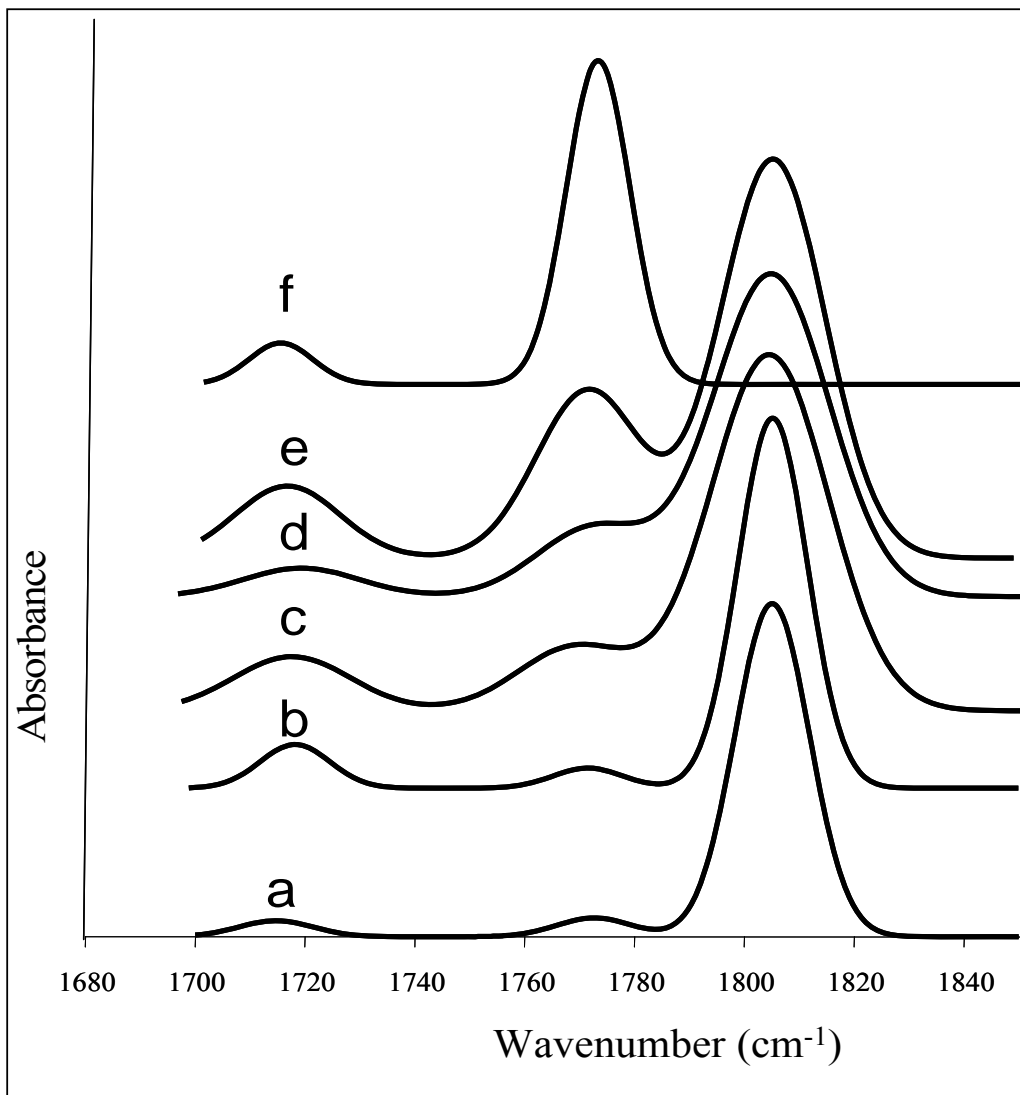
Figure 3.8 represents the FT-IR spectra of C=O stretching region of Nanocomposites containing 5 wt % Nanomer I.24 TL clay and different copolymer compositions (a) PVPh10 (b) PVPh20 (c) PVPh30 (d) PVPh40 (e) PVPh50 (f) PVPh

The ratio of these absorption coefficients, K_1 is calculated using the method of Coleman and Painter.[93, 96, 97]

$$K = \frac{A_{HB}^{T_2} - A_{HB}^{T_1}}{A_F^{T_1} - A_F^{T_2}}$$

where $A_{HB}^{T_2}$ and $A_{HB}^{T_1}$ are hydrogen bonded absorption intensities at temperatures T_1 and T_2 and $A_F^{T_1}$ and $A_F^{T_2}$ are non-hydrogen bonded absorption intensities at temperatures T_1 and T_2. In our experiments, T_1 was room temperature (24 °C) and T_2 was 180°C.

This analysis requires that the change in absorption coefficient with temperature be insignificant and there must be a large transformation between free and hydrogen bonded groups with temperature change. The absorption coefficient ratio of the hydrogen-bonded C=O band to the free C=O band in the C=O stretching mode remains low (usually between 1.0 and 1.7) and almost constant with temperature and blend composition which makes it convenient for quantitative analysis. For our system, the K value was determined for the nanocomposites containing different copolymer compositions and then averaged as a whole.

The curve fitting procedure was carried out for the nanocomposites with different copolymer compositions ranging from 10-50% vinyl phenol. The carbonyl stretching vibration is resolved into three peaks. A_1 is defined as the area of free carbonyl peak, A_2 is the area associated with the monomeric hydrogen bonded carbonyls and A_3 is associated with dimeric hydrogen bonded carbonyls. Table 3.1 shows how the deconvolution results provide the absorptivity ratio for both the dimeric hydrogen bonded and monomeric hydrogen bonded carbonyls. An average K value of 1.6 was determined

Table 3.1Deconvolution Results of the C=O stretching region of nanocomposites containing 20-50% vinyl phenol copolymers measured at 25º C and 180º C to determine the absorptivity ratios.

%vinyl phenol	Temp ºC	Free C=O			Monomeric H-bonded C=O			Dimeric H-bonded C=O			$K_{monomeric}$	$K_{dimeric}$
		υ cm^{-1}	$W_{1/2}$ cm^{-1}	A_1	υ cm^{-1}	$W_{1/2}$ cm^{-1}	A_2	υ cm^{-1}	$W_{1/2}$ cm^{-1}	A_3		
0.2	25	1805	28.2	8.5	1772	26.3	0.5	1719	27.8	1.6	1.67	1.45
	180	1805	28.2	8.6	1772	26.3	0.4	1719	27.5	1.5		
0.3	25	1805	24.3	7.6	1770	28.9	1.3	1720	30.4	1.6	1.64	1.41
	180	1805	24.5	7.7	1770	28.9	1.3	1720	30.2	1.5		
0.4	25	1805	22.6	7.5	1773	32.4	2.0	1722	25.4	0.9	1.63	1.41
	180	1805	22.8	7.6	1773	32.3	1.9	1722	25.3	0.90		
0.5	25	1805	21.5	6.3	1771	34.6	2.6	1714	28.9	1.4	1.64	1.45
	180	1805	21.5	6.3	1771	34.2	2.5	1714	28.4	1.4		
									Average K		1.6	1.4

* fixed during curve fitting

for monomeric hydrogen bonding and 1.4 for dimeric hydrogen bonding. The absorption intensities (A_2 and A_3) were then corrected by dividing the experimentally determined areas by their respective K values ($A_2' = A_2 / K_{inter}$) and ($A_3' = A_3 / K_{intra}$). Followed by this correction, the percentage of carbonyl groups that participate in monomeric hydrogen bonding are then calculated by:

$$\% \ C{=}O_{monomeric} = \frac{A_2'}{A_1 + A_2' + A_3'}$$

And the percentage of C=O groups participating in dimeric hydrogen bonding are calculated by using the equation:

$$\% \ C{=}O_{intra} = \frac{A_3'}{A_1 + A_2' + A_3'}$$

Table 3.2 shows the curve fitting analysis of carbonyl stretching region to determine the amount of free, monomeric and dimeric hydrogen bonded C=O and Table 3.2 represents the determination of percentage of free, monomeric and dimeric hydrogen bonded C=O as a function of copolymer composition. Figure 3.9 displays the plot of percentage of free, monomeric and dimerically hydrogen bonded carbonyls as a function of the composition of copolymer in the nanocomposite. This data shows that with the increase in the amount of vinyl phenol (10-100%) in the copolymer, the percentage of carbonyl groups in the clay that are involved in monomeric hydrogen bonding increase from 2.1 to 80.5. The percentage of dimerically hydrogen bonded –C=O does not change significantly with copolymer composition in the nanocomposite. The free –C=O groups decrease dramatically as the monomeric hydrogen bonding increases.

Table 3.2 Results of the curve fitting to the C=O stretching region for nanocomposites containing 0-100% vinyl phenol content at room temperature.

%vinyl phenol	Free C=O			Monomeric H-bonded C=O			Dimeric H-bonded C=O		
	v^* cm^{-1}	$W_{1/2}$ cm^{-1}	A_1	v^* cm^{-1}	$W_{1/2}$ cm^{-1}	A_2	v^* cm^{-1}	$W_{1/2}$ cm^{-1}	A_3
10	1805	30.4	9.1	1772	24.6	0.3	1715	22.5	1.4
20	1805	28.2	8.5	1772	26.3	0.5	1719	27.8	1.6
30	1805	24.3	7.6	1770	28.9	1.3	1720	30.4	1.6
40	1805	22.6	7.5	1773	32.4	2.0	1722	25.4	0.9
50	1805	21.5	6.3	1771	34.6	2.6	1714	28.9	1.4
100	NA	NA	NA	1771	37.5	8.3	1714	30.2	1.7

Table 3.3Percentage of free, monomeric H-bonded and Dimeric H-bonded C=O as a function of copolymer composition in the 5% Nanomer I.24 TL nanocomposites

Copolymers	% free C=O	% monomeric H-bonded C=O	% Dimeric H-bonded C=O
PVPh10	88.2	2.1	9.7
PVPh20	86.1	2.9	11.0
PVPh30	80.2	8.6	11.4
PVPh40	80.2	12.8	7.0
PVPh50	70.8	17.8	11.4
PVPh	0	80.5	19.5
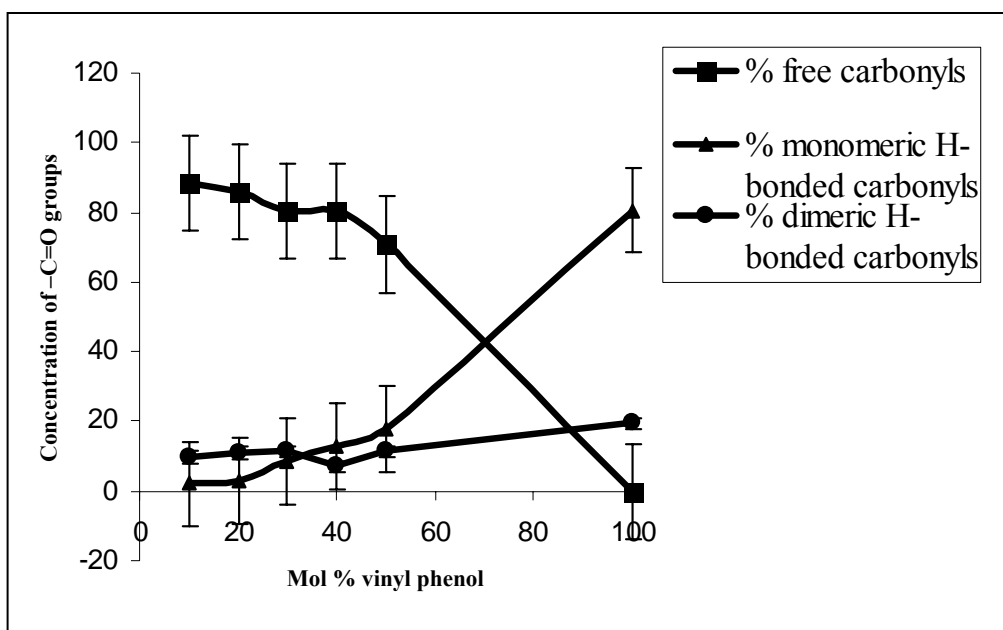
Figure 3.9The percentage of carbonyl groups involved in free, monomeric- and dimeric H-bonding as a function of copolymer composition.

Unfortuantely, it is not possible to resolve the monomeric hydrogen bonding into contributions from the hydrogen bonding between the –C=O of the clay and –OH of the polymer or hydrogen bonding between -C=O and –OH group of another carboxylic acid in the clay. Therefore the carbonyl stretching analysis is ambiguous in defining the extent of clay-copolymer intermolecular hydrogen bonding. However, if this data is combined with the analysis of the hydroxyl vibration, insight into the extent of intermolecular hydrogen bonding is possible.

Qualitative Analysis of the hydroxyl stretching vibration in the pure copolymers and nanocomposites

Although quantitative evaluation of hydroxyl stretching vibration is difficult due to vibrational overlap and and possible changes in absorption coefficients of the intra- and inter-associated O-H component, the hydroxyl stretching vibration in the region (3100-3700 cm^{-1}) can be analysed to provide a qualitative measure of the extent of hydrogen bonding interactions in a mixture.

Peak fitting Analysis of pure copolymers

The FTIR spectra of pure copolymers are shown in the Figure 3.10. A sharp peak is observed for the free hydroxyl groups in the region 3532-3545 cm^{-1} and a broad peak pertaining to intra-molecular hydrogen bonding in the pure copolymers appears between 3380-3440 cm^{-1}. The hydrogen-bonded –OH peak becomes broader when the molar composition of the copolymer increases from PVPh10 to PVPh (100% poly(vinyl phenol)), while the area under the free –OH peak decreases. The area under the peak provides a qualitative measure of the contribution of the respective absorbances to the overall curve. Hydroxyl stretching region in the FTIR spectra has been deconvoluted
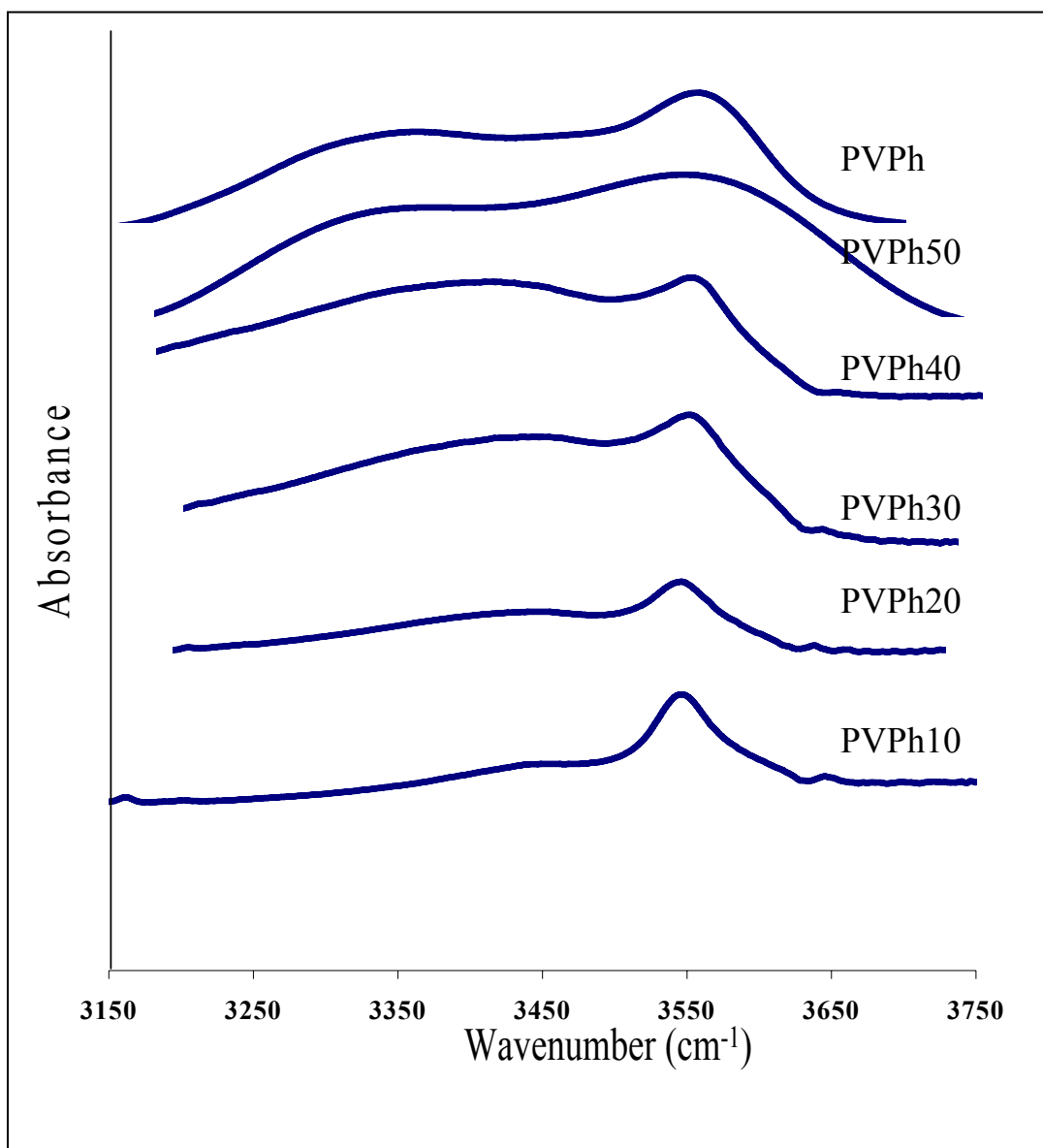
Figure 3.10 TIR spectra of pure copolymers
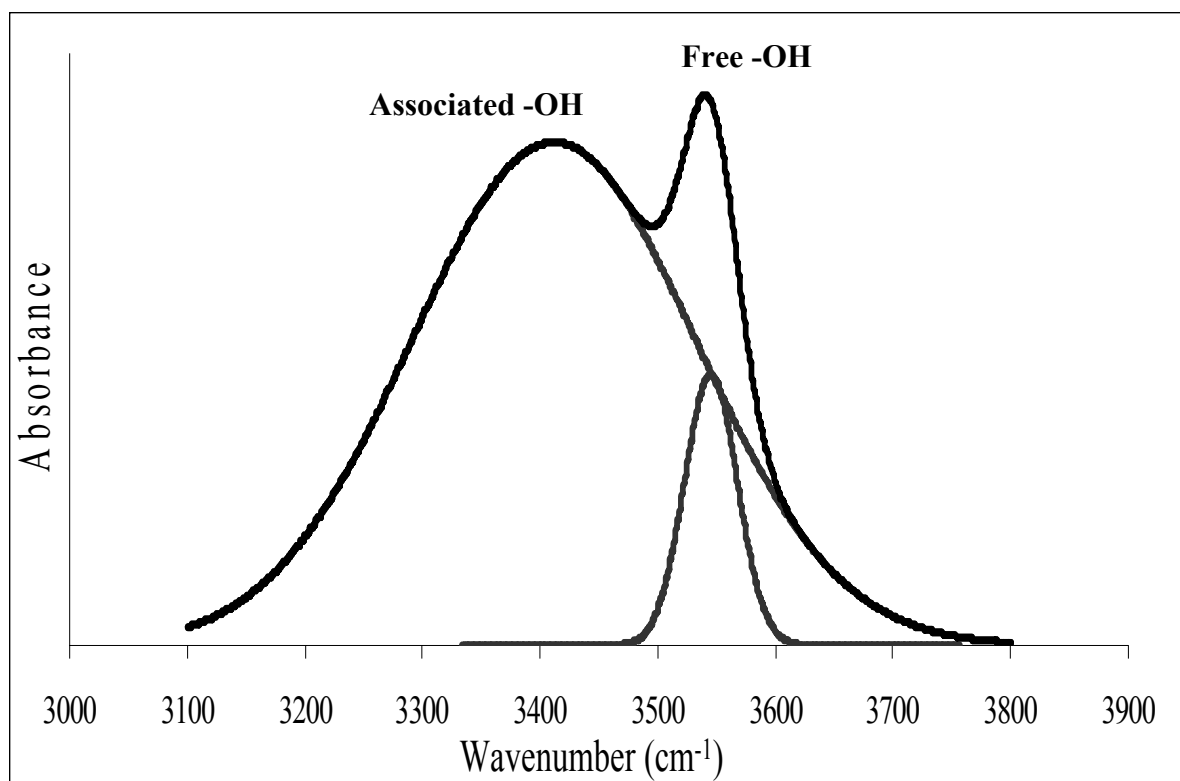
Figure 3.11 Deconvoluted IR spectra of PVPh40

using Peakfit v.4.11 software. In all fitting procedures, a Gaussian band shape has been assumed. The –OH region between 3100-3700 cm^{-1} was resolved into free and associated –OH groups for the pure copolymers. Figure 3.11 shows the deconvolution carried for the PVPh40 copolymer.

Similarly, the –OH stretching vibration was resolved using Peakfit software for all the copolymers. The contribution from the free and intra-associated hydroxyls was assessed using Beer- Lambert law,[98] which relates the concentration of the relevant vibration groups to the absorbance by the relationship:

$$A = a * b * c \qquad\qquad (3.1)$$

where A is the absorbance of a given vibration, a represents the absorption coefficient, b the thickness of the film, and c is the concentration of the species. In the copolymers of styrene and 4-vinyl phenol (PVPh), some of the hydroxyl groups are free and others are involved in intra-molecular hydrogen bonding. On varying the vinyl phenol content in the copolymer, the concentration of free and associated –OH groups varies. Also the total concentration of –OH groups changes with the vinyl phenol content in the copolymer. Therefore the total concentration of the hydroxyl groups must be calculated for each copolymer. The total –OH concentration in the sample can be calculated from:

$$C_T = (d * w * f_{VPh}) / M \qquad\qquad (3.2)$$

Where d is the density of the polymer, w is the weight fraction of the polymer in the nanocomposite, f_{VPh} is the molar fraction of vinyl phenol in the copolymer and M is the molar mass of the vinyl phenol repeat unit. The total concentration of –OH in the copolymer can also be expressed as:

$$C_T = C_F + C_{AS} \qquad\qquad (3.3)$$

Where C_T is the total –OH concentration, C_F is the concentration of free –OH groups and $C_{AS,}$ is the concentration of –OH that participate in intra-molecular hydrogen bonding. The concentration of free OH is calculated by rearranging equation 3.1 as:

$$A = a * b * c$$

$$C = A / (b * c)$$

Therefore, $\qquad\qquad C_F = A_F / (a_F * b)$ $\qquad\qquad\qquad$ (3.4)

In this equation, A_F represents the absorbance for free –OH peak which is the area under this peak. The absorption coefficient for the free –OH vibration (a_F) is determined from the reported values of free –OH concentration, absorbance, and film thickness of PVPh[99] and is used for all copolymer and nanocomposite samples. Once the concentration of free –OH is known using equation 3.4, the concentration of intra-associated –OH is then determined by subtracting the concentration of free –OH from the total concentration of –OH. Table 3.4 displays the deconvolution results for the pure copolymers. Figure 3.12 is a plot of the ratios C_F / C_T and C_{AS} / C_T as a function of mol% of vinyl phenol in the copolymer. The fraction of free –OH decreases on increasing the vinyl phenol content in the copolymer and at the same time the contribution of the intra-molecularly associated –OH increases. The C_F/C_T observed in PSVPh10 is 0.75 which decreases to 0.04 in PSVPh50 and finally to 0.01 in PVPh. The contribution from intra-molecular association observed in case of PSVPh10 is 0.25 and increases to 0.95 in PVPh40. The polymer with 100% vinyl phenol (PVPh) shows a very high contribution ($C_{AS}/ C_T = 0.99$) from the intra-molecular association of the hydroxyl groups.

Table 3.4 Curve Fitting Analysis of pure copolymers

	1.1	Free OH			Intra OH				C_F/C_T	C_{AS}/C_T
Copolymers	υ (cm⁻	$W_{1/2}$	A_F (cm	C_F	υ (cm⁻	$W_{1/2}$	A_{AS} (cm⁻	C_{AS}		
PVPh10	3545	65	61.9	102	3444	150	38.1	339	0.7	0.2
PVPh20	3545	65	27	447	3417	260	73	157	0.2	0.7
PVPh30	3543	65	16.7	276	3413	272	83.3	275	0.0	0.9
PVPh40	3540	65	11.5	190	3398	279	88.5	364	0.0	0.9
PVPh50	3539	64	11	182	3390	285	89	461	0.0	0.9
PVPh	3532	65	7.7	127	3381	320	92.3	987	0.0	0.9
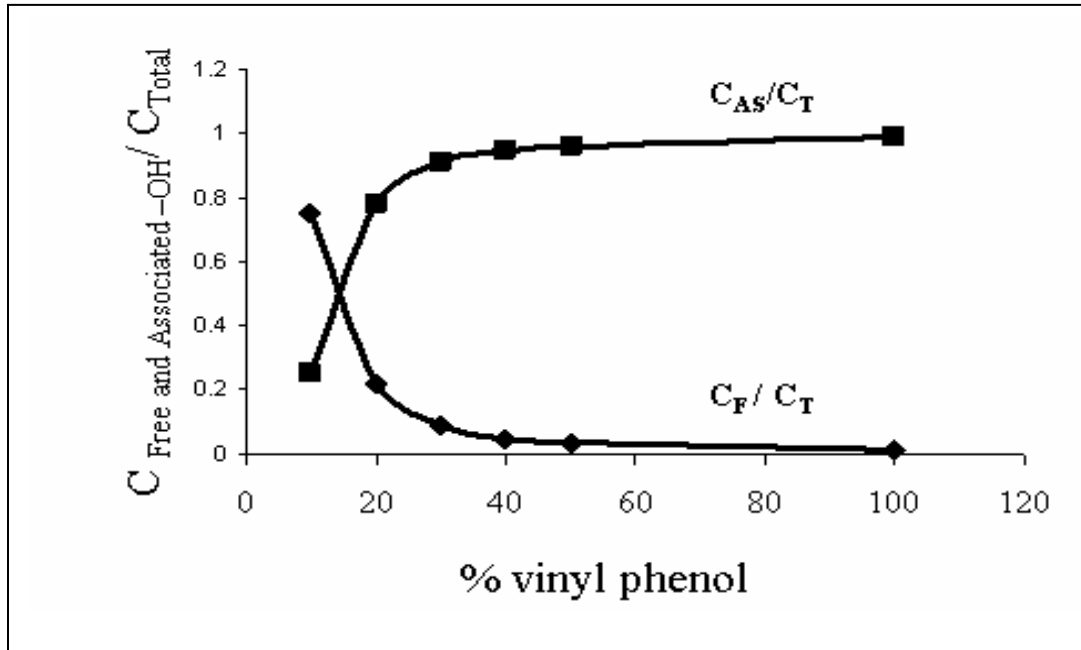
Figure 3.12 Plot of the ratio of calculated CF / CT and CAS / CT as a function of

Peak fitting Analysis of Nanocomposites

A similar analysis is completed for the nanocomposites with 5 % Nanomer I.24 TL. Figure 3.13 shows the IR spectra of the nanocomposites containing 5 wt % Nanomer I.24 TL. The IR spectra of the nanocomposites show discernible differences relative to that of the pure copolymers in the hydrogen bonded region of hydroxyls. The hydrogen bonded hydroxyl peak of the nanocomposites becomes broader and there exists a separation of peaks into intra- and inter-molecular association. A representative example of the deconvolution of the hydroxyl region of the IR spectrum in the nanocomposite PVPh40 is shown in the Figure 3.14. During the deconvolution process of the nanocomposite analysis, the position and width of the free and intra-associated hydrogen bonded-OH groups were fixed at those observed for the pure copolymer. The position and width of the inter-associated –OH were allowed to vary in the fitting process. The presence of inter-molecular association in the nanocomposite results in the need to add one more term to the relationship of equation 3.3. Thus the total –OH concentration in the nanocomposite must be expressed as

$$C_T = C_F + C_{AS} + C_I \qquad (3.5)$$

Where C_I and C_{AS} represent the concentration of inter-molecularly hydrogen bonded and intra-molecularly associated -OH groups respectively in the nanocomposite. The values for C_I and C_{AS} are determined using equations 3.6 and 3.7.

$$C_I = A_I/(a_{as} * b) \qquad (3.6)$$

$$C_{AS} = A_{AS}/(a_{as} * b) \qquad (3.7)$$

In these equations, A_I and A_{AS} represent the absorbances for the inter and intra-
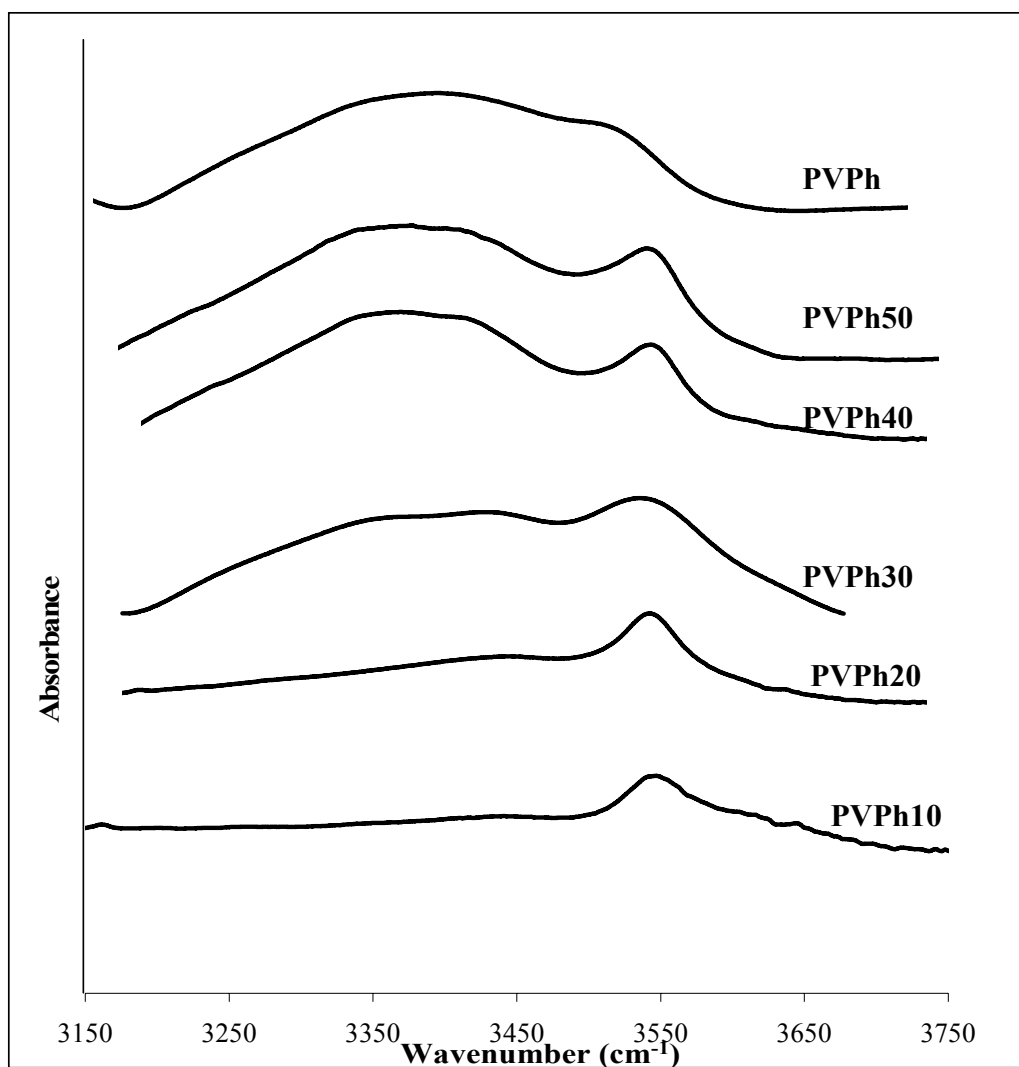
**Figure 3.13 FTIR spectra of Nanocomposites containing 5 wt%
Nanomer I.24 TL clay**
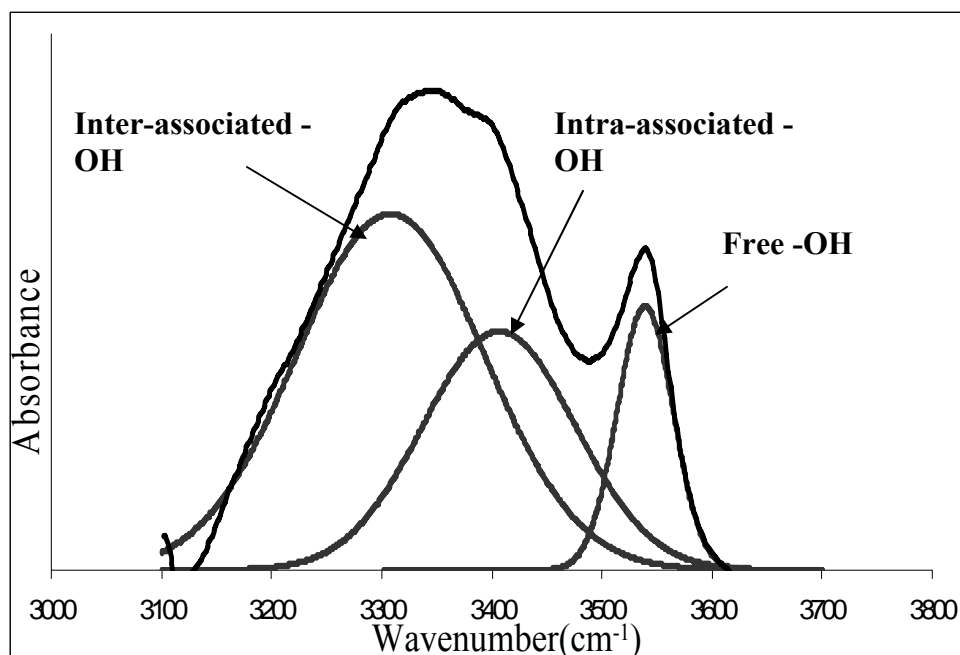
Figure 3.14 Deconvoluted IR spectra of PVPh40/Nanomer I.24TL

molecularly associated hydroxyl groups. The absorption coefficient a_{as} is assumed to be

similar for both inter- and intra-molecularly associated –OH groups, an assumption that

has been shown to be generally valid.[99] This approximation is a potential source of error

in quantifying the –OH concentration. It is important to emphasize that due to this

uncertainty, the values obtained using this analysis do not indicate an absolute percent of

–OH that are free or hydrogen bonded in each sample, but do provide qualitative

information on these variables. To determine the value of the absorption coefficient a_{as},

C_{AS} is first calculated for the pure copolymer samples using equation 3.7 followed by

$$a_{as} = A_{AS}/(C_{AS}* b) \tag{3.8}$$

Since the concentration of the total and free hydroxyl groups is different for each

polymer, the concentration of the associated hydroxyl groups determined by equation 3.7 varies with copolymer composition. Therefore the absorption coefficient for the associated –OH can be calculated for each copolymer system using the concentration of associated –OH for that particular copolymer. Then C_I (the concentration of inter-molecularly H-bonded –OH) is calculated for all nanocomposites with different copolymer composition, followed by the determination of C_F (concentration of free –OH). The concentration of intra-molecularly associated –OH, C_{AS} is calculated by subtracting the sum of C_I and C_F from the total –OH concentration, which is determined using equation 3.5. Table 3.5 summarizes the curve fitting results for all nanocomposites in the hydroxyl stretching region. Figure 3.15 shows the plot of C_F / C_T, C_{AS} /C_T and C_I/C_T as a function of copolymer composition in the nanocomposite.

The deconvolution results show that the incorporation of clay to the copolymer increases the contribution of the free –OH to the total –OH relative to that of the pure copolymers. For instance, the C_F/C_T of the pure PVPh10 increases from 0.75 to 0.87 in the PVPh nanocomposite. Similarly, nanocomposites formed with other copolymer compositions show an increase in C_F / C_T on forming nanocomposites. The contribution from intra-molecular hydrogen bonding increases with increasing vinyl phenol in the copolymer, however the values are significantly lower that those of pure copolymers. For instance, C_{AS} /C_T of the 40% and 50% neat copolymers were 0.95 and 0.96 respectively, while these contributions decrease to 0.36 and 0.24 respectively, on forming nanocomposites. This data demonstrates that rather than engaging in intra-molecular hydrogen bonding, the –OH groups predominantly engage in inter-molecular hydrogen bonding with the clay. The frequency of the inter-molecularly hydrogen bonded –OH is

Table 3.5 Curve Fitting results for Nanomer I.24TL/ PVPh Nanocomposites

Mol%	Free -OH				Intra-molecluarly H-bonded OH				Inter-molecularly H-bonded OH				C_F/C_T	C_{AS}/C_T	C_I/C_T
	υ (cm^{-1})	$W_{1/2}$	A_F (cm^{-1})	C_F	υ (cm^{-1})	$W_{1/2}$	Aas (cm^{-1})	C_{AS}	υ (cm^{-1})	$W_{1/2}$	A_I (cm^{-1})	C_I			
10	3545	65	75.7	1123	3444	150	17	120	3390	100	7.34	52	0.87	0.09	0.04
20	3545	65	46.5	840	3417	260	30.8	621	3385	110	22.7	458	0.43	0.32	0.24
30	3543	65	24.7	526	3413	272	35.5	1109	3324	130	39.8	1244	0.18	0.39	0.43
40	3540	65	14.7	315	3398	279	33.7	1316	3341	137	51.6	2015	0.09	0.36	0.55
50	3539	64	14.3	344	3390	285	22	1081	3319	142	63.7	3130	0.08	0.24	0.69
100	3532	65	24.0	971	3381	320	42.9	6264	3237	126	33.5	2264	0.14	0.48	0.38
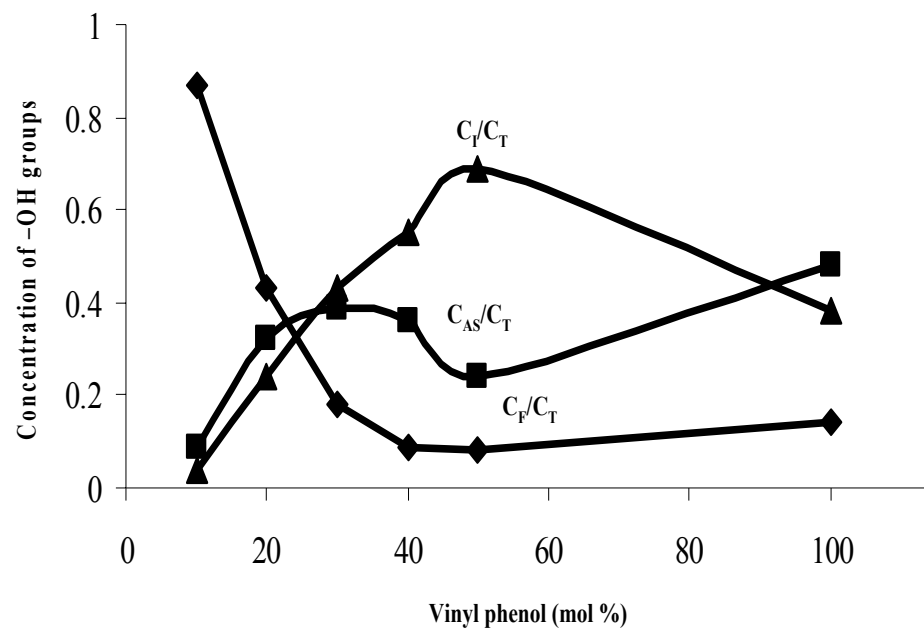
Figure 3.15 Plot of CF / CT, CAS/CT and CI/ CT versus the mol% of vinyl phenol present in the 5 % Nanomer I.24 TL nanocomposite.

at a lower wavenumber than the intra-molecularly hydrogen bonds. Both –COOH and oxide ions of the clay are capable of undergoing stronger hydrogen bonding interaction than the –OH------OH hydrogen bond within the copolymer chains. Nanocomposites containing PVPh40 and PVPh50 show significant extent of inter-molecular hydrogen bonding, with values of C_I/C_T of 0.55 and 0.69, respectively, in comparison to PVPh10 and PVPh20 which have values of 0.04 and 0.24. The presence of a large number of hydroxyl groups in PVPh40 and PVPh50 copolymers facilitates more of inter-molecular hydrogen bonding, resulting in better interaction between the polymer and clay, which affects the morphological behavior of these nanocomposites. Correlation of these molecular level interactions to the morphology will be discussed in next section. The C_I/C_T in the PVPh nanocomposite is 0.38 and the fraction of hydroxyls involved in intra-molecular association is much higher, C_A/C_T is 0.48. On increasing the vinyl phenol content in the copolymer, the proximity between the –OH groups increases, presumably favoring intra-molecular hydrogen bonding relative to inter-molecular hydrogen bonding.

3.2.3 *Correlating Intermolecular hydrogen bonding to the dispersion in nanocomposites*

For the nanocomposites containing the copolymers PS, PVPh10 and PVPh20, poor dispersion of the clay sheets is observed by SAXS and TEM. Furthermore, semi-quantitative analysis of the –OH region indicates minimal inter-molecular association between the copolymer and clay. As fewer hydroxyl groups are present in the copolymer chain, very little hydrogen bonding is possible with the clay surface. Thus mixing of the clay with these polymers does not provide sufficient enthalpic gain for the entry of

polymer chains in the interlayers resulting in a conventional composite with clay aggregates.

The nanocomposite containing the 30% poly(vinyl phenol) copolymer with 5% Nanomer I.24 TL clay shows a broad peak in SAXS, suggesting an intermediate structure between exfoliation and intercalation while the TEM also confirms this interpretation. The analysis of its IR spectrum indicates an increase in inter-molecular hydrogen bonding (C_I/C_T=0.43) which improves the molecular dispersion in the nanocomposite to some extent corroborating the fact that specific interactions are desired to facilitate the polymer permeation in the clay sheets. These results are in accordance with the improved morphological behavior of the nanocomposite.

As the vinyl phenol content increases in the PVPh40 and PVPh50 nanocomposites, further increase in inter-molecularly associated –OH is observed (C_I/C_T = 0.55 and 0.69 for PVPh40 and PVPh50, respectively). The SAXS curves of these samples demonstrate that these samples are really entirely exfoliated. This improved dispersion is attributed to the large number of hydroxyl groups which can orient themselves to the hydrogen acceptor group on the clay and form an inter-molecular hydrogen bond. These favorable interactions provide the driving force for increased polymer permeation of the clay sheets, leading to significant exfoliation.

Furthermore, the nanocomposite containing 100% Poly(vinyl phenol) shows intercalation from TEM and SAXS analysis. It shows better dispersion than PS, PVPh10 and PVPh20. The results show that the dispersion of the PVPh nanocomposite is between that observed in the PVPh20 and PVPh30 nanocomposites. The analysis of IR spectrum shows that the extent of inter-molecular hydrogen bonding in this nanocomposite is less

74

than that of the PVPh40 and PVPh50 nanocomposites. The intra-molecular association among the polymer chains is found to increase in this sample, presumably hindering intermolecular hydrogen bonding and results in an intercalated morphology.

3.2.4   Thermal behavior of Nanocomposites

The impact of the extent of intermolecular interaction and morphology on the thermal properties of the nanocomposites is also studied. Determination of glass transition temperature was carried out for the nanocomposites. The glass transition temperature is the temperature where the polymer changes from a hard, glassy state to a rubbery state. This transition is marked by increase in the segmental motion of the polymer chains. It is known that the segmental mobility of the polymer chains is affected by the presence of a filler in the matrix. For instance, the relaxation dynamics of a polymer chain in clay nanocomposites is dependent on the size scale of the clay, its morphology and the dispersion in the matrix. [100] Local and global conformation of polymer chains within host galleries are expected to be different from those observed in the bulk not only due to the confinement of the polymer chains but also due to polymer-surface interactions not observed in the bulk.[101] Polymer-surface interactions play a dominant role in determining the relaxation dynamics of the polymer chains thus affecting the glass transition temperature. Table 3.6 shows the change in the glass transition temperature as determined by DSC for the various nanocomposites. The nanocomposites show excellent correlation between the increase in glass transition temperature of the nanocomposite and the degree of exfoliation in the nanocomposites. An increase in the hydroxyl content of the copolymer from 0-50% results in an increase in the glass transition temperature relative to that of the neat polymers. However, for the

Table 3.6 Change in Glass transition temperature of nanocomposites

Nanocomposite	T_g (copolymer)	Increase in T_g	Structure
PS	107° C	3 ° C	Poor dispersion
PVPh10	111° C	3 ° C	Poor dispersion
PVPh 20	114° C	7°C	Little exfoliation
PVPh30	125° C	9° C	Mixed structure (Intercalated and exfoliated)
PVPh40	122° C	16° C	Mostly exfoliated
PVPh50	127° C	18° C	Completely exfoliated
Poly(vinyl phenol)	145° C	8° C	Intercalated

PVPh nanocomposite, the increase in T_g was less than that of PVPh30 and more than the PVPh20 nanocomposite. This correlates well to the morphology which indicate that PVPh is intercalated while PVPh30 nanocomposite is mostly exfoliated with some intercalated regions temperature. These results suggest that the degree of exfoliation in the nanocomposite affects the thermal behavior to large extent. For the PS and PVPh10 nanocomposites, poorly dispersed morphology results in a slight change in glass transition temperature, an increase of 3 °C. As the vinyl phenol content increases to 20 %, ΔT_g increases to 7 °C, where morphology studies suggest some exfoliated regions. Further increase in exfoliation, as in PVPh30 nanocomposite, increases the ΔT_g. A large increase in the glass transition temperature to 16 °C for the PVPh40 nanocomposite and 18 °C for the PVPh50 nanocomposite suggests that the exfoliated structure is required to provide significant improvement in the thermal properties of the polymer at these low

loadings of the clay. As the nanoscale dispersion of the clay increases in the polymer matrix, this leads to the potential interfacial interaction between the polymer and clay. This can result in lower segmental mobility of the polymer chains that interact with the stiff clay sheets, thus increasing the glass transition temperature.

3.3 Summary and Conclusion

The control of hydrogen bonding between clay and polymer provides a mechanism to tune the dispersion of nanoparticles in polymer matrix. In this chapter, the results that indicate that we have been able to optimize intermolecular hydrogen bonding between the polymer and clay are presented. Varying the copolymer composition from 0-50 % poly (vinyl phenol) increases the dispersion of the clay sheets in the polymer matrix which can be correlated to an increase in the extent of intermolecular hydrogen bonding between the clay and the polymer. This extent of inter-molecular hydrogen bonding is determined by FT-IR spectroscopy and provides a fundamental explanation for the observed morphologies. Nanocomposites containing 0-10 % poly (vinyl phenol) showed poor dispersion due to no or very little hydrogen bonding between the polymer and clay. Increase in the vinyl phenol content to 20 %, resulted in a decrease in the intensity of the clay peak in the SAXS curve suggesting some exfoliation which is also evident in the thermal properties which show an increase in the glass transition temperature of 7 °C over that of the neat polymer. Nanocomposites containing 50 % poly(vinyl phenol) and 40 %poly (vinyl phenol) showed very high exfoliation as evident by SAXS and TEM. The thermal properties of these nanocomposites were also enhanced showing an 18 °C and 16 °C rise in the glass transition temperature relative to that of the neat polymer. The

extent of intermolecular hydrogen bonding in these nanocomposites was also the largest of all studied.

However, as the vinyl phenol content increases to 100 %, the dispersion of the clay sheets in the polymer matrix is significantly reduced resulting in an intercalated morphology due to lower inter-molecular hydrogen bonding. These polymer chains preferably engage in intra-molecular hydrogen bonding as shown by semi-quantitative analysis of the IR spectrum. This also results in only a modest increase in the Tg of the nanocomposite over that of the copolymer ($\Delta T_g = 8$ °C).

Clearly, there exists a correlation between the extent of intermolecular hydrogen bonding between the clay and polymer matrix and the morphology and the thermal properties of the resulting nanocomposite. Moreover, it appears that the extent of intermolecular interaction between the polymer and clay can be controlled by copolymer composition and thus these results provide guidelines by which the dispersion and properties of polymer clay nanocomposites can be controlled.

CHAPTER 4 EFFECT OF CLAY SURFACTANT ON ABILITY TO FORM INTERMOLECULAR INTERACTIONS IN POLYMER/CLAY NANOCOMPOSITES

4.1   Introduction

In this chapter, the importance of surfactant structure on the formation of intermolecular interactions between clay and polymer, and the impact of these interactions on the dispersion of polymer/clay nanocomposites will be evaluated. Chapter 3 documents how the extent of hydrogen bonding between the polymer and clay impacts the dispersion of clay platelets in a polymer matrix, where the extent of the interaction was varied by controlling the amount of hydroxyl groups in the polymer matrix. The role of the surfactant on this process will be further clarified by completely similar studies with clays that contain various surfactants.

Clays selected for the study (Table 4.1) are organically modified montmorillonites (Nanomer I.24 TL and Cloisite 25A) and pristine montmorillonite (Cloisite Na$^+$). Cloisite Na$^+$ is pristine clay which does not contain any organic modifier and is highly hydrophilic due to the charged surface of clay. On the other hand, Nanomer I.24 TL and Cloisite 25A are organophilic in nature which is attributable to the presence of long chain organic surfactants. The organophilic clay, Nanomer I.24 TL, has been modified by 12-aminododecanoic acid, a long chain surfactant with a polar functional group, –COOH, which has the capability to undergo hydrogen bonding with hydroxyl groups, whereas the Cloisite 25A does not contain any polar functionality in its organic modifier. The importance of the presence of the functional group in Nanomer I.24 TL on the extent of

Table 4.1 Surfactants of the Clays examined

Clays	Surfactants
Nanomer I.24 TL	12-amino dodecanoicacid
Cloisite 25A	dimethyl, dehydrogenated tallow, 2-ethylhexyl quaternary ammonium $$CH_3 - \overset{\overset{\displaystyle CH_3}{\displaystyle |}}{\underset{\underset{\displaystyle HT}{\displaystyle |}}{N^+}} - CH_2CHCH_2CH_2CH_2CH_3 \quad \overset{\displaystyle CH_2}{\underset{\displaystyle CH_3}{}}$$
Cloisite Na$^+$	Na$^+$

hydrogen bonding between the polymer and clay can provide insight into the fundamental processes that govern the formation of polymer clay nanocomposite. Montmorillonite clay itself has the ability to form hydrogen bonds with polar functionalities of a polymer due to the presence of oxide ions on the silicate surface and hydroxyl groups present in the interlayers. This affects the ability of the clay to be dispersed as opposed to the one having a completely non-polar surfactant in the clay. Therefore, all three clays are capable of forming hydrogen bonds with the polymer, regardless of the structure of the surfactant.

Random copolymers of styrene and vinyl phenol with varying amount of hydrogen bonding monomer, 4-vinyl phenol, have been synthesized to prepare the nanocomposites. The clay loading was kept constant at 5 wt % and nanocomposites were

prepared by dissolving the copolymer and clay in tetrahydrofuran (THF) followed by precipitation in a non-solvent.

Intermolecular interactions between the polymer and clay in the nanocomposites were investigated by FT-IR spectroscopy. The understanding of these molecular level interactions will provide insight into the thermodynamic stability of the nanocomposites. The morphology of the composites and the dispersion of the clay are studied using small angle x-ray scattering (SAXS) and transmission electron microscopy (TEM). Thermal behavior is investigated by differential scanning calorimetry (DSC).

4.2 Results and Discussion

4.2.1 Morphological studies

Small angle x-ray scattering (SAXS) and transmission electron microscopy (TEM) were used to determine the morphology of the resultant nanocomposites. Figure 4.1 shows the small angle x-ray scattering curves of the pristine clay and the clays containing different surfactants. The peak in the SAXS curve can be utilized to determine the d-spacing of the clays as:

$$d = 2\pi/q$$

where q (scattering vector) is the position of the peak in the scattering curve and d represents the d-spacing of the clay.

Clay sheets are crystalline in nature and have a stacking order. Thus, they exhibit a characteristic peak in the SAXS pattern at a q that corresponds to the Van der Waal spacing (d-spacing). Therefore the changes in the SAXS pattern can be monitored to
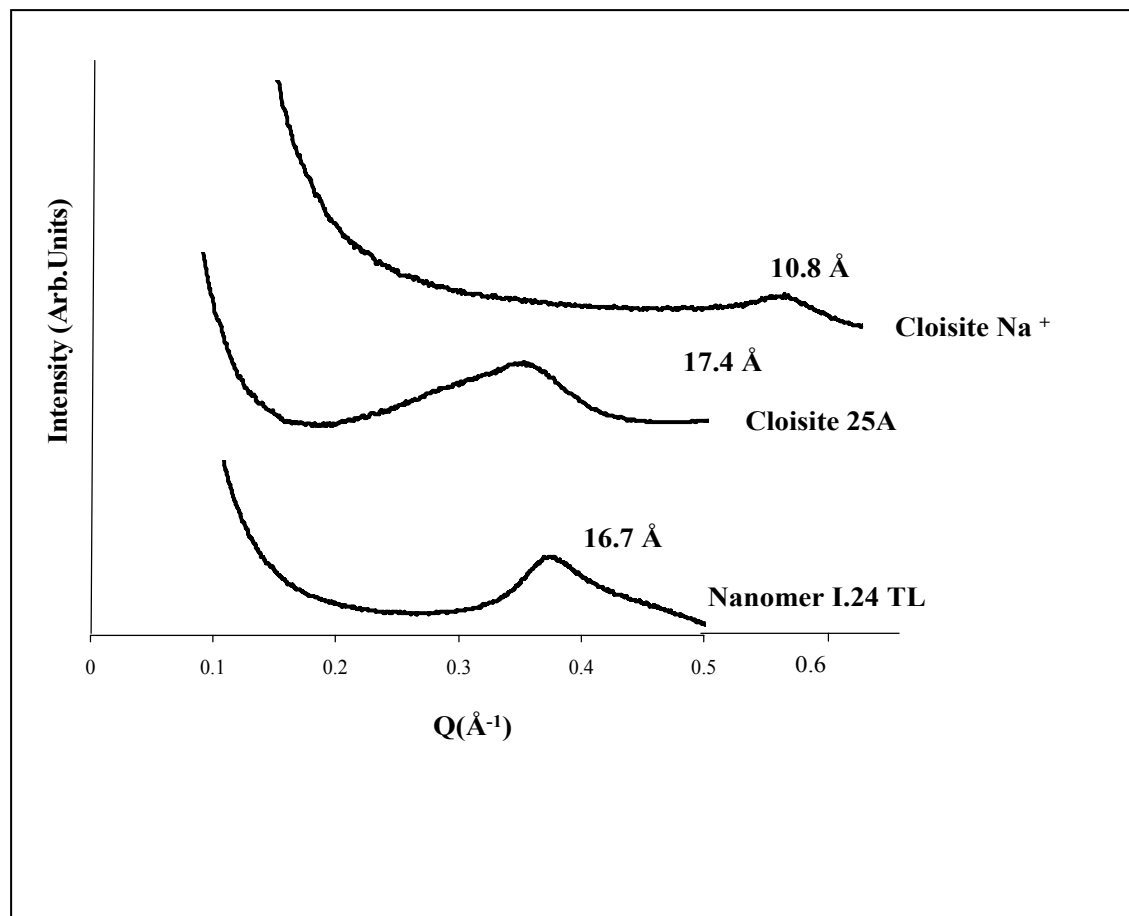
Figure 4.1 SAXS curves for Different clays

discern changes in the clay stacking or it's d-spacing. This d-spacing is affected by the permeation of polymer chains in the clay galleries. If there is no discernible change in the d-spacing as exhibited in the SAXS pattern, a traditional composite with chemically distinct phases (polymer and clay) has been formed. However, a shift towards a higher d-spacing reflects the formation of an intercalated nanocomposite and the complete loss of a characteristic peak is indicative of an exfoliated morphology, which should also be verified using transmission electron microscopy.

Small angle x-ray scattering results for the Clays

Pristine clay (sodium montmorillonite) is highly hydrophilic due to its charged surface. It has only sodium ions in its gallery which leads to a peak at a very narrow d-spacing of 10.8 Å. The other clays have been modified by long chain organic surfactants whose presence tends to push the clay sheets apart leading to an increase in the d-spacing. A higher d-spacing of the clay plays a vital role in facilitating polymer permeation and, thus, the presence of organic surfactant enhances the compatibility between the polymer and the clay.

Nanomer I.24 TL modified by 12-amino dodecanoic acid has a d-spacing of 16.7 Å, whereas the d-spacing of Cloisite 25A was 17.4 Å. A higher d-spacing is expected for Cloisite 25A due to the presence of long chain surfactant (C-18), whereas carbon chain length is twelve in the Nanomer I.24 TL.

The dispersion of these three clays in a polymer matrix was investigated where Polystyrene (0% vinyl phenol), PVPh10 (10% vinyl phenol), PVPh20, PVPh30, PVPh40, PVPh50 and PVPh (100%) were used as polymer matrices. The molecular weights,

polydispersity indices and actual mole percentage of 4-vinyl phenol present in these copolymers are tabulated in chapter 2.

Small Angle X-ray Scattering Results of the nanocomposites

Figure 4.2 illustrates the SAXS curves for Nanocomposites containing the Nanomer I.24 TL. Nanomer I.24 TL shows a characteristic peak at the q value of 0.376 Å^{-1} on forming a composite with polystyrene, PS, which is indicative of very little dispersion of the clay in the polymer matrix. The observation that the clay sheets retain their stacked structure with a similar d-spacing implies that a poor dispersion of clay sheets in the polymer matrix is realized. Similarly, PS/Cloisite 25A and PS/Cloisite Na$^+$ composites also exhibit peaks that correspond to the d-spacing of the respective clays, indicating that the disruption of stacked clay structure has not taken place (refer Figures 4.3 and 4.4).

TEM images as demonstrated in Figure 4.5 also corroborate the presence of clay tactoids for all polystyrene nanocomposites. It is known that mixing clay with a polymer is entropically unfavorable as the polymer chains cannot adopt as many conformations in the confined state as in bulk. To facilitate mixing, favorable energetics is required between the polymer and the clay. In the absence of these favorable energetic interactions, polymer chains are restricted from entering the clay galleries as it would result in the loss of entropy and therefore poor dispersion is obtained.

On increasing the mole percent of vinyl phenol to 10 % in the copolymer, Nanomer I.24 TL and Cloisite 25A composites (SAXS Figures 4.2 and 4.3) displayed essentially the same results where the d-spacing is in the same region as the neat clay
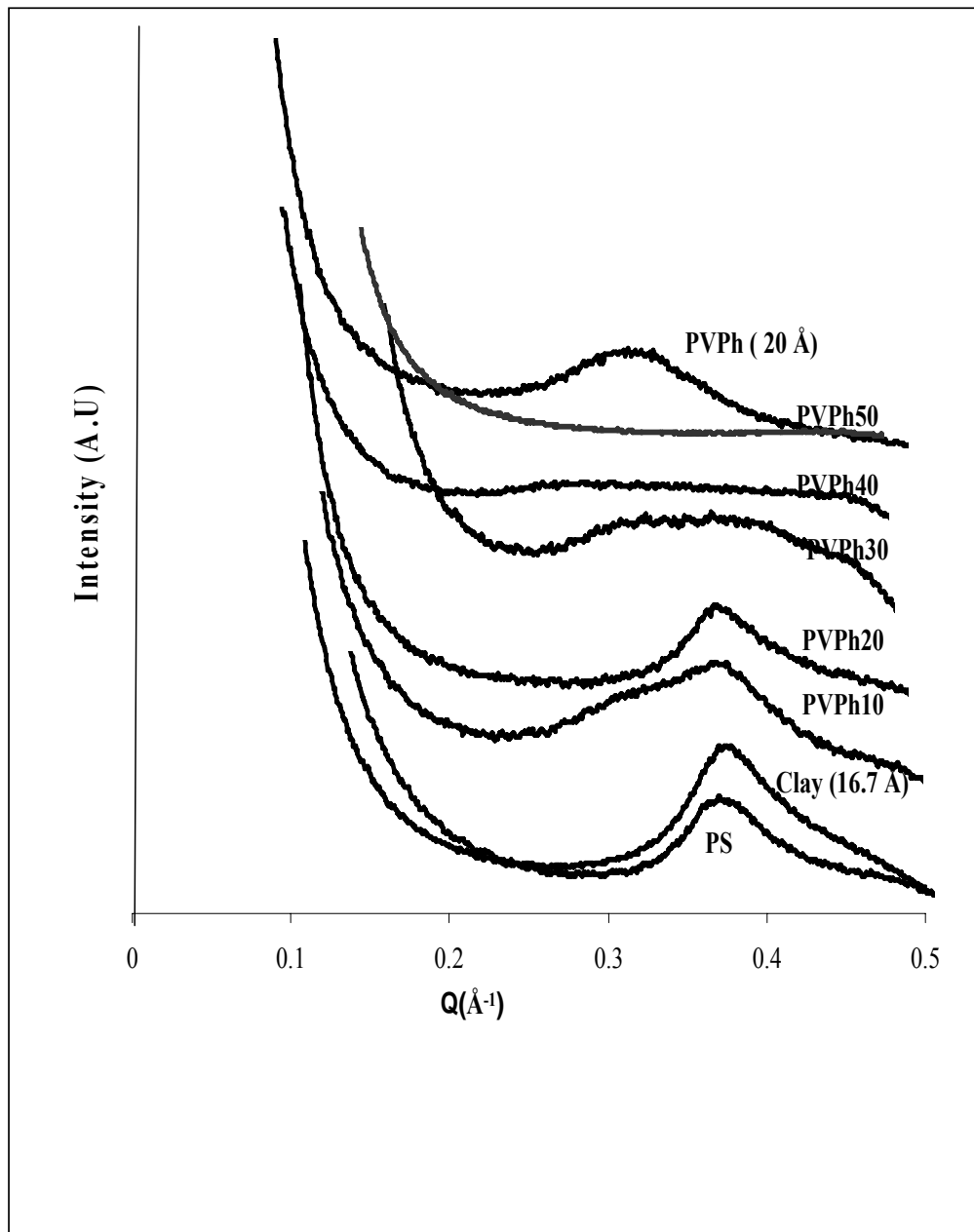
Figure 4.2 SAXS curves for Nanomer I.24 TL/ PVPh Nanocomposites
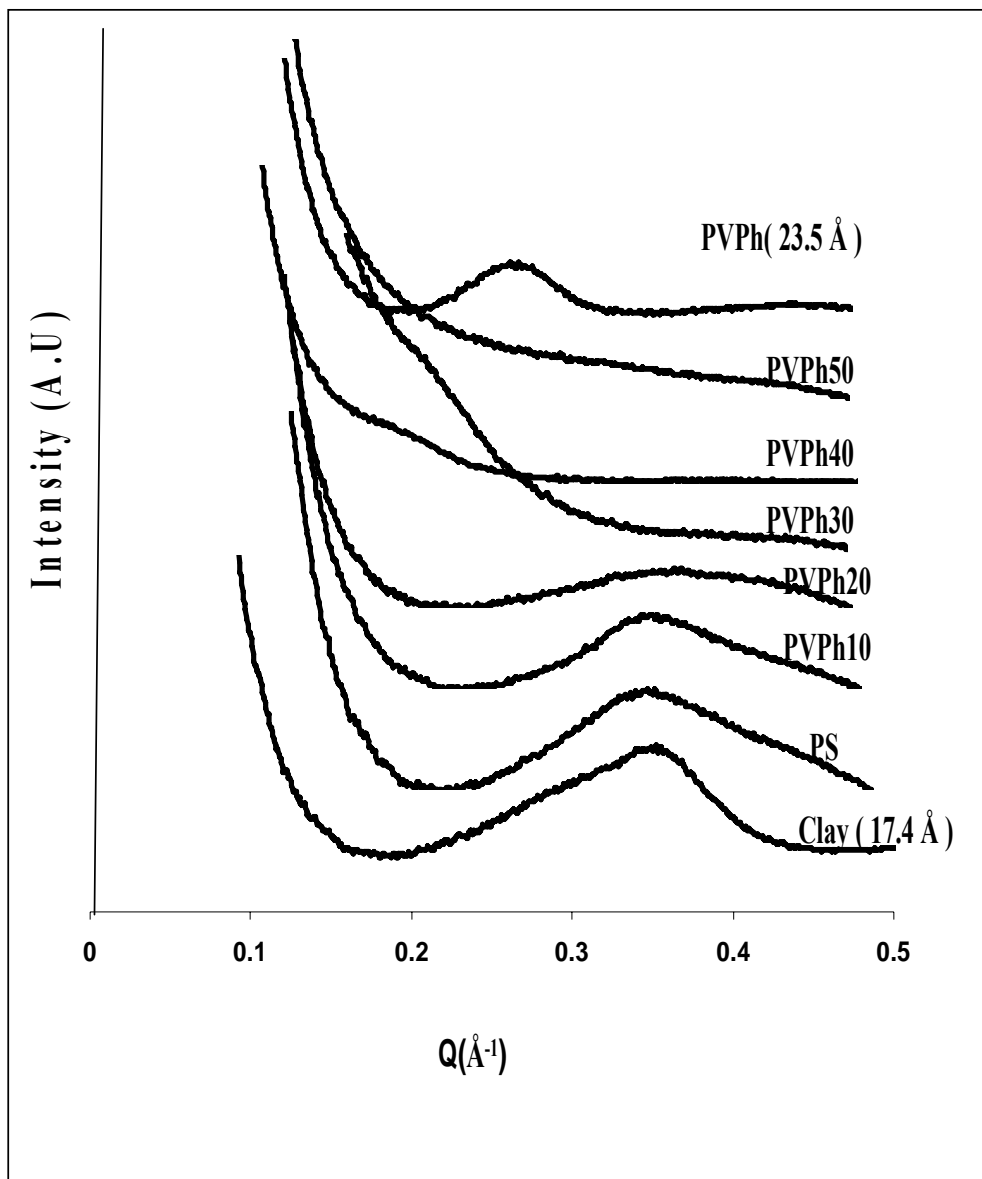
Figure 4.3 SAXS curves for Cloisite 25A / PVPh Nanocomposites
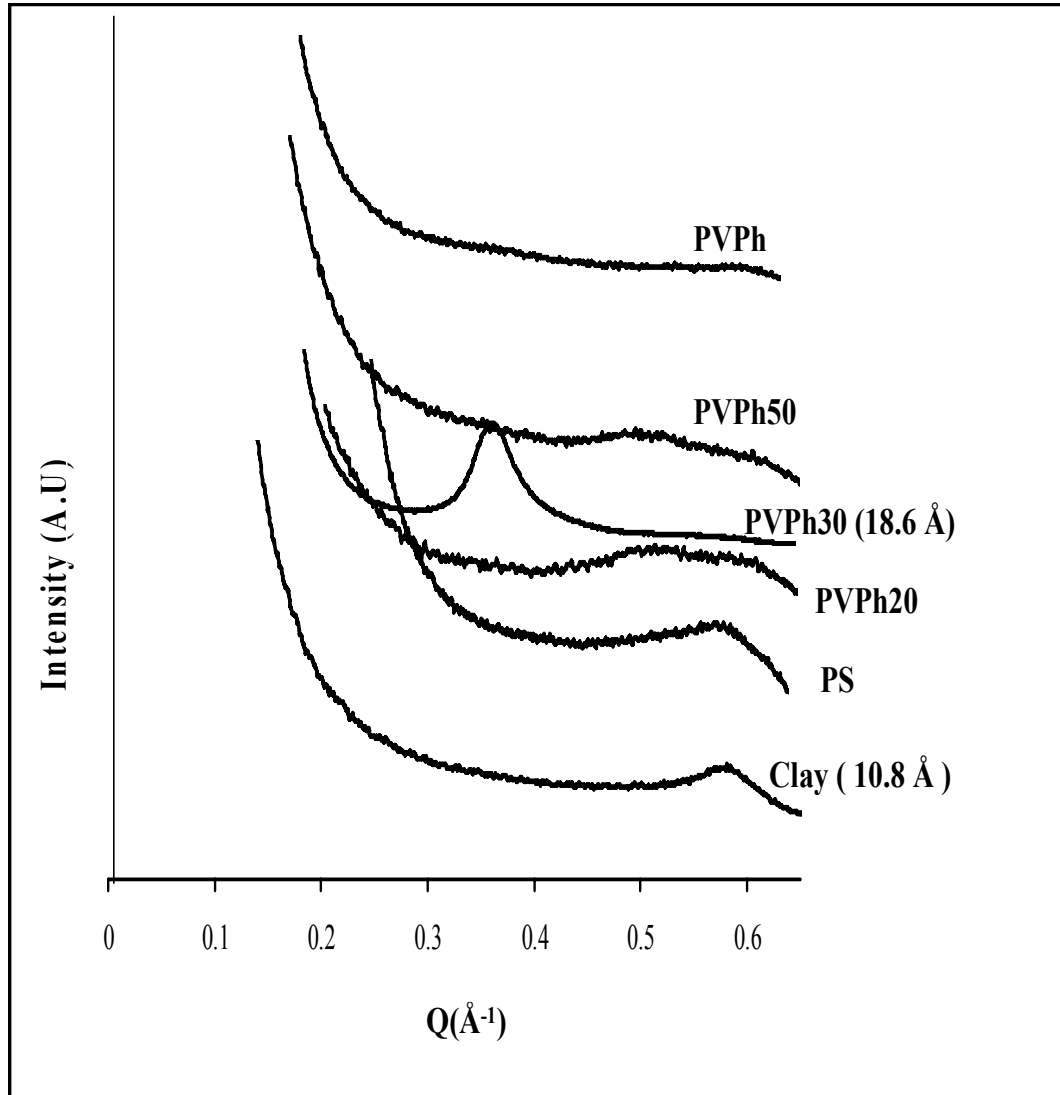
Figure 4.4 SAXS curves for Cloisite Na+/ PVPh Nanocomposites

Nanomer I.24 TL

Cloisite 25A

Cloisite Na$^+$
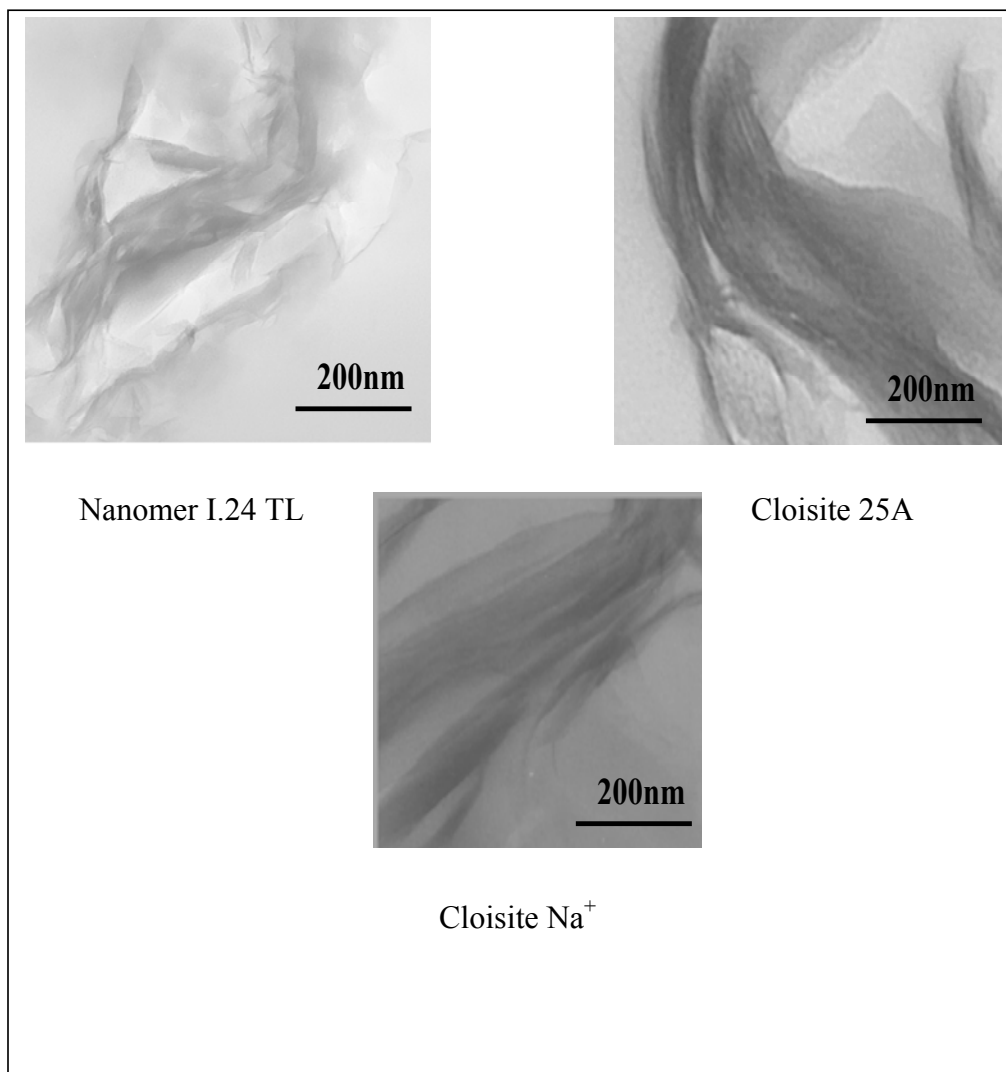
Figure 4.5 TEM Micrographs of Polystyrene nanocomposites containing different clays

with no decrease in the peak intensity, indicating no improvement in the dispersion. This is not surprising as the PVPh10 copolymer has fewer –OH groups that can engage in inter-molecular hydrogen bonding, thus poor dispersion of the clay results. SAXS curves in Figures 4.2, 4.3 and 4.4 for PVPh20 nanocomposites show a slight decrease in the intensity of the peaks in for all the clays, indicating the presence of fewer clay aggregates than in PS and PVPh10 composites. However, as the mole percentage of vinyl phenol is increased in the copolymer to 30%, the Nanomer I.24 TL nanocomposites shows a system with both intercalated and exfoliated structures, as revealed by a broad peak in the SAXS curve in the region of clay d-spacing (Figure 4.2). This improved dispersion is verified by TEM micrographs, depicted in Figure 4.6, where both individually dispersed and stacked clay sheets were observed. For the Cloisite 25A nanocomposite, intercalation was observed as elucidated by a shoulder in the SAXS curve of this nanocomposite at q, 0.245 Å^{-1}, which corresponds to a d-spacing of 25.6 Å.

The peak has been shifted in the nanocomposite from the original d-spacing of 17.4 Å exhibited by Cloisite 25A. Additional support for the intercalated structure is observed through TEM (Figure 4.6) where the Cloisite 25A/PVPh30 nanocomposite shows an intercalated morphology with well-ordered but separated clay sheets present in the polymer matrix. Similarly, in the Cloisite Na^{+}/ PVPh30 nanocomposite, a peak shift is exhibited from the original d-spacing of 10.8 Å in the clay to 18.6 Å, as shown in Figure 4.4, which is indicative of an intercalated structure. This is further confirmed by the presence of swollen clay sheets in the polymer matrix as manifested by TEM in Figure 4.6. The increase in the amount of polar hydroxyl groups in PVPh30 is expected to provide an increase in the intermolecular hydrogen bonding with the clay functionalities

Nanomer I.24 TL

Cloisite 25A

Cloisite Na⁺ Clay
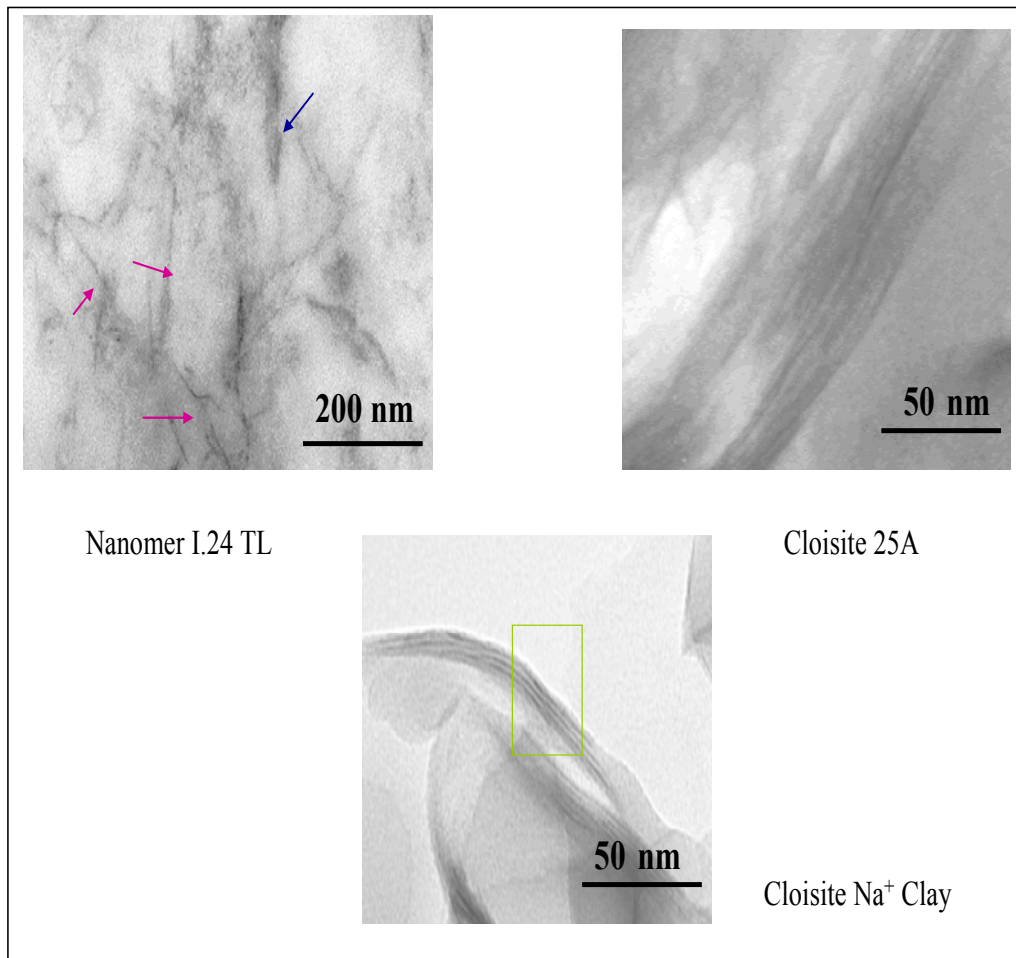
Figure 4.6 TEM Micrographs of PVPh30 nanocomposites containing different clays

(-COOH, -OH and oxide ions), which provides favorable enthalpic interactions for the permeation of polymer chains into the clay galleries.

The PVPh40 nanocomposite with Nanomer I.24 TL shows no peak at q = 0.376 Å^{-1} in the Figure 4.2. But a small shoulder is observed for this nanocomposite at q = 0.26 Å^{-1}. This corresponds to a d spacing of 24 Å. According to the spectra, some intercalation has taken place but mostly the nanocomposite should be exfoliated. Similarly, the cloisite 25A nanocomposite with PVPh40 shows a mostly exfoliated structure as evident by the presence of a small shoulder at q = 0.195 Å^{-1} (d-spacing = 32.2 Å) on the SAXS curve (Figure 4.3). On increasing the percentage of vinyl phenol repeat units in the copolymer to 50% in the Nanomer I.24 TL nanocomposites, a complete disappearance of the peak in SAXS curves is observed. This absence of a peak indicates a complete loss of registry between the clay layers, and thus, the silicate sheets are homogeneously and individually dispersed in the polymer matrix. TEM in Figure 4.7 further verifies this morphology for the PVPh50 nanocomposites. Nanomer I.24 TL nanocomposite shows complete exfoliation. The spacing between the clay sheets as observed in TEM is greater than 100 Å and the clay sheets can be considered exfoliated at this separation. The Cloisite 25A/PVPh50 nanocomposite also did not show a distinguishable peak in the region of the clay d-spacing, indicative of uniform dispersion of clay sheets. The PVPh50/Cloisite Na^+, however, shows a small broadened peak centered at q = 0.468 Å^{-1} corresponding to a d-spacing of 13.3 Å. Since the pure cloisite Na^+ has a d-spacing of 10.8 Å, this small shift in the nanocomposite suggests that an intercalated morphology has been attained here. Also, the intensity of this peak is small
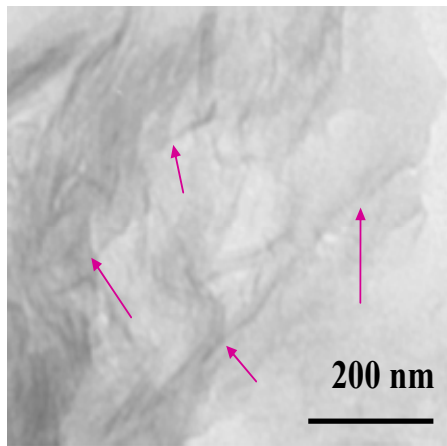
Nanomer I.24 TL
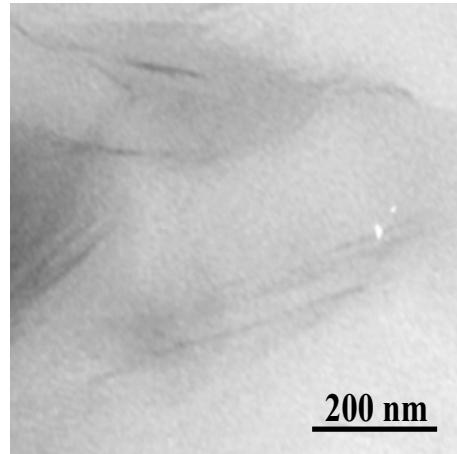
Cloisite 25A
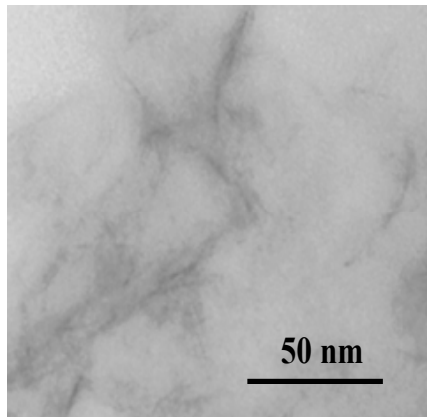
Cloisite Na⁺

Figure 4.7 TEM Micrographs of PVPh50 nanocomposites containing different clays.

relative to the strong peak observed for PVPh30 / Cloisite Na$^+$ nanocomposite, which implies that there exist some exfoliated regions of clay in the polymer matrix. The improved dispersion in the PVPh40 and PVPh50 nanocomposites may be attributed to the enthalpic gain provided by efficient intermolecular hydrogen bonding in these nanocomposites.

When 100% poly(vinyl phenol) (PVPh) was utilized with Nanomer I.24 TL to prepare the nanocomposite, a shift in the SAXS peak to indicate a d-spacing of 20 Å (Figure 4.2) was observed relative to 16.7 Å was found for this pure clay. The Cloisite 25A clay has a d-spacing of 17.4 Å and its nanocomposite with PVPh exhibits a peak in the SAXS curve that indicates a d-spacing of 23 Å (Figure 4.3). On switching the clay to form a Cloisite Na$^+$/ PVPh nanocomposite (Figure 4.4), the peak in the SAXS curve completely disappears suggesting an exfoliation of these nanocomposites. The PVPh is highly hydrophilic due to the presence of –OH groups on every repeat unit and it is not surprising that it very compatible with the hydrophilic clay(Cloisite Na$^+$) leading to a superior dispersion of the clay sheets in this polymer matrix. It is expected that the charged oxide ions present on the silicate surface can have favorable enthalpic interactions with the –OH groups of the polymer, thus promoting the inclusion of polymer chains in the clay galleries, which results in a thermodynamically stable nanocomposite. This can be further illustrated by TEM (Figure 4.8) where individually dispersed clay platelets are observed in the polymer matrix.

On the other hand, the surfactants in the Nanomer I.24 TL and Cloisite 25A clays have long non-polar alkyl chains do not appear to mix well with the hydrophilic polymer. Figure 4.8 corroborates these results, where TEM micrographs show clay platelets that

Nanomer I.24TL

Cloisite 25A

Cloisite Na$^+$
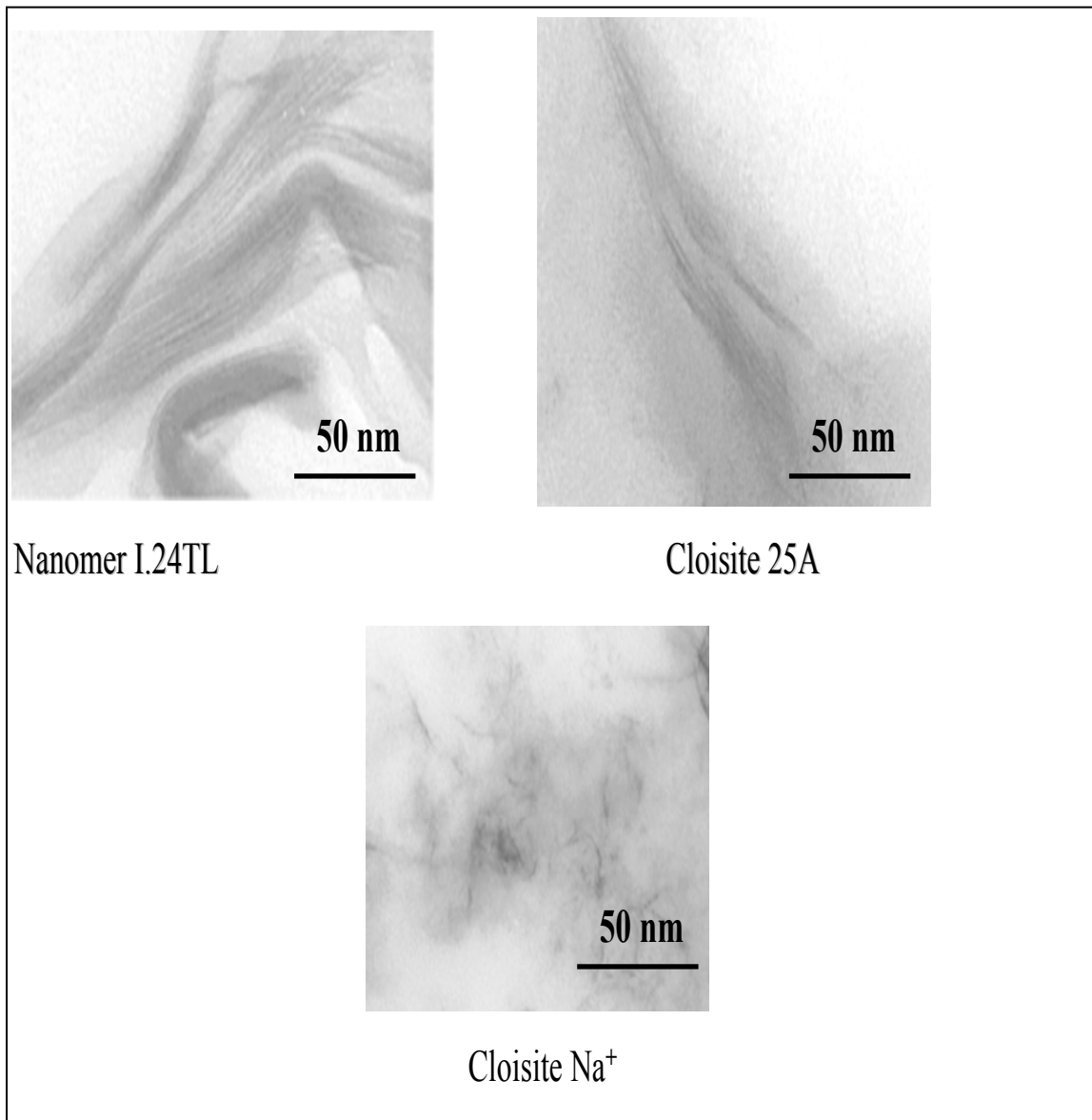
Figure 4.8 TEM Micrographs of PVPh nanocomposites containing different clay

are intercalated by the polymer in these nanocomposites. The results will be further examined by investigating the molecular interactions between clay and polymer by using FT-IR and examining the thermal properties of the nanocomposites with differential scanning calorimetry (DSC).

4.2.2   FT-IR studies of Intermolecular Interactions

The polymer and the clay have the ability to undergo hydrogen bonding when mixed with each other which plays a critical role in determining the dispersion of the clay sheets in the polymer matrix. The hydrogen bonding interaction is stronger than ordinary van der Waal interactions with the energy ranging from 2 to10 kcal/mol. Moreover, infra-red spectroscopy is a powerful tool to investigate hydrogen bonding interactions. In chapter three, the vibration of the carbonyl bond was examined to quantify the extent of hydrogen bonding interactions between the polymer and montmorillonite clay. The Nanomer I.24 TL utilized in that study has a carbonyl group which can act as either proton acceptor or proton donor. However, Nanomer I.24TL is the only clay with a carbonyl functional group in the surfactant, therefore the analysis of the carbonyl stretch can not be employed for a quantitative analysis of these clays. Therefore analysis of the hydroxyl stretching region (3100-3700 cm^{-1}) will thus be completed to provide information on the extent of hydrogen bonding in these nanocomposites.

It has already been mentioned in chapter 3 that the quantitative analysis of the hydroxyl region is difficult due to vibration overlap coming from the proximity of the CH_2 assymetric and symmetric vibrations and possible changes in the absorption coefficients of intra- and inter- associated hydroxyl groups.[94] Therefore, the –OH analysis

that will be utilized is only semi-quantitative in nature and can only be utilized in comparing the extent of interaction in these nanocomposites. Figures 4.9, 4.10 and 4.11 show the FT-IR spectra in the hydroxyl region of the nanocomposites formed using Nanomer I.24 TL clay, Cloisite 25A and Closite Na$^+$ respectively for the various copolymers which range from 0-100 % vinyl phenol. A sharp peak which is characteristic of the free hydroxyl groups is observed in the 3532-3545 cm^{-1} region while the broad hydrogen bonded peak in the 3380-3440 cm^{-1} region comprises the contribution both from intramolecular and intermolecularly associated –OH groups. To determine the contribution from the free, intra- and inter- associated –OH groups, the FT-IR data in the region 3100-3700 cm^{-1} was deconvoluted using Peakfit v.4.11 software. In all fitting procedures, a Gaussian band shape has been assumed. Figure 4.12 shows the representative example of the deconvolution for the poly(vinyl phenol) (PVPh)/Nanomer I.24 TL clay nanocomposite.

Intermolecular Interactions in Nanomer I.24 TL nanocomposites

During the deconvolution process, the position and width of the free and intra-molecularly hydrogen bonded -OH groups were fixed at those observed for the pure copolymer. The position and width of the inter-molecularly associated –OH groups were allowed to vary in the fitting process. The contributions from free (C_F/C_T), intra-(C_{AS}/C_T) and inter-molecularly associated –OH (C_I/C_T) to the IR curve were calculated using the method described in Chapter 3. Tables 4.2 and 4.3 summarize the results obtained from this analysis for the pure copolymers and the Nanomer I.24 TL nanocomposites. Figure 4.13 shows plots of C_F / C_T, C_{AS} /C_T and C_I/ C_T as a function of the copolymer
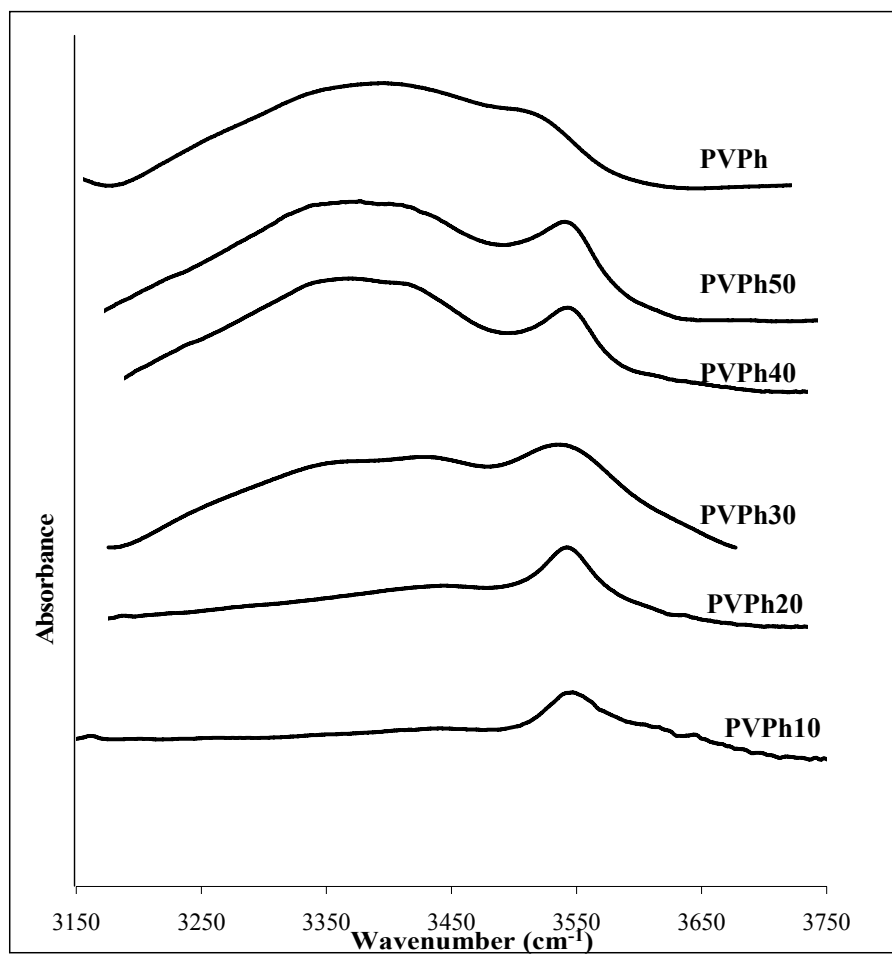
Figure 4.9 FT-IR Spectra of Nanomer I.24 TL/ PVPh Nanocomposites
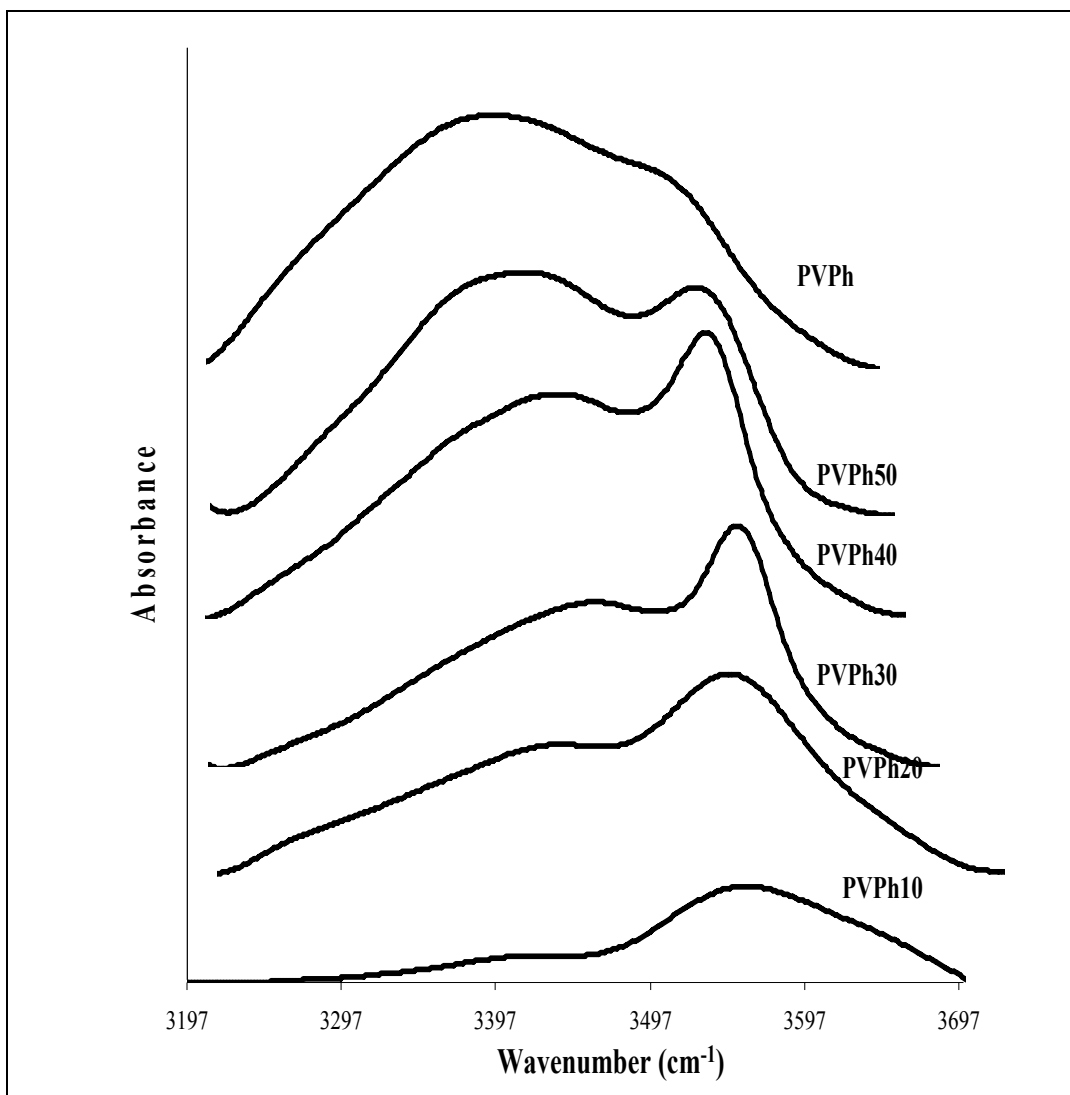
Figure 4.10 FT-IR spectra of Cloisite 25A/PVPh Nanocomposites
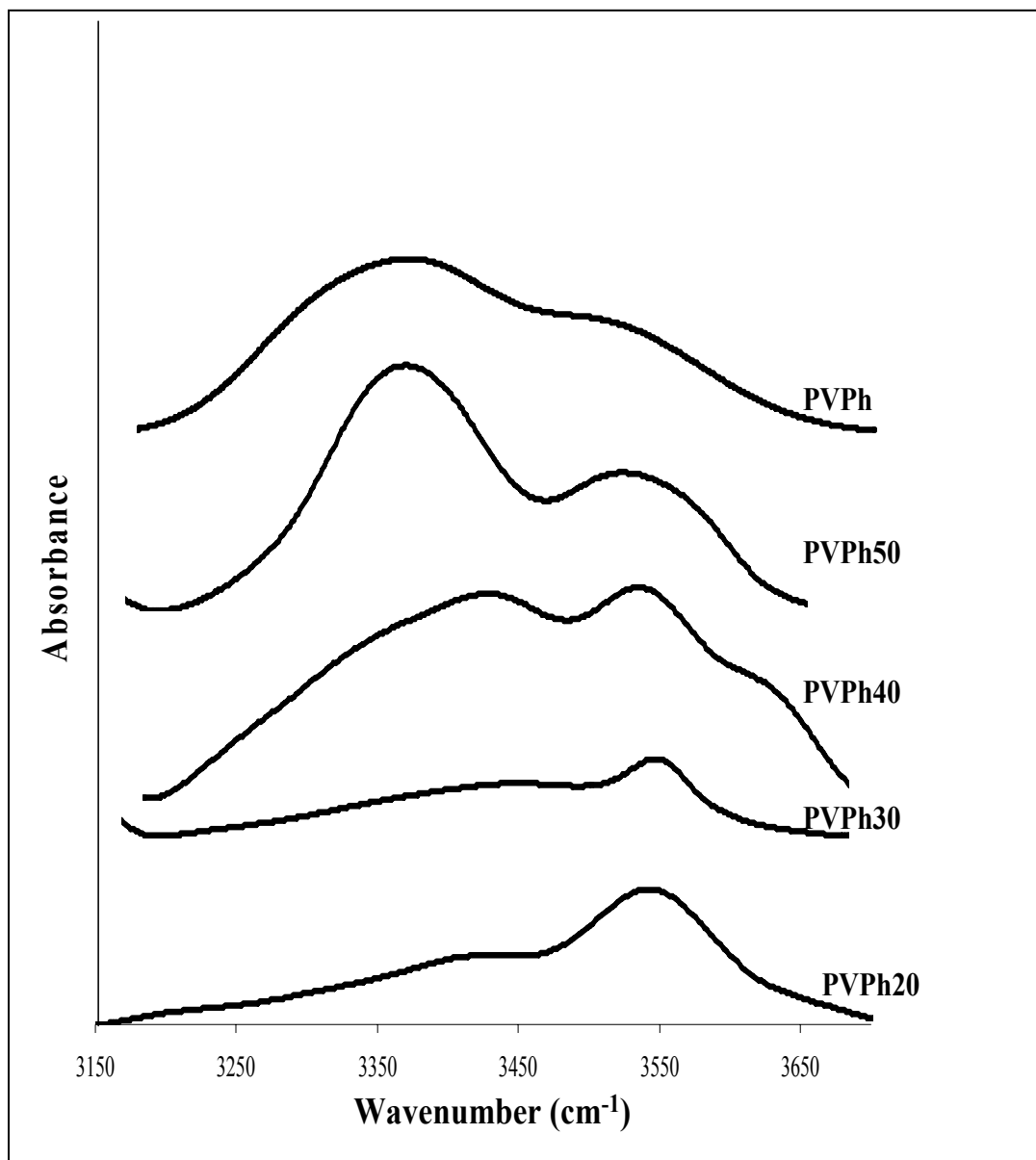
Figure 4.11 FT-IR Spectra of Cloisite Na+ / PVPh Nanocomposites
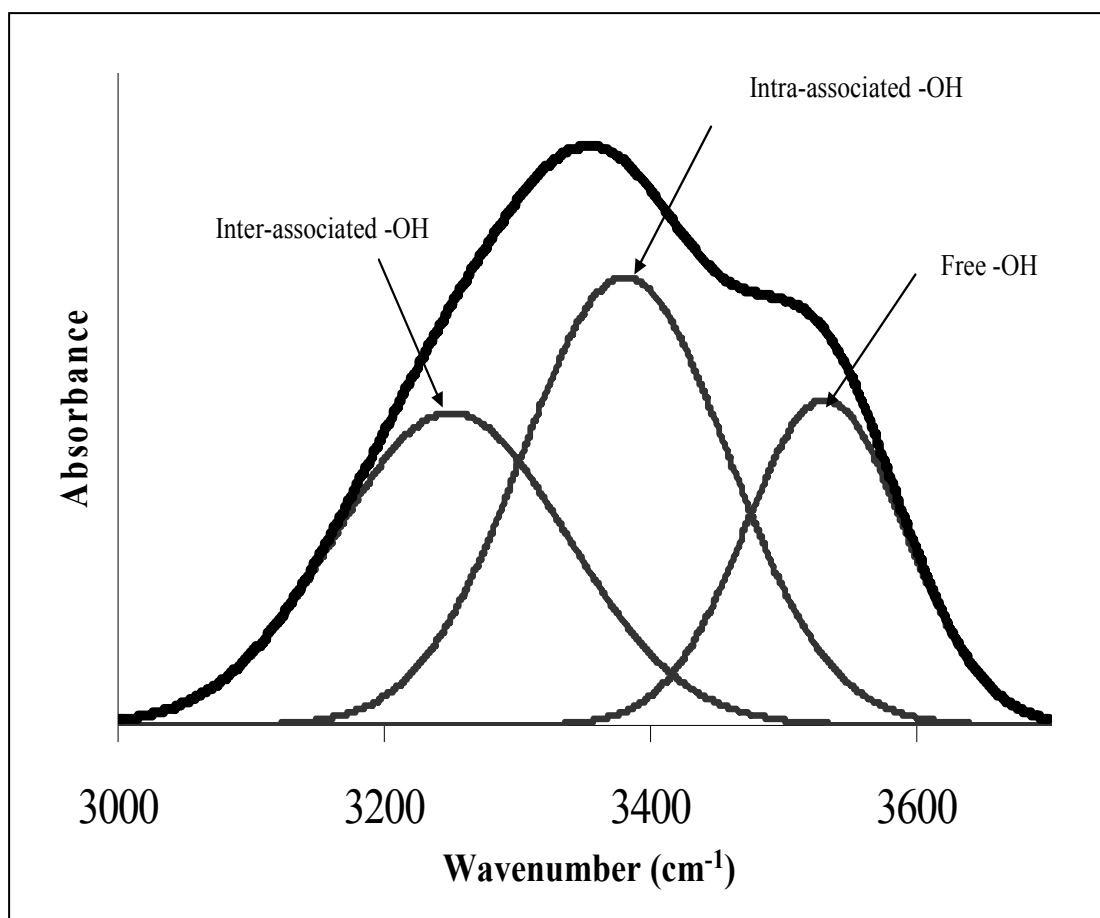
Figure 4.12 Deconvoluted IR spectra of PVPh/Nanomer I.24TL Nanocomposite

Table 4.2 Curve Fitting Results of Pure Copolymers

Copolymers	Free OH				Intra OH				$C_F/$ C_T	$C_{AS}/$ C_T
	υ (cm^{-1})	$W_{1/2}$	A_F (cm^{-1})	C_F	υ (cm^{-1})	$W_{1/2}$	A_{AS} (cm^{-1})	C_{AS}		
PVPh10	3545	65	61.9	1025	3444	150	38.1	339	0.75	0.25
PVPh20	3545	65	27	447	3417	260	73	1574	0.22	0.78
PVPh30	3543	65	16.7	276	3413	272	83.3	2755	0.09	0.91
PVPh40	3540	65	11.5	190	3398	279	88.5	3649	0.05	0.95
PVPh50	3539	64	11	182	3390	285	89	4613	0.04	0.96
PVPh	3532	65	7.7	127	3381	320	92.3	9872	0.01	0.99

Table 4.3 Curve Fitting results for Nanomer I.24TL/ PVPh Nanocomposites

Mol %	Free -OH				Intra-molecluarly H-bonded OH				Inter-molecluarly H-bonded OH				C_F/C_T	C_{AS}/C_T	C_I/C_T
	υ (cm^{-1})	$W_{1/2}$	A_F (cm^{-1})	C_F	υ (cm^{-1})	$W_{1/2}$	Aas (cm^{-1})	C_{AS}	υ (cm^{-1})	$W_{1/2}$	A_I (cm^{-1})	C_I			
10	3545	65	75.7	1123	3444	150	17	120	3390	100	7.34	52	0.87	0.09	0.04
20	3545	65	46.5	840	3417	260	30.8	621	3385	110	22.7	458	0.43	0.32	0.24
30	3543	65	24.7	526	3413	272	35.5	1109	3324	130	39.8	1244	0.18	0.39	0.43
40	3540	65	14.7	315	3398	279	33.7	1316	3341	137	51.6	2015	0.09	0.36	0.55
50	3539	64	14.3	344	3390	285	22	1081	3319	142	63.7	3130	0.08	0.24	0.69
100	3532	65	24	971	3381	320	42.9	6264	3237	126	33.5	2264	0.14	0.48	0.38
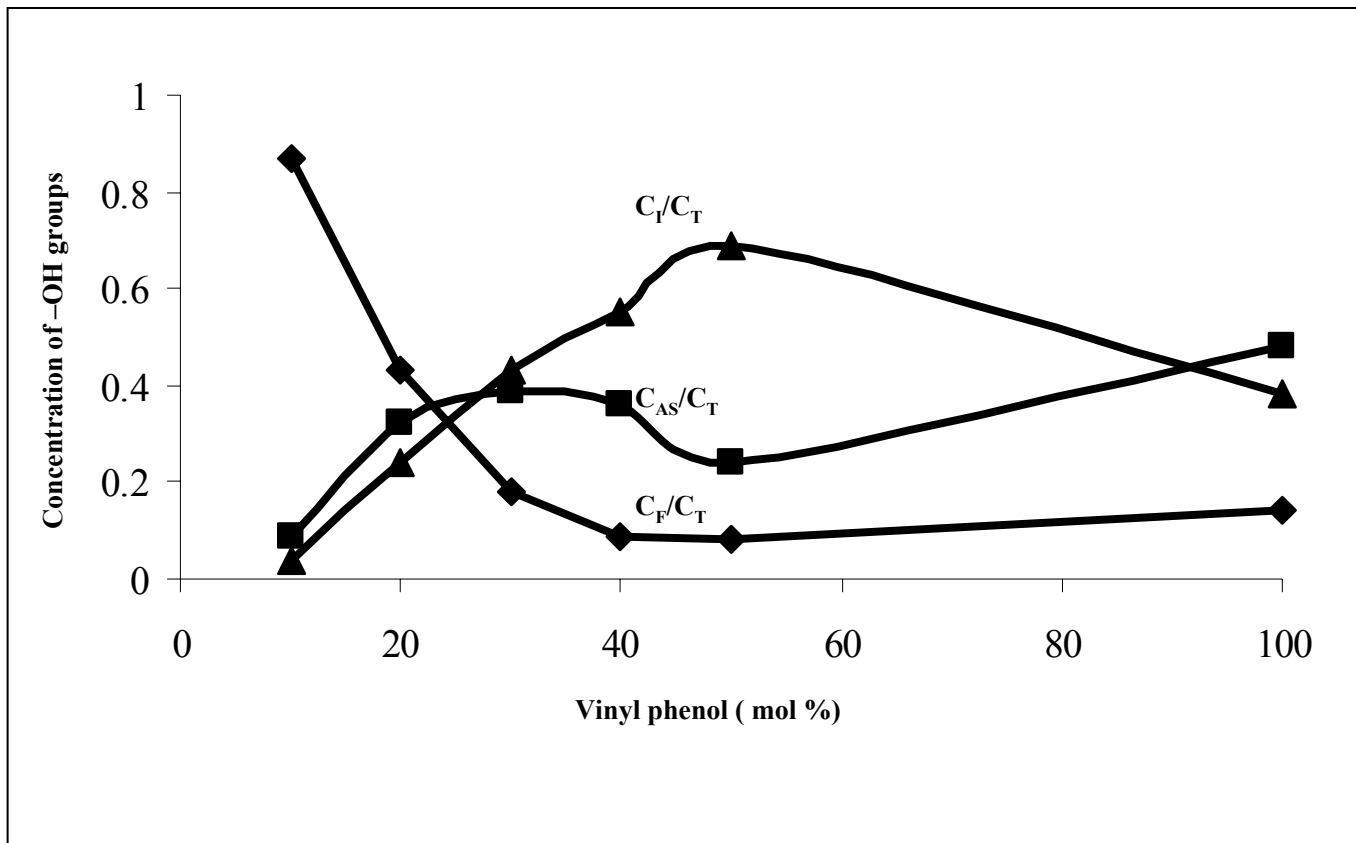
Figure 4.13 Plot of CF / CT, CAS / CT and CI / CT versus the mol% of vinyl phenol present in Nanomer I.24 TL nanocomposite.

composition in the nanocomposite. It shows that the extent of inter-molecular hydrogen bonding (C_I/C_T) increases on increasing the vinyl phenol content from 10 to 50%. A relatively low fraction of the hydroxyl groups are engaged in inter-molecular hydrogen bonding in the PVPh10 and PVPh20 nanocomposites with C_I/C_T values of 0.04 and 0.24 respectively. As the copolymer composition increases to 30% vinyl phenol, the contribution from –OH groups involved in intermolecular association, C_I/C_T, reaches 0.43. The PVPh50 nanocomposite shows an optimum extent of inter-molecular hydrogen bonding with the clay with C_I/C_T reaching its maximum at 0.69.

We have reported previously in Chapter 3 that the pure copolymers display greater extent of intra-molecular hydrogen bonding relative to the respective nanocomposites. As a representative example, the C_{AS} / C_T for the pure copolymers (PVPh40 and PVPh50) were 0.95 and 0.96 respectively. But these contributions decreased to 0.36 and 0.24 on forming nanocomposites. It was shown that the –OH groups are predominantly engaged in inter-molecular hydrogen bonding with the clay in the nanocomposite. Moreover, the intermolecular hydrogen bonding between the polymer and the clay was found to be stronger than the intra-hydrogen bonding between the polymer chains as exhibited by the shift of the broad hydrogen bonded peak towards lower wavenumber.

However, in the PVPh (100% vinyl phenol) nanocomposite, there is a dominating tendency to form intra-molecular hydrogen bonds among the polymer chains rather than form inter-molecular hydrogen bonding with the clay. Calculated fraction of intra-molecularly associated –OH increases from 0.24 in the PVPh50 nanocomposite to 0.48 in the PVPh nanocomposite. At the same time, the fraction of inter-molecular association

decreases from 0.69 in the PVPh50 nanocomposite to 0.38 in the PVPh nanocomposite. This can be understood by recalling the interpretation of the SAXS and TEM data, which discussed the unfavorable interaction between the non-polar surfactants present in the clay and the hydrophilic PVPh. As a result, these polymeric chains predominantly engage in intra-molecular association (OH…OH) which results in an intercalated morphology.

Analysis of the Infrared spectra of the Cloisite 25A Nanocomposites

The Cloisite clay and Nanomer I.24 TL have both oxide ions and hydroxyls which can engage in inter-molecular hydrogen bonding with the polymer. Moreover, the Cloisite 25A nanocomposites show similar morphologies as Nanomer I.24 TL nanocomposites. Thus an analysis of the IR spectrum of these nanocomposites can provide insight into the role of these moieties on the formation of hydrogen bonding and resultant morphology of these nanocomposites. Table 4.4 summarizes the analysis of the IR spectrum of the Cloisite 25A nanocomposites. Figure 4.14 shows the plot of C_F/C_T, C_{AS}/C_T and C_I/C_T as a function of copolymer composition in the Cloisite 25A nanocomposites. Increasing the % VPh in the copolymer from 10 to 50 % results in an increase in the fraction of hydroxyl groups involved in inter-molecular hydrogen bonding (C_I/C_T). The inter-molecular contribution to the IR curve increases from 0.02 in PVPh10 to 0.54 in PVPh50. There is a noticeable change in the calculated fraction of inter-molecularly hydrogen bonded –OH groups from PVPh10 to PVPh20, 0.02 to 0.28 which further increases until it reaches its maximum value at PVPh50, similar to the Nanomer I.24 TL nanocomposites.

Table 4.4 Curve Fitting results for Cloisite 25A/ PVPh Nanocomposites

Mol %	Free -OH				Intra-molecularly H-bonded OH				Inter-molecularly H-bonded OH						
	υ (cm^{-1})	$W_{1/2}$	A_F (cm^{-1})	C_F	υ (cm^{-1})	$W_{1/2}$	A_{as} (cm^{-1})	C_{AS}	υ (cm^{-1})	$W_{1/2}$	A_I (cm^{-1})	C_I	$C_F/$ C_T	$C_{AS}/$ C_T	$C_I/$ C_T
10	3545	65	89.4	1225	3444	150	6.3	45	3387	96	3.7	26	0.95	0.03	0.02
20	3545	65	59.1	1097	3417	260	13.8	279	3382	102	27	545	0.57	0.15	0.28
30	3543	65	40.0	973	3413	272	27.7	866	3330	126	33.3	1041	0.34	0.3	0.36
40	3540	65	28.2	569	3398	279	35.8	1398	3343	140	43	1679	0.16	0.38	0.46
50	3539	64	24.4	840	3390	285	26	1277	3319	150	49.6	2437	0.18	0.28	0.54
100	3532	65	23.2	1306	3381	320	49	5716	3237	126	27.7	2477	0.14	0.55	0.31

106
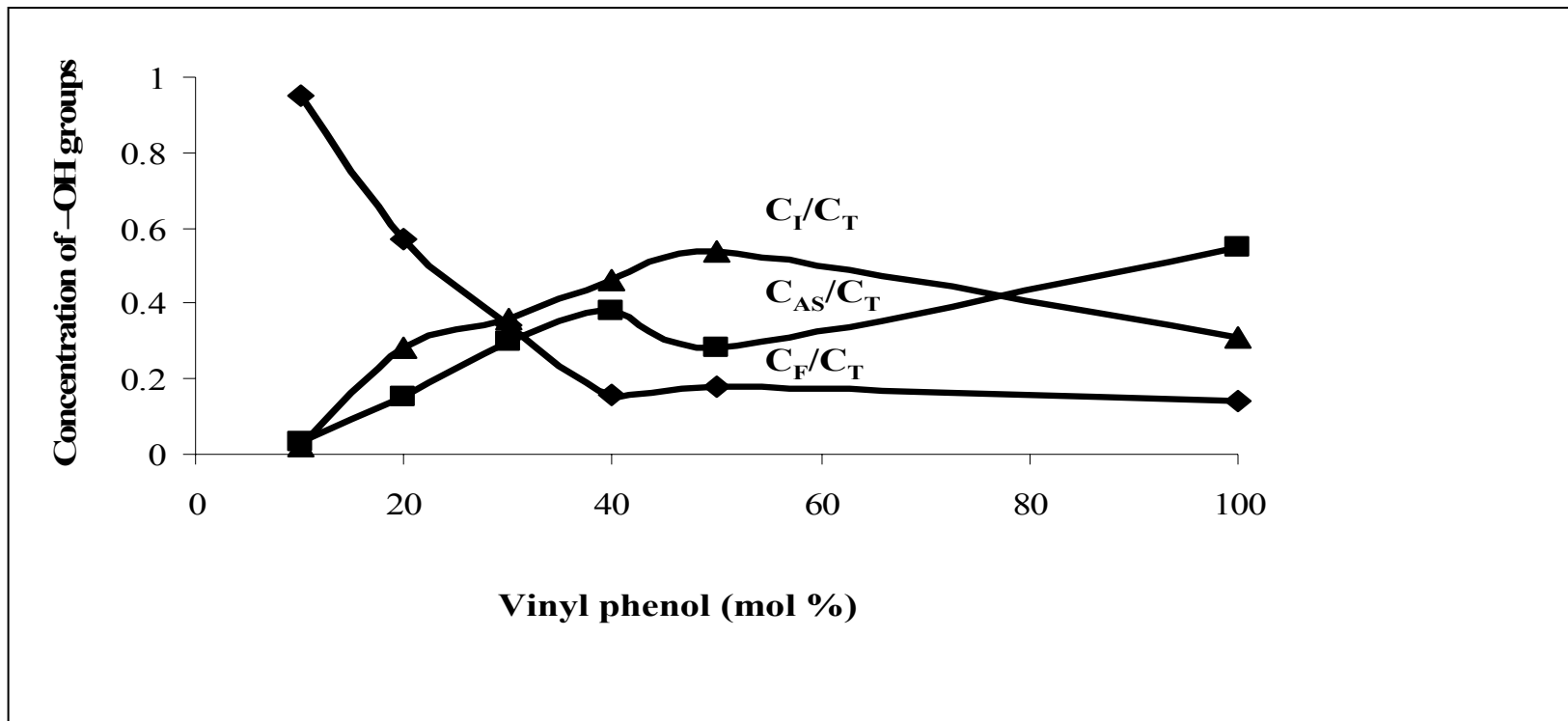
Figure 4.14 Plot of CF/CT, CAS/CT and CI/CT versus the mol% of vinyl phenol present in Cloisite 25A nanocomposite.

On increasing the vinyl phenol content to 100 % in the matrix, the contribution from inter-molecular association reduces to 0.31 and the fraction of intra-molecularly associated –OH increases to 0.55. Thus, as in the Nanomer I.24 TL nanocomposites, the hydroxyl groups in the PVPh are predominantly engaged in intra-molecular hydrogen bonding. As in Nanomer I.24 TL, the surfactant on the Cloisite 25A is non-polar, and thus does not mix well with the hydrophilic PVPh, mitigating the formation of inter-molecular hydrogen bonding between the polymer and clay. This correlates well with morphological behavior observed through SAXS and TEM where intercalated clay sheets were observed.

Infrared Analysis of Cloisite Na$^+$ nanocomposites

Table 4.5 lists the results of the analysis of the FTIR spectrum for the Cloisite Na$^+$ nanocomposites and Figure 4.15 show the fraction of free, inter-molecular, intra-molecularly associated –OH to the total –OH concentration as a function of the composition of the copolymer matrix. The results reveal that there exists significant improvement in the fraction of –OH involved in inter-molecular hydrogen bonding (C_I/C_T) as the vinyl phenol content in the copolymer is increased from PVPh20 (C_I/C_T = 0.15) to PVPh30 (C_I/C_T = 0.41) in the copolymers. On further increasing the vinyl phenol content of the copolymer to 50%, a maxima in the extent of inter-molecular hydrogen bonding (C_I/C_T = 0.54) is observed followed by a decrease to 0.38 in the PVPh nanocomposite. The intra-molecular hydrogen bonding between the polymer chains is also enhanced on increasing the mol % of vinyl phenol upto PVPh40 followed by a small

Table 4.5 Curve Fitting results for Cloisite Na+/ PVPh Nanocomposites

| Mol%	Free -OH				Intra-molecularly H-bonded OH				Inter-molecularly H-bonded OH						
	υ (cm^{-1})	$W_{1/2}$	A_F (cm^{-1})	C_F	υ (cm^{-1})	$W_{1/2}$	A_{as} (cm^{-1})	C_{AS}	υ (cm^{-1})	$W_{1/2}$	A_I (cm^{-1})	C_I	C_F / C_T	C_{AS} / C_T	C_I / C_T
20	3545	65	60.5	1015	3417	260	12.8	91	3389	106	26.6	189	0.78	0.07	0.15
30	3543	65	40	628	3413	272	25.1	506	3332	128	38.9	785	0.33	0.26	0.41
40	3540	65	17.8	310	3398	279	38.3	1197	3338	146	43.9	1372	0.1	0.42	0.48
50	3539	64	21.4	538	3390	285	29.6	1156	3320	150	50	1952	0.14	0.32	0.54
100	3532	65	44.8	133	3381	320	21.8	2152	3237	147	33.2	2270	0.37	0.25	0.38
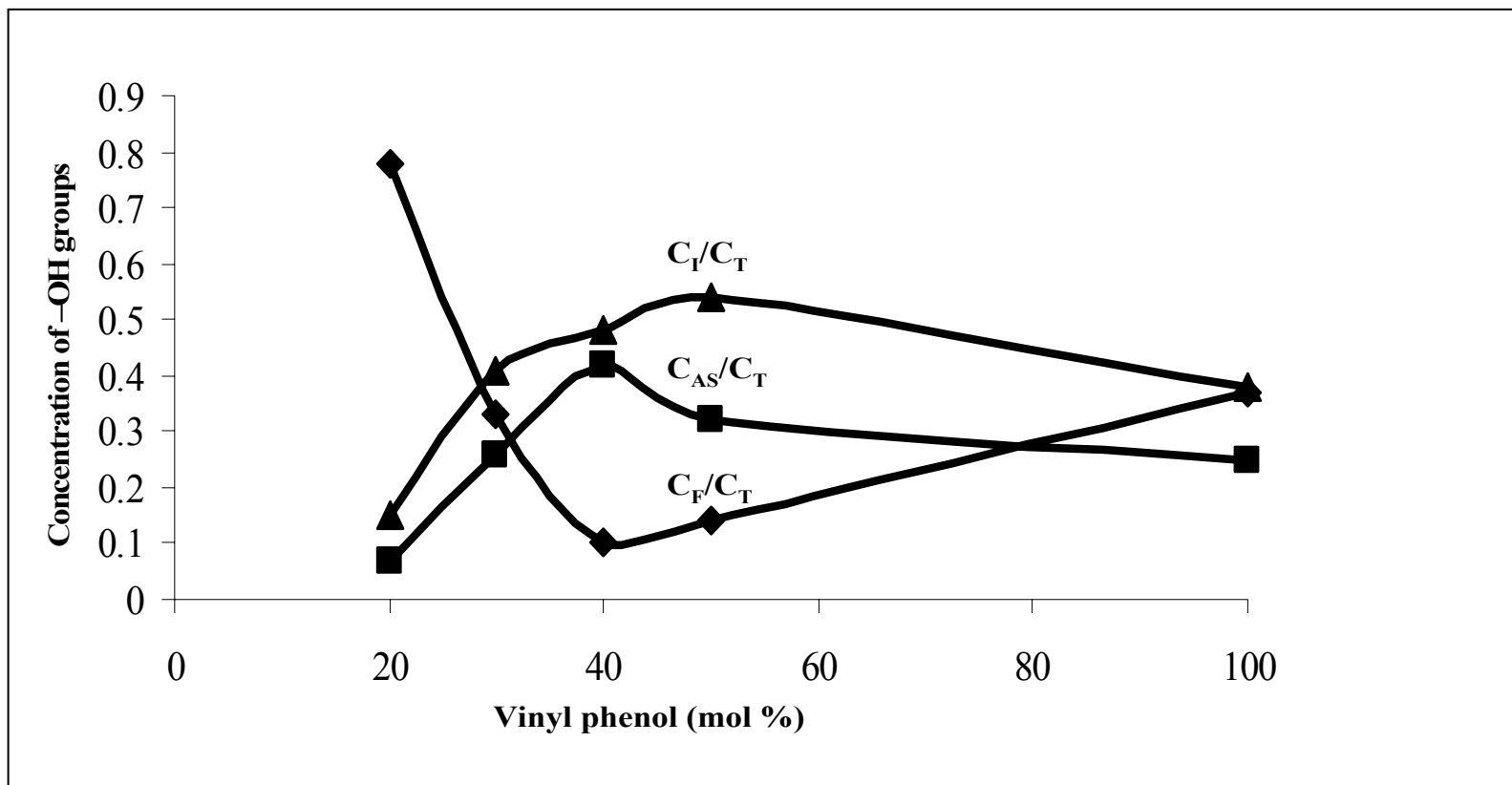
Figure 4.15 Plot of CF / CT, CAS/CT and CI/ CT versus the mol% of vinyl phenol present in Cloisite Na+ nanocomposite.

decrease at PVPh50, although the fraction of inter-molecularly associated –OH remains larger than the intra-molecularly associated –OH. The Cloisite Na$^+$/ PVPh nanocomposite displays a higher contribution from the inter-molecularly associated –OH (0.38) than the intra-molecularly associated –OH. This is interpreted to be a result of the fact that there is no organic surfactant in this clay and therefore it does not undergo repulsive interactions with the hydrophilic PVPh chains as they try to permeate inside the clay galleries. Additionally, the Cloisite Na$^+$ clay has oxide ions and hydroxyl groups which can form inter-molecular hydrogen bonding with the polar –OH groups of the PVPh chains resulting in enhanced dispersion.

4.2.3   *Correlating inter-molecular hydrogen bonding to the dispersion in Nanocomposites*

The analysis of the hydroxyl vibration in the IR spectrum indicates that the Closite 25A and Nanomer I.24 TL show similar trends in the extent of inter-molecular hydrogen bonding where the inter-molecular association between the polymer and the clay increases on increasing the vinyl phenol content in the copolymer from 10 to 50 %. These inter-molecular interactions correlate well with the increase in dispersion displayed by the nanocomposite where the Nanomer I.24 TL and Cloisite 25A nanocomposites show significant disruption of clay aggregates, resulting in homogeneous dispersion of clay platelets in the polymer matrix. When the % vinyl phenol in the copolymer increases from 10 to 50 %, an increase in the inter-molecular hydrogen bonding between the polymer and clay provides the required energetic gain to overcome the entropic loss which occurs as the polymer chains permeate inside the clay gallery.

When the vinyl phenol content in the copolymer increases to 100% in the nanocomposites, C_I / C_T (fraction of inter-associated –OH) is 0.38 and 0.31 in the Nanomer I.24 TL and Cloisite 25A nanocomposites, respectively. The contribution from intra-molecular hydrogen bonding is higher than the intermolecular hydrogen bond in these nanocomposites This tendency to form intra-associated hydrogen bonds within the polymer chains dominates the structure of the resulting nanocomposite. As was discussed previously, both Nanomer I.24 TL and Cloisite 25A have long hydrophobic alkyl chains present in their organic modifiers, which exhibit limited interaction with the hydrophilic PVPh. As a result, the association between the segments of polymer chains is favored over polymer-clay interaction leading to an intercalated morphology.

In the absence of any organic modifiers, the Cloisite Na^+ clay is highly hydrophilic. The nanocomposites containing Cloisite Na^+ clay show an increase in the extent of inter-molecular association as the vinyl phenol content is increased from 10 % to 50 % in the copolymer matrix, similar to that observed for the Nanomer I.24 TL and Cloisite 25A nanocomposites. It appears that increasing the number of the hydrogen bonding moieties (-OH) in the nanocomposites increases the extent of inter-molecular hydrogen bonding between the polymer and clay. These specific interactions result in an enthalpic gain, which provides the driving force for the permeation of polymer chains into the clay galleries. Further increase of the vinyl phenol content to PVPh (100% vinyl phenol), decreases the fraction of inter-molecular association to 0.38. However, this contribution from inter-molecular association remains higher than the intra-molecular associated –OH, which is 0.25.

In comparison to the Cloisite 25A and Nanomer I.24 TL nanocomposites, where

PVPh nanocomposite exhibits intercalation and a predominance of intra-association among the polymer chains, the Cloisite Na$^+$ nanocomposite exhibits significant disruption of the clay sheets in the polymer matrix. PVPh has a hydrogen bonding site (-OH) on every repeat unit, making it highly hydrophilic and therefore very compatible with the hydrophilic clay, Cloisite Na$^+$. Polymer-clay interactions are thus favored in the Cloisite Na$^+$/PVPh nanocomposites, resulting in the formation of a thermodynamically stable exfoliated nanocomposite.

4.2.4 Correlating the thermal properties to Dispersion and Interactions

The Glass transition temperature is the temperature where the polymer changes from a hard, glassy state to a rubbery state. It is known that this transition is marked by an increase in the segmental motion of the polymer chains. Segmental mobility of a polymer chain is affected by the presence of filler in the matrix. For instance, the relaxation dynamics of polymer chain in clay nanocomposites is dependent on the size scale of the clay, its morphology and the dispersion of the clay in the matrix. [100] Table 4.6 shows the change in the glass transition temperature of the nanocomposites examined in this study.

It is known that clay sheets have large surface areas (700-800 m^2/g), which can result in extensive interfacial interaction with the polymer in which it is dispersed. In a study carried out by Schiraldi, [101] it was emphasized that the interfacial interactions play a dominant role in determining the T_g of a clay composite. On forming an exfoliated composite, the large surface area of dispersed clay can lead to extensive interfacial interactions between the polymer and clay. This can result in a reduction in the relaxation dynamics of the polymer chain and an increase in T_g for the resultant nanocomposites.

113

Table 4.6 Change in Glass transition temperature of nanocomposites

Nanocomposites	Increase in T_g (° C)		
	Nanomer I.24 TL	Cloisite 25A	Cloisite Na$^+$
PS	3	3	2
PVPh10	3	3	3
PVPh20	7	5	5
PVPh30	9	7	8
PVPh50	18	16	23
PVPh	8	7	12

The glass transition temperature can also be altered by the presence of attractive interactions between the polymer and clay such as hydrogen bonding which reduces the mobility of polymeric chains and increases the glass transition temperature.

For all three clays examined, the polystyrene (PS) and PVPh10 nanocomposites show no significant improvement of the glass transition temperature (T_g) over that of the neat copolymers, where a moderate increase of 3 °C was observed. As the presence of any impenetrable surface can raise the T_g of a polymer slightly, thus this change can be realized by mixing a polymer with any filler, and its efficient dispersion is not required. The FT-IR results, indicate that the PVPh10 nanocomposites display very little inter-molecular hydrogen bonding. Thus it appears that the mobility of the polymer chains is not affected to a great extent by the presence of the clay, presumably due to the lack of interaction between the clay and polymer.

As the vinyl phenol content is increased to 30 %, an increase in T_g of 7-9 °C is observed for all the clays studied. The FTIR analysis indicates that the extent of intermolecular hydrogen bonding in the PVPh30 nanocomposites increases which implies that hydrogen bonding between the clay and polymer impacts the relaxation dynamics of the polymer chains. The PVPh50 nanocomposites show drastic enhancement in the glass transition temperature of the polymer matrix for all three clays, which again correlates well with the fraction of inter-molecularly hydrogen bonded –OH (C_I/C_T). This seems to indicate that the strong specific interactions restrict the segmental mobility of the polymer chains and thus leads to a significantly higher glass transition temperature.

A further increase in the content of vinyl phenol (PVPh) in the copolymer results in a reduction in the extent of inter-molecular hydrogen bonding between the polymer and clay, where intra-molecular association between the polymer chains dominates over the inter-molecular hydrogen bonding between the polymer and clay. This reduction in the polymer-clay interaction is reflected in a modest increase in glass transition temperature of the nanocomposite. The Nanomer I.24 TL and Cloisite 25A nanocomposites show changes of 8 and 7 °C, respectively, whereas the Cloisite Na, has a slightly larger increase in T_g, 12 °C. This makes sense as this nanocomposite has more intermolecular hydrogen bonds than the other PVPh nanocomposites. However, the increase is not as large as the PVPh50 nanocomposites as the extent of intermolecular hydrogen bonding between clay and polymer is not as large in the PVPh nanocomposite than the PVPh50 nanocomposites. This observation is important as it emphasizes the importance of the extent of hydrogen bonding between polymer and clay on the change in T_g of the nanocomposite. Clearly the extent of hydrogen bonding is the controlling factor

in determining the glass transition temperature of the resultant nanocomposite. The extent of dispersion is related to this in that it will impact the extent of interface available for the formation of hydrogen bonds between the clay and matrix. However, it is not the controlling factor in this process.

4.3   Summary and Conclusion

The role of hydrogen bonding on the morphology and thermal properties of nanocomposites containing the organically modified clays, Nanomer I.24 TL and Cloisite 25A and pristine clay, has been investigated in this chapter.

The nanocomposites of Nanomer I.24 TL, Cloisite 25A and Cloisite Na$^+$ show similar morphological behavior, where the dispersion of the clay sheets is found to improve on increasing the vinyl phenol content from 10 to 50 % in the copolymer. The results demonstrate that the PVPh50 nanocomposites have a significant number of hydroxyl groups that can engage in efficient inter-molecular hydrogen bonding with the clay. This results in outstanding improvement in glass transition temperature for these nanocomposites and excellent dispersion. The large increase in T_g is related to the extensive inter-molecular hydrogen bonding between the polymer and the clay. On increasing the vinyl phenol content to 100% in the polymer matrix, inter-molecular hydrogen bonding between the polymer and the clay diminished resulting in reduced dispersion for the Cloisite 25A and Nanomer I.24 TL where an intercalated morphology was attained. In these nanocomposites, intra-molecular association among the polymer chains was found to dominate over inter-molecular hydrogen bonding between the polymer and clay. This results in reduced polymer-clay interactions and thus intercalation

116

was observed and only modest increases in the glass transition temperature. The Cloisite Na$^+$ nanocomposite with PVPh on the other hand, predominantly engages in inter-molecular hydrogen bonding leading to better polymer-clay interaction and greater increase in T$_g$ than the Cloisite 25A and Nanomer I.24 TL nanocomposites. Although Closite Na$^+$/PVPh nanocomposite also shows mostly exfoliated morphology like Cloisite Na$^+$/PVPh50, but the increase in glass transition temperature was much higher for PVPh50 nanocomposite than PVPh nanocomposite. This has been attributed to the greater extent of intermolecular hydrogen bonding exhibited by PVPh50 nanocomposite than PVPh nanocomposite. Therefore, attractive interactions like inter-molecular hydrogen bonding play a crucial role in determining the relaxation dynamics of the polymer chains and thus affecting the glass transition temperature.

CHAPTER 5 SOLUBILITY PARAMETER STUDIES FOR POLYMER/CLAY NANOCOMPOSITES

5.1   Introduction

Traditionally, the Hildebrand solubility parameter concept[102] has been used to estimate the miscibility of two materials. According to the concept, two materials with matching solubility parameters have balanced intermolecular interactions and therefore should be miscible. To determine the solubility parameter of a compound, the following relationship is used:

$$\delta = \Sigma\ F_i/V \tag{5.1}$$

where F_i is the molar attraction constant, V is the molar volume and δ is the solubility parameter. From the solubility parameters, the polymer-polymer interaction parameter, χ can be calculated according to[102,103]:

$$\chi = \frac{V_r}{RT}\left(\delta_A - \delta_B\right)^2 \tag{5.2}$$

where V_r is the molar volume of the the repeat unit, and δ_A and δ_B are the solubility parameters of the two polymers. This relationship was introduced by Flory[104] to describe semiempirically the energetic interactions between different polymers and provides a measure of the degree of phase separation in a given system of polymers. This parameter contributes to the free energy of mixing as:

$$\Delta G_m = RTV_c[(\Phi_A/N_A)\ln\Phi_A + (\Phi_B/N_B)\ln\Phi_B + \chi_{AB}\Phi_A\Phi_A]$$

where ΔG_m is the Gibbs free energy of mixing, Φ_A and Φ_B are the volume fractions of polymers A and B ($\Phi_A + \Phi_B = 1$) and N_A and N_B are the number of reference units with

the molar volume V_c of a given reference unit.

Thus the determination of the solubility parameters of the polymer and the clay for the nanocomposites can provide insight into their interactions, miscibility and the morphology.

Previously, Ho and Glinka[105] investigated the effect of the solubility parameter of clays on their dispersion in various solvents. Studies were carried out using Small Angle neutron scattering (SANS) and Wide Angle X-ray Scattering (WAXS). They observed that the dispersion forces present in the solvent are highly significant in determining whether the organically modified clay remains suspended in the solvent whereas polar and hydrogen bonding interactions determine the degree of exfoliation of the clay in the solvent.

Since dispersive, polar and hydrogen bonding interactions are all essential in determining the miscibility of polymer and the clay in a composite, the individual contributions of each to the total solubility parameter of the clay must be examined.

5.2   Results and Discussion

Determination of solubility parameter of the clays

It must be emphasized that the calculations performed here are only approximate but can serve as guidelines to understand polymer-clay interactions. Clay sheets have a hydrophilic surface with long chain organic surfactants attached electro-statically to the surface. The long chain organic surfactant is expected to play a major role in defining the interaction with the polymer, as the hydrophobic tail of the surfactant and styrenic (hydrophobic) portion of the copolymer are relatively compatible. Table 5.1 shows the

structures of the surfactants present in the clays studied here. The Nanomer I.24 TL contains 12-amino dodecanoic acid as the long chain surfactant. The polar –COOH functionality present in the clay is capable of undergoing polar and hydrogen bonding interactions, therefore group contributions for polar forces and hydrogen bonding must be considered for the computation of its solubility parameter. On the other hand, Cloisite 25A has a non-polar surfactant where only dispersive forces are needed to compute its solubility parameter.

Table 5.2 displays the solubility parameters of the surfactants present in the clays Nanomer I.24 TL and Cloisite 25A. In the determination of the solubility parameter of

Table 5.1Different Clays used in the study
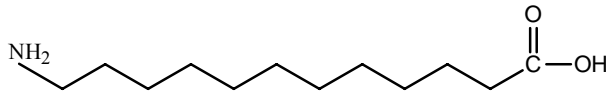
Clays	Surfactants
Nanomer I.24 TL	12-amino dodecanoicacid
Cloisite 25A	dimethyl, dehydrogenated tallow, 2-ethylhexyl quaternary ammonium
Cloisite Na$^+$	Na$^+$

Table 5.2 Solubility parameter of the surfactants in the clays

Clay	Surfactant	Solubility Parameter $(J^{1/2}/cm^{3/2})$
Nanomer I.24 TL	12-amino dodecanoic acid	19.3
Cloisite 25A	dimethyl, dehydrogenated tallow, 2-ethylhexyl quaternary ammonium	17.5

these surfactants, it was assumed that the long chain of the surfactant dominates the solubility parameter as the ammonium ion is connected electrostatically to the clay layer and therefore shielded. Therefore the ammonium ion was excluded from this calculation. To determine of the solubility parameter of the pristine montmorillonite clay with a general formula of $Al_4Si_8O_{20}(OH)_4$, it is assumed that only the silicate tetrahedral sheets interact with the polymeric chain. The building blocks of the clay consist of silicon-oxygen tetrahedral $(Si_2O_5^{2-})$ and aluminium octahedral $[Al(OH)_6]^-$.[106] Since the silicon-oxygen tetrahedra is present at the surface whereas aluminium octahedra is sandwiched in between the silicon tetrahedras, only the silicon-oxygen layer interacts with the polymer chains as they permeate inside the clay galleries. The silicon-oxygen tetrahedral, with the repeat unit of Si_2O_5, can interact with the polar –OH groups present in the polymeric structure through its oxide ions. The solubility parameter of pristine montmorillonite clay was calculated to be 35.1 including dispersive, polar and hydrogen bonding contributions.

It must also be noted that in Nanomer I.24 TL and Cloisite 25A both the inorganic

clay surface (Si_2O_5) and the surfactants are capable of interacting with the polymeric chains permeating inside the clay galleries. Contributions from both are required in the determination of solubility parameter of these clays. But it is imperative to investigate how much of the pristine montmorillonite clay surface is covered by the organic surfactant in the respective clays to evaluate the contributions of both towards the solubility parameter. The cation exchange capacity of the pristine montmorillonite clay was calculated based on percent weight loss on ignition to be 388meq/100g clay. This means that there are 388 meq of exchangeable Na^+ ions in the pristine clay, whereas Cloisite 25A has 95meq of organic modifier as reported by Southern Clay Products. Based on these values, 24.4 % of Na^+ ions in the interlamellar space have been substituted by the organic surfactant. Thus the solubility parameter of the clays was then calculated using the formula:

$$\delta = (x/100) * \delta_{surfactant} + ((100-x)/100) * \delta_{inorganic-clay} \qquad (5.3)$$

Where x represents the percentage of surface covered by surfactant, $\delta_{surfactant}$ is the solubility parameter of the long chain surfactant and $\delta_{inorganic-clay}$ is the solubility parameter of $Si_2O_5^{2-}$. $\delta_{surfactant}$ for Nanomer I.24 TL was determined to be 19.3 $J^{1/2}/cm^{3/2}$ $J^{1/2}/cm^{3/2}$ and 17.5 for Cloisite 25 A. Table 5.3 exhibits the calculated solubility parameters for Nanomer I.24 TL and Cloisite 25A using this method.

Determination of the solubility parameter of the copolymers

Random copolymers are used as the matrix in these nanocomposites, thus the contribution of each repeating unit must be included in the calculation of the solubility

Table 5.3 Solubility Parameter of the surfactants in the clays

Clays	Solubility Parameter ($J^{1/2}/cm^{3/2}$)
Nanomer I.24 TL	31.1
Cloisite 25A	30.8

parameter of the copolymers. The equation to determine the solubility parameter of the random copolymer is thus:

$$\delta_{\text{random-copolymer}} = x_{\text{styrene}}\delta_{\text{styrene}} + x_{\text{vinylphenol}}\delta_{\text{vinylphenol}} \tag{5.4}$$

Where δ_{styrene} is the solubility parameter of styrene, $\delta_{\text{vinylphenol}}$ is the solubility parameter of vinyl phenol, x_{styrene} is the mole fraction of styrene and $x_{\text{vinylphenol}}$ is the mole fraction of vinyl phenol in the copolymer. Additionally, partial solubility parameters were introduced by Hansen to account for intermolecular interactions in polar substances.[107] The total solubility parameter, δ_t is split into three parts, the atomic dispersion forces, δ_d, dipole–dipole forces, δ_p, and molecular hydrogen bonding, δ_h. The Hansen parameters are correlated to the total (Hildebrand) solubility parameters δ_t as shown in Eq. (3):

$$\delta_t = (\delta_d^2 + \delta_p^2 + \delta_h^2)^{1/2} \tag{5.5}$$

δ_d, δ_p, and δ_h can be calculated as follows:

$$\delta_d = \sum \frac{F_{d,i}}{V_m} \tag{5.6}$$

$$\delta_p = \frac{\left(\sum F_{p,i}^2\right)^{1/2}}{V_m} \tag{5.7}$$

$$\delta_h = \frac{\left(\sum E_{coh}^2\right)^{1/2}}{V_m^{1/2}}$$
(5.8)

where $F_{d,i}$ and $F_{p,i}$ are the group contributions for dispersive and polar forces and E_{coh} is the group contribution for hydrogen bonding.

Table 5.4 lists the solubility parameters of the copolymers with vinyl phenol content ranging from 0-100%. Using the calculated solubility parameter of the clays and copolymers, the difference in solubility parameters is determined for all nanocomposites studied, shown in Table 5.5. These calculations reveal that the solubility parameter difference decreases on increasing the vinyl phenol content of the copolymers, irrespective of the clay utilized, with the minimum occurring at PVPh for all clays. These results indicate that the PVPh should exhibit the best compatibility with the clays. However, it has been demonstrated that the PVPh50 nanocomposites individually disperses the clay platelets. This disparity is expected to be a result of the variation in the extent of intermolecular hydrogen bonding among the copolymers which is not taken into account in the calculation of the solubility parameter of the copolymers. To account for this, the extent of intermolecular hydrogen bonding in each nanocomposites will be accounted for in the solubility parameter calculations in this equation:

$$\delta_t = (\delta_d^2 + \delta_p^2 + (\delta_h * C_I/C_T)^2)^{1/2}$$
(5.9)

$\delta_{NanomerClay}*$, $\delta_{CloisiteClay}*$ and $\delta_{PristineClay}*$ were calculated to be 31.1, 30.8 and 35.1 respectively.

Where C_I/C_T is a measure of the hydroxyls that inter-molecularly hydrogen bond to the

Table 5.4Solubility Parameters of the Copolymers

Copolymers	Molar Content (4-vinyl phenol)	Molar Content (Styrene)	Solubility Parameter ($J^{1/2}/cm^{3/2}$)
PS	0	1	18.6
PVPh10	0.135	0.865	19.5
PVPh20	0.2	0.8	19.9
PVPh30	0.3	0.7	20.6
PVPh40	0.38	0.62	21.2
PVPh50	0.475	0.525	21.8
PVPh	1	0	25.4

Table 5.5 Solubility parameter Difference for Clay Nanocomposites

Copolymers	Solubility Parameter ($\delta_{Copolymer}$)	$\delta_{NanomerClay}* - \delta_{Copolymer}$	$\delta_{CloisiteClay}* - \delta_{Copolymer}$	$\delta_{PristineClay}* - \delta_{Copolymer}$
PS	18.6	12.5	12.2	16.5
PVPh10	19.5	11.6	11.3	15.6
PVPh20	19.9	11.2	10.9	15.2
PVPh30	20.6	10.5	10.2	14.5
PVPh40	21.2	9.9	9.6	13.9
PVPh50	21.8	9.3	9.0	13.3
PVPh	25.4	5.7	5.4	9.7

clay in the nanocomposite. Table 5.6, 5.7 and 5.8 show the solubility parameter difference calculations for the nanocomposites after accounting for the extent of intermolecular hydrogen bonding in the nanocomposite. Figure 5.1 is a plot of the solubility parameter differences between the clays and copolymers as a function of the copolymer composition. The solubility parameter difference exhibits a mimimum for the copolymers with 50% vinyl phenol irrespective of the clay structure. This indicates that the extent of H-bonding is a critical factor in defining the compatibility of the polymer and clay.

This calculation assumes that the cation exchange capacity defines the coverage of the surface of the clay by the surfactants. If this is not assumed, the data can also be interpreted to provide information on the extent of interaction of the copolymer with the clay surface and the surfactant. The PVPh50 copolymer displays the best compatibility

Table 5.6 Solubility parameter Difference for Nanomer I.24 TL Nanocomposites

Copolymers	Contribution towards Inter-molecular hydrogen bonding	Solubility Parameter ($\delta_{Copolymer}$)	$\delta_{NanomerClay}{}^{*}$ - $\delta_{Copolymer}$
PVPh10	0.04	20.9	10.2
PVPh20	0.24	21.2	9.9
PVPh30	0.43	21.8	9.3
PVPh50	0.49	22.0	9.1
PVPh	0.38	21.6	9.5

Table 5.7 Solubility parameter Difference for Cloisite 25A Nanocomposites

Copolymers	Contribution towards Inter-molecular hydrogen bonding	Solubility Parameter ($\delta_{Copolymer}$)	$\delta_{CloisiteClay}$* - $\delta_{Copolymer}$
PVPh10	0.02	20.9	9.9
PVPh20	0.28	21.3	9.5
PVPh30	0.36	21.5	9.3
PVPh50	0.54	22.3	8.5
PVPh	0.31	21.4	9.4

Table 5.8 Solubility Parameter Difference for Cloisite Na+ Nanocomposites

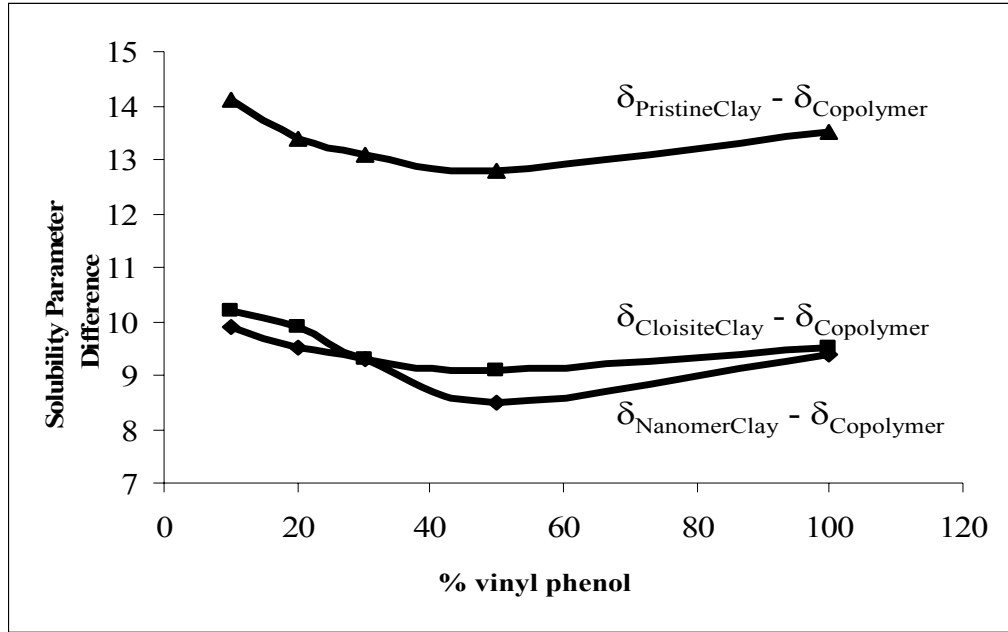| Copolymers	Contribution towards Inter-molecular hydrogen bonding	Solubility Parameter ($\delta_{Copolymer}$)	$\delta_{PristineClay}$* - $\delta_{Copolymer}$
PSVPh10	0.15	21.0	14.1
PSVPh20	0.41	21.7	13.4
PSVPh30	0.48	22.0	13.1
PSVPh50	0.54	22.3	12.8
PVPh	0.38	21.6	13.5

Figure 5.1 Plot representing the solubility parameter difference between the copolymer and clays versus the vinyl phenol content in the copolymers.

with the clay therefore they must have similar solubility parameters. If it is assumed that this polymer and the clay have equal solubility parameters, the following equation is valid:

$$\delta_{PVPh50} = x_{surfactant} * \delta_{surfactant} + (1-x)_{clay} * \delta_{clay}$$

(5.10)Where δ_{PVPh50} is the solubility parameter of PVPh50, $\delta_{surfactant}$ is the solubility parameter of the surfactant, δ_{clay} is the solubility parameter of the clay, $x_{surfactant}$ represents the percent of the surface that is covered in the surfactant and x_{clay} is the percent of inorganic clay surface that is exposed to the copolymer. Table 5.9 displays the solution to this equation for the PVPh50 copolymer and inorganic clay surface ($Si_2O_5^{2-}$).

These results imply that as the polymer chain permeates inside the clay galleries, it primarily interacts with the surfactant, but also the clay surface. The interaction with

Table 5.9 Interaction of the copolymer PVPh50 with the inorganic clay surface and the surfactant

Clay	$X_{surfactant}$	X_{clay}
Nanomer I.24 TL	0.805	0.195
Cloisite 25A	0.69	0.31

the clay surface is not insignificant as the oxide ions present on the surface have the ability to strongly interact with the –OH groups of the polymer. It can also be seen that in the Nanomer I.24 TL clay, the polymer interaction with the surfactant is higher relative to that in the non-polar Cloisite 25A. This makes sense as the polar PVPh50 prefers a more polar environment. In Cloisite 25A, the non-polar surfactant drives the PVPh50 copolymer more towards the inorganic surface where more friendly polar oxide ions can be found. It should be noted that these trends remain regardless whether the solubility parameters in equation 5.10 are equal or differ by a small (<2) factor.

5.3   Summary and Conclusion

This chapter estimates the solubility parameter of the clays in the nanocomposites in an attempt to understand the morphology of the examined systems.

The solubility parameter difference decreases with the vinyl phenol content of the copolymers in the nanocomposites irrespective of the clay utilized, with the minimum occurring at PVPh. These results indicated that PVPh should exhibit optimum compatibility with the clays. However, PVPh50 shows the best dispersion in these

nanocomposites. This deviation is explained by accounting for the extent of intermolecular hydrogen bonding in the nanocomposites in the calculation of the solubility parameter of the copolymers. This emphasizes the importance of the extent of intermolecular interaction between the polymer and clay to obtain miscible polymer/clay hybrids. It was also determined that PVPh50 copolymer interacts with the surfactant of the Nanomer I.24 TL clay more extensively than in Cloisite 25A clay. The presence of the polar -COOH in Nanomer I.24 TL surfactant drives the PVPh50 polymer chains away from the hydrophilic inorganic surface, whereas the polymer interacts more with the Cloisite 25A surface as it has a non-polar surfactant.

CHAPTER 6 EFFECT OF CLAY LOADING ON THE DISPERSION AND THERMAL PROPERTIES OF NANOCOMPOSITES

6.1 Introduction

In Chapter 3, the optimization of the extent of intermolecular hydrogen bonding in a polymer clay nanocomposite had been investigated by controlling the distribution of hydroxyl groups in a copolymer. This was realized by synthesizing copolymers of styrene and 4-vinyl phenol where styrene is a non-hydrogen bonding monomer and 4-vinyl phenol can participate in hydrogen bonding via its hydroxyl group. The results indicated that tuning the inter-molecular hydrogen bonding tends to optimize the interaction between the polymer and the filler resulting in improved dispersion of clay sheets and considerable improvement in the thermal properties of the nanocomposites relative to the pure polymer. In this chapter, the importance of clay loading on the dispersion and thermal properties has been studied where the loadings are varied from 1-8 wt % which are being mixed with the various copolymers (0-100) mole percent vinyl phenol. It will be determined utilizing SAXS, TEM and DSC, which clay loading provides optimum morphological and thermal improvements.

6.2 Results and Discussion

6.2.1 Thermal Behavior

The temperature at which the long-range segmental motion of the polymer chains starts is termed as glass transition temperature. Cooperative relaxation of chains is affected by the presence of stiff filler particles in the polymer matrix, their weight percentage and aspect

ratio in the polymer matrix. It has been emphasized in Chapter 4 that the interfacial interactions play a dominant role in determining the T_g of a clay composite. On forming an exfoliated composite, the large surface area of dispersed clay can lead to extensive interfacial interactions between the polymer and clay. This can result in a reduction in the relaxation dynamics of the polymer chain and an increase in T_g for the resultant nanocomposites. The glass transition temperature can also be altered by the presence of attractive interactions between the polymer and clay such as hydrogen bonding which reduces the mobility of polymeric chains and increases the glass transition temperature.

Clay loadings ranging from 1-8 wt % were mixed with the copolymers (0-100 % vinyl phenol) using solution blending. Table 6.1 shows the increase in glass transition temperature observed for these nanocomposites relative to the pure copolymers. For all the polymers examined, 8 wt% clay loading showed least increase in the glass transition temperature whereas 3% and 5% clay nanocomposites displayed optimum increase in T_g. 1% clay loading, although seemingly little has still provided enormous improvement in glass transition temperature for all the nanocomposites.

Considering 3 and 5 wt % clay loadings, where nanocomposites have shown optimum increase in T_g, as the vinyl phenol content in the copolymer was increased from 0-50 %, these clay loadings increase the T_g's of the nanocomposites significantly. PS and PVPh10 show only moderate increase of 3 - 4 °C. As the presence of any impenetrable surface can raise the T_g of a polymer slightly, thus this change can be realized by mixing a polymer with any filler, and its efficient dispersion is not required. The FT-IR results indicated that the PVPh10 nanocomposites display very little inter-molecular hydrogen

Table 6.1 Increase in Glass Transition temperature for the nanocomposites relative to pure copolymers

Nanocomposite	Increase in T_g (ºC) with different Clay Loading (%)			
	1	3	5	8
PS	4	3	3	1
PVPh10	3	4	3	2
PVPh20	9	9	7	6
PVPh30	7	7	9	5
PVPh40	**10**	**16**	**16**	**12**
PVPh50	**9**	**16**	**18**	**12**
PVPh	3	13	9	5

bonding. Thus it appears that the mobility of the polymer chains is not affected to a great extent by the presence of the clay, presumably due to the lack of interaction between the clay and polymer.

PVPh20 and PVPh30 nanocomposites with higher vinyl phenol content show larger increases in T_g relative to PS and PVPh10 for all the clay loadings. Increase of 7-9 ºC was observed for PVPh20 and PVPh30 nanocomposites for 1-5 % clay loadings. On further increase of the clay loading to 8 wt %, increase in the glass transition temperature observed was 5-6 ºC. It is believed that increasing the clay concentration increases the clay-clay interaction due to electrostatic interaction between the oxide ions and positively charged cations in the interlayer which results in the aggregation of clay sheets and reduced intermolecular interaction between the polymer and clay. This diminished interfacial interaction affects the relaxation dynamics of polymer chains. Therefore the change exhibited by 8% composites in glass transition temperature is lower relative to 3 and 5% composites.

PVPh40 and PVPh50 nanocomposites demonstrated remarkable improvement in the glass transition temperature. An increase of T_g as high as 18 ºC was recorded for PVPh50-5% clay nanocomposite. PVPh40 with 3 and 5% clay loadings shows an increase of 16 ºC. Even 8% clay nanocomposites with PVPh40 and PVPh50 show significant improvement in T_g. An increase of 12 ºC was observed for both the nanocomposites containing 8 % clay. The PVPh40 and PVPh50 nanocomposites show drastic enhancement in the glass transition temperature of the polymer matrix for all the clay loadings, which correlates well with the fraction of inter-molecularly hydrogen bonded –OH (C_I/C_T). This seems to indicate that the strong specific interactions restrict

134

the segmental mobility of the polymer chains and thus leads to a significantly higher glass transition temperature.

Although on increasing the concentration of clay to 8 %, change in glass transition temperature observed for the nanocomposite was less relative to 3 and 5 % but was still noteworthy. It is believed that the tendency of clay sheets to aggregate in PVPh10 and PVPh20 matrices is much more pronounced than with PVPh40 and PVPh50 due to the presence of fewer hydrogen bonding sites. Increase in glass transition temperature of 12 °C observed at this clay loading for the nanocomposites supports the aforementioned explanation.

A further increase in the content of vinyl phenol (PVPh) in the copolymer results in a reduction in the extent of inter-molecular hydrogen bonding between the polymer and clay, where intra-molecular association between the polymer chains dominates over the inter-molecular hydrogen bonding between the polymer and clay. This reduction in the polymer-clay interaction is reflected in a modest increase in glass transition temperature of the nanocomposite. It shows an increase of 13 °C for 3% clay loading whereas an increase of 9 °C was observed for 5% clay nanocomposite. On further increase of clay loading to 8%, increase in T_g observed was 5 °C. Increase in glass transition temperature observed for PVPh nanocomposites was not as large as that for PVPh40 and PVPh50 nanocomposites due to diminished intermolecular hydrogen bonding between the polymer and clay. This observation emphasizes the importance of the extent of intermolecular hydrogen bonding between the polymer and clay on the change in T_g of the nanocomposite.

6.2.2 *Morphological Studies*

Random copolymers of poly(styrene-co-vinyl phenol) mixed with 1-8 % clay were analysed by SAXS and TEM for their morphology. Figure 6.1 represents the SAXS curve for Nanomer I.24 TL which exhibits the d-spacing of 16.7 Å. Details of how d-spacing can be utilized to determine the morphological state of the nanocomposites have been described in chapter 4. Figure 6.2 and 6.3 depict the SAXS pattern for PS and PVPh10 composites for all the clay loadings (1-8 %). 1 and 3 wt % loadings do not show any characteristic peak in the region of clay d-spacing of Nanomer I.24 TL for PS and PVPh10 composites, but TEM micrographs represented in Figures 6.4 and 6.5 show aggregated regions of clay present for all the clay loadings (3-8 wt %) in polystyrene and PVPh10 composites suggesting poor dispersion. This is expected as both PS and PVPh10 do not have sufficient –OH to engage in hydrogen bonding with the clay.

In the absence of any enthalpic interactions, the ability of clays to be uniformly dispersed on the nanoscale level in the polymer matrix of PS and PSVPh10 will be hindered irrespective of the clay loading. Entropic loss which occurs as the polymer chains try to intercalate cannot be compensated by these none/minimal energetic interactions. FT-IR also supports that PVPh10's contribution towards inter-molecular hydrogen bonding ($C_I/C_T = 0.04$) with Nanomer I.24 TL is very low. TEM micrographs show the formation of more clay aggregates in PS and PVPh10 as the clay loading is increased from 3 to 8 wt %. It is believed that an increase in the clay loading enhances the interaction between the clay sheets which increases the tendency of clay particles to form a distinct phase in the polymer matrix. PS and PVPh10 do not have enough
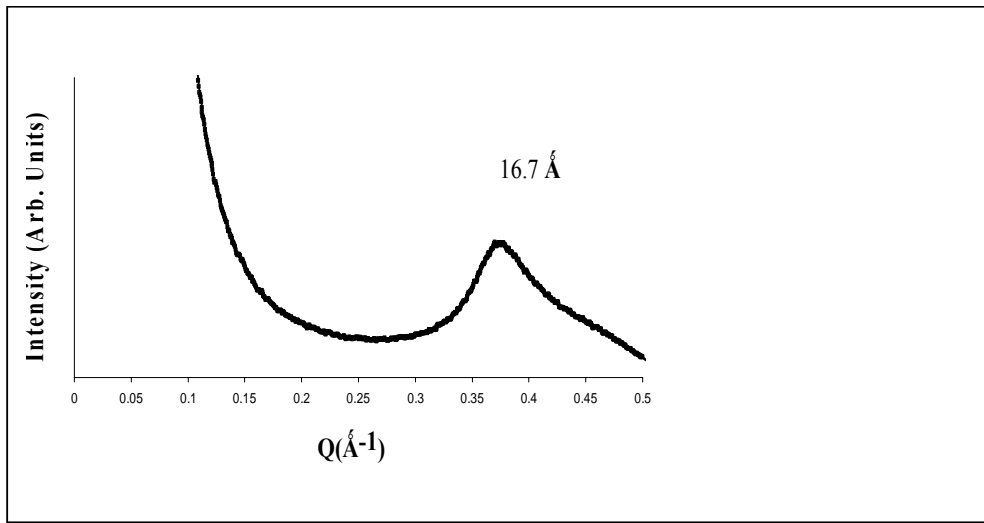
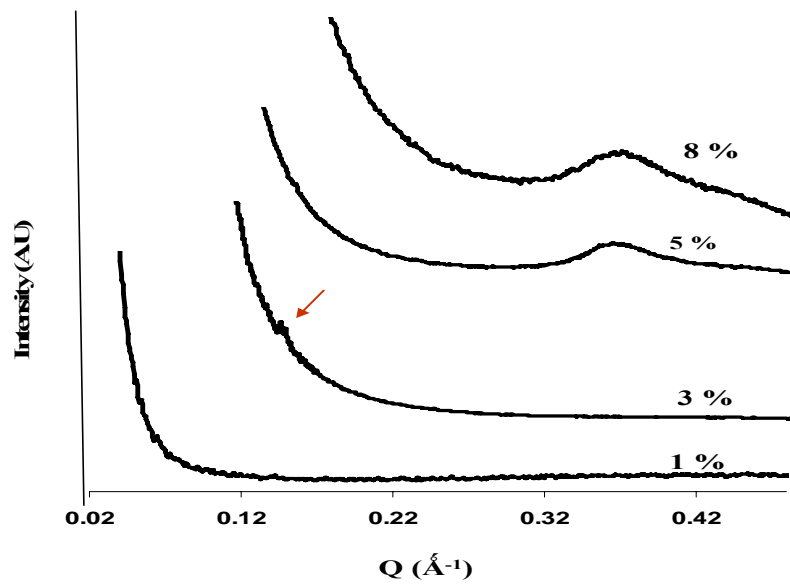**Figure 6.1 SAXS Pattern for Nanocor I.24 TL Clay**

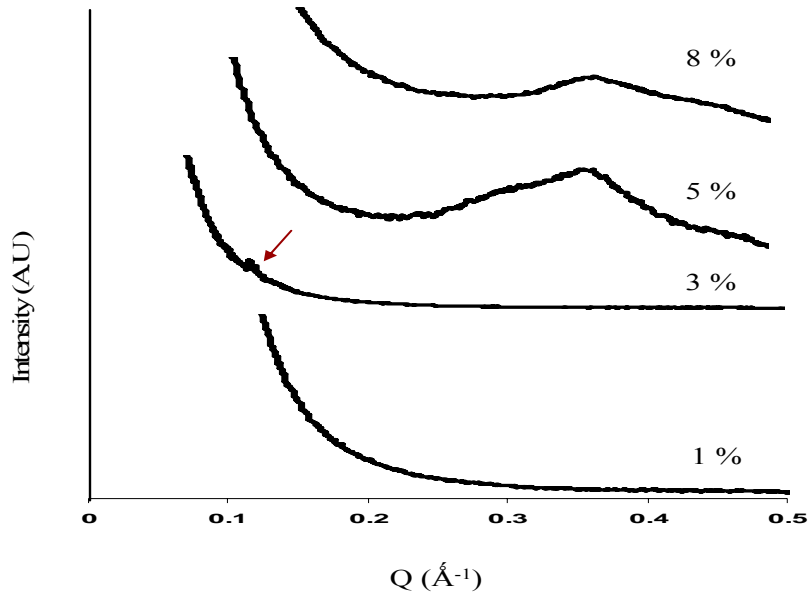**Figure 6.2 SAXS Pattern for Polystyrene Nanocomposites**

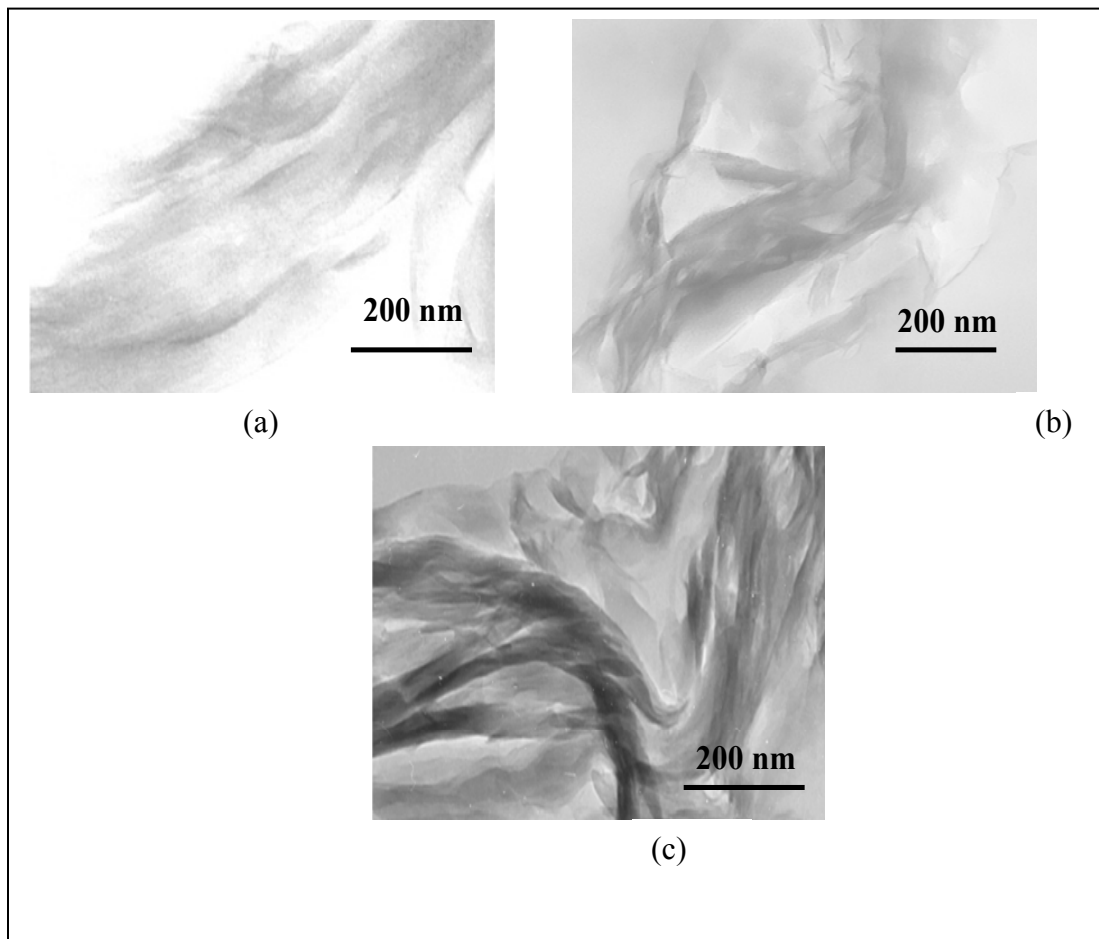**Figure 6.3 SAXS Pattern for PVPh10 Nanocomposite for different clay loadings**

Figure 6.4 Transmission Electron Micrographs for Polystyrene Nanocomposites (a) 3% clay (b) 5% clay (c) 8%clay
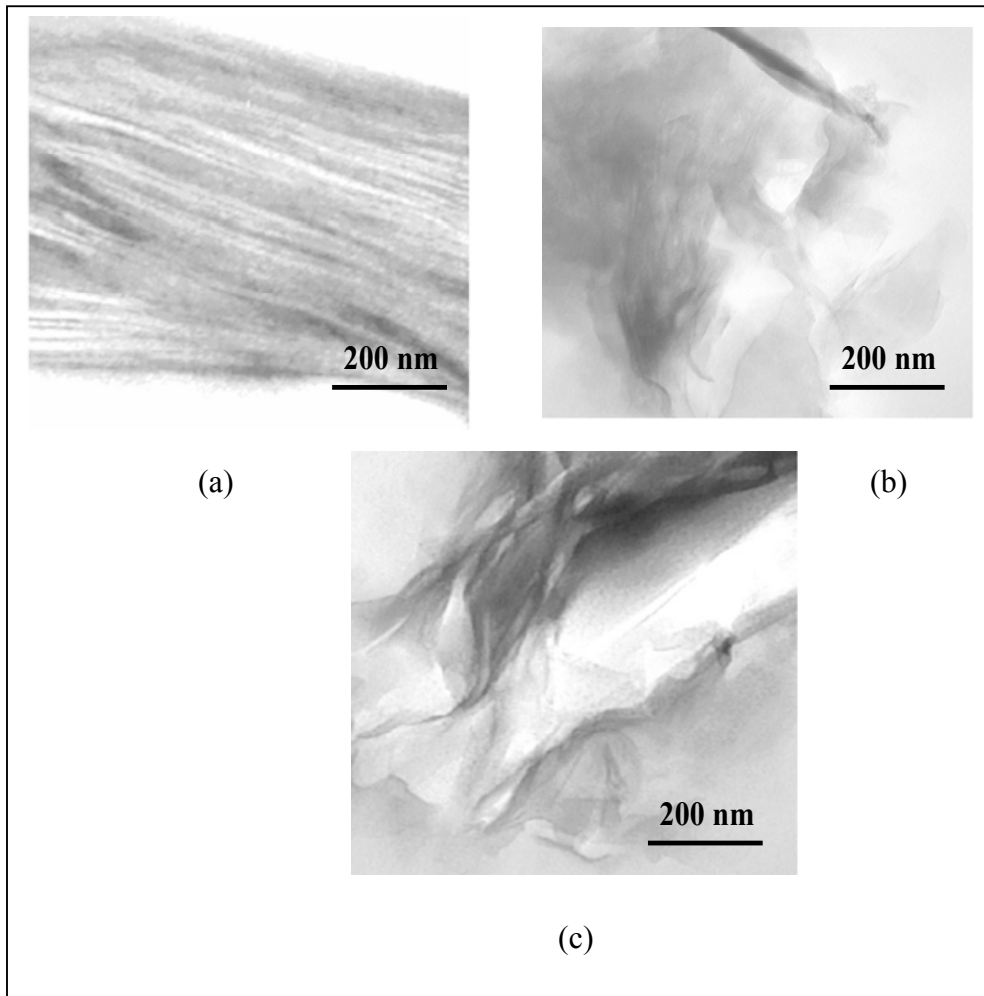
Figure 6.5 Transmission Electron Micrographs for PVPh10 Nanocomposites (a) 3% clay (b) 5% clay (c) 8%clay

hydroxyl groups which can disrupt the like-like interaction between the clay sheets and therefore the miscibility between the polymer and the clay is greatly reduced leading to poor dispersion. Additionally, increase in the volume fraction of the clay in the nanocomposite would lead to greater entropic loss as the polymer chains try to penetrate the clay galleries. These two factors would affect the dispersion of the clay sheets in the polymer matrix.

On further increasing the vinyl phenol content to 20 % as in PVPh20, contribution towards intermolecular hydrogen bonding with Nanomer I.24 TL clay was found to increase relative to PVPh10 as reported by FTIR. SAXS curves in Figure 6.6 show no characteristic peak for 3 wt% loading. Also few individual clay platelets are observed in the TEM, Figure 6.7 for 3 wt % loading nanocomposite. But on enhancing the clay content in the polymer matrix to 8 wt %, tendency of clay sheets to aggregate increased and more clay agglomerates could be observed in TEM images relative to 3 and 5 % composites. Results observed for 8 % PVPh20 composites are similar to those observed for PS and PVPh10 composites.

On increasing the vinyl phenol content to 30 % in the copolymer PVPh30, TEM images reveal good dispersion for 3 % clay loading composite where individually dispersed clay sheets could be observed. At 5 % clay loading, region of clay d-spacing as represented by SAXS, Figure 6.8 became broader indicative of the presence of both intercalated and exfoliated structures. TEM suggests that clay sheets are better dispersed in PVPh30 relative to PVPh20 nanocomposite. However, on increasing the clay loading to 8 wt%, more stacked clay platelets were observed in TEM, Figure 6.9. Moreover, at 8

141

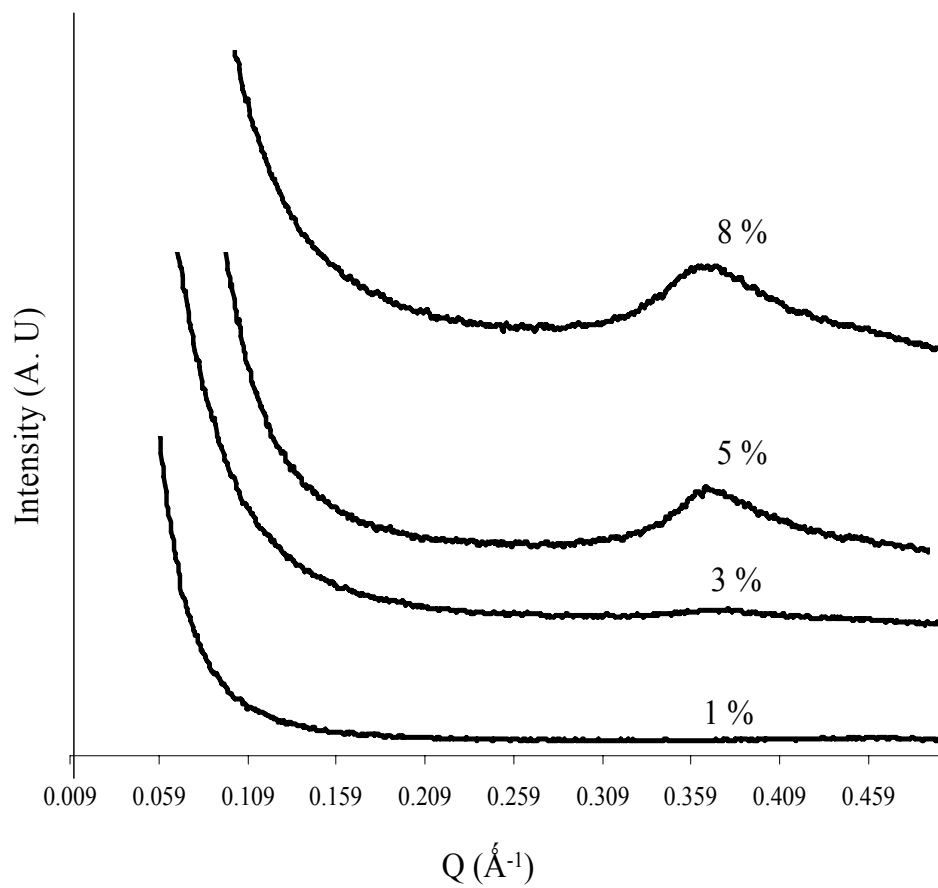**Figure 6.6 SAXS Pattern for PVPh20 Nanocomposite for different clay loadings**
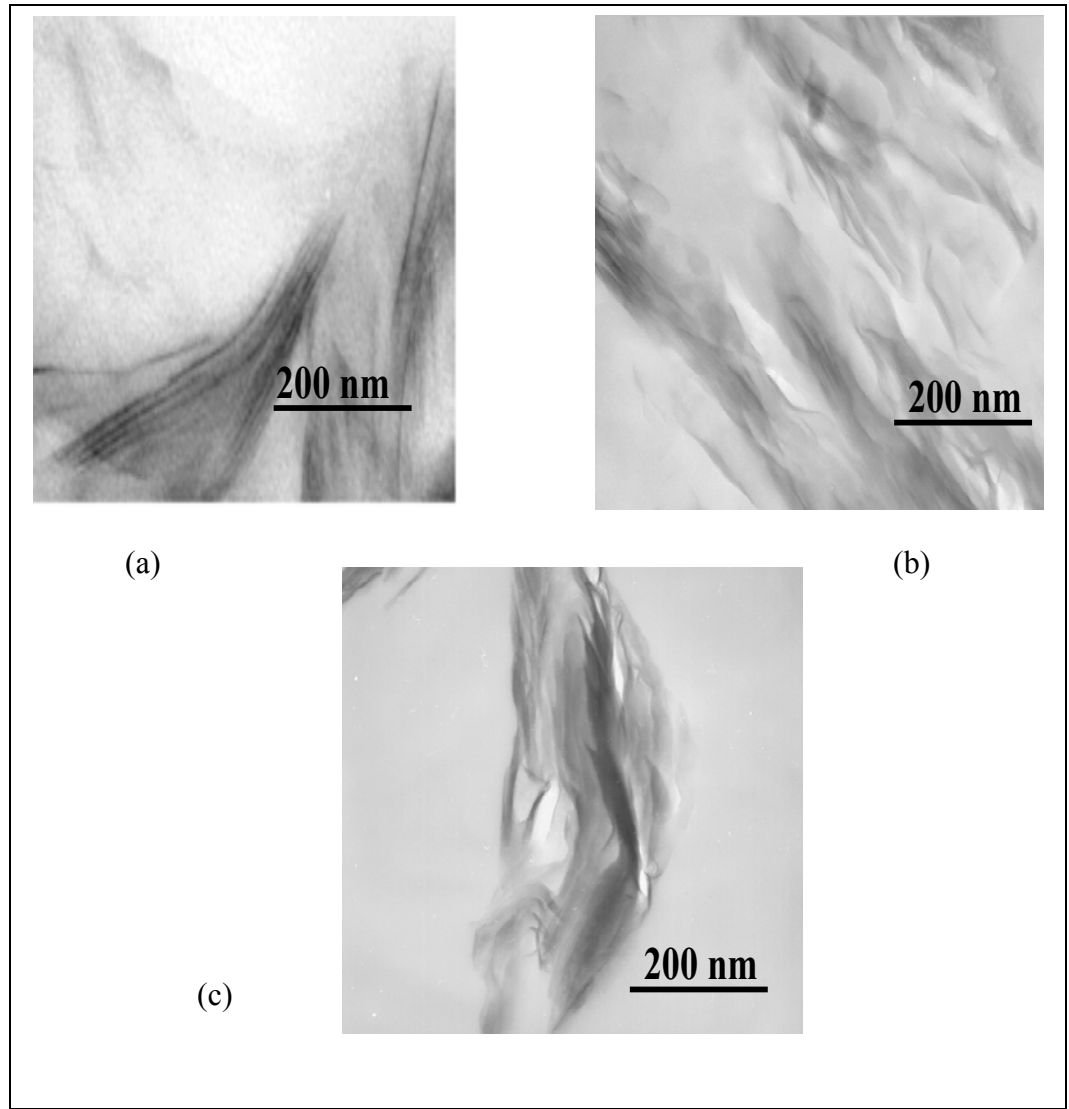
(a)

(b)

(c)

Figure 6.7 Transmission Electron Micrographs for PVPh20 Nanocomposites (a) 3% clay (b) 5% clay (c) 8%clay
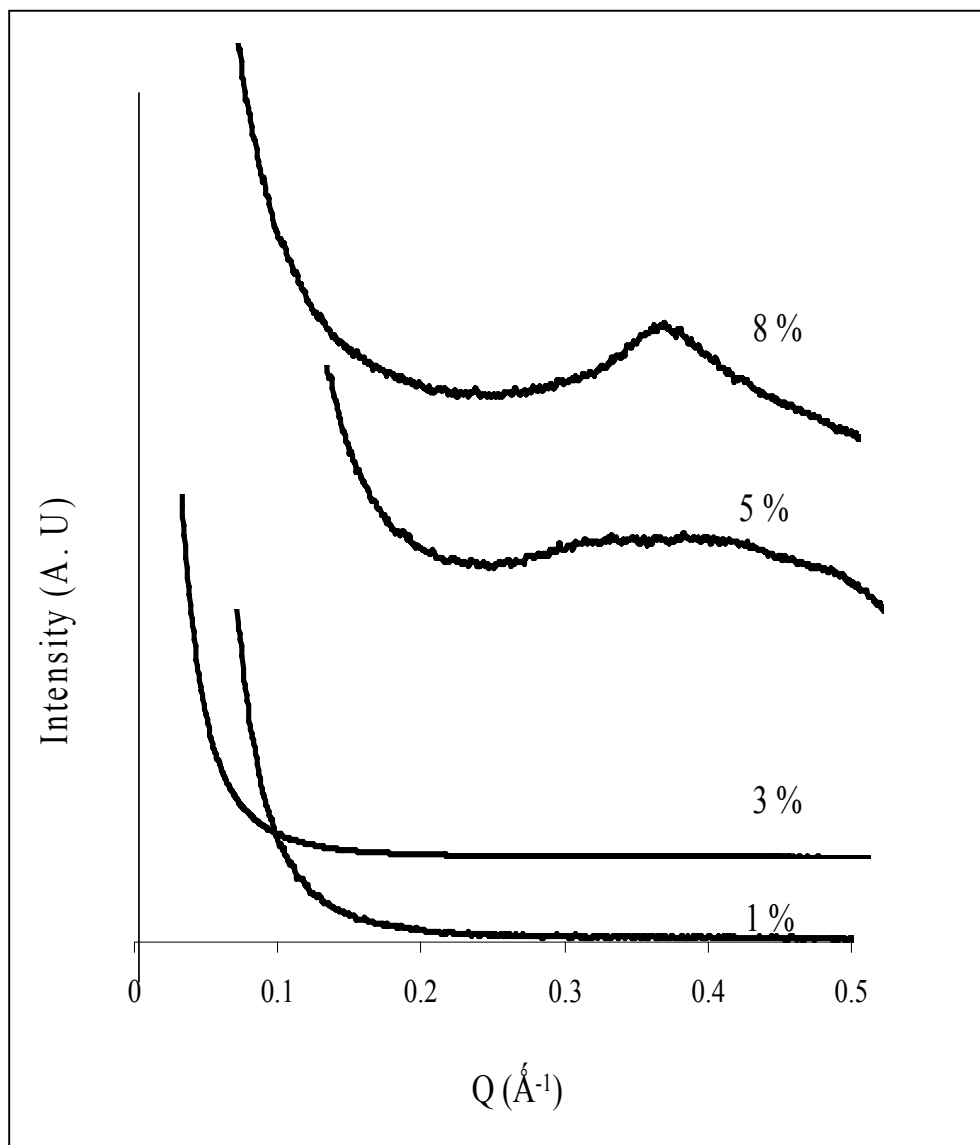
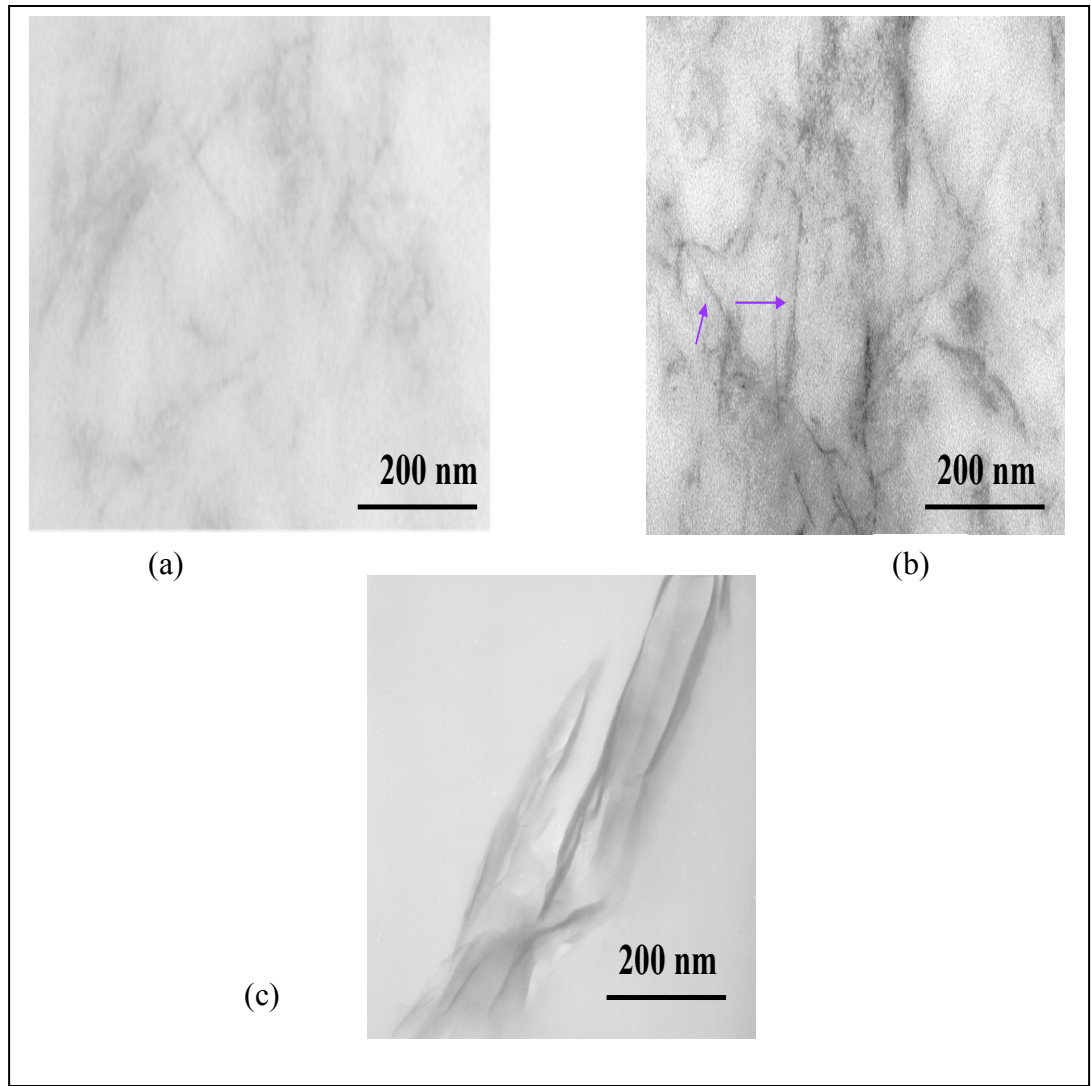**Figure 6.8 SAXS Pattern for PVPh30 Nanocomposites for different clay loadings**

Figure 6.9 TEM for PVPh30 Nanocomposites for different Clay Loadings (a) 3% clay (b) 5% clay (c) 8%clay

wt % clay loading, PVPh30 nanocomposite exhibits a distinct peak in the d-spacing region of Nanomer I.24 TL clay which is also indicative of poor dispersion relative to 3 and 5 % PVPh30 composites. The increase in the amount of polar hydroxyl groups in PVPh30 is expected to provide an increase in the intermolecular hydrogen bonding with the clay functionalities (-COOH, -OH and oxide ions), which provides favorable enthalpic interactions for the permeation of polymer chains into the clay galleries.

For PVPh40 nanocomposites, none of the clay loadings ranging from 1-8 % showed any discernible peak in the SAXS pattern, Figure 6.10. 5%-PVPh40 nanocomposite exhibited a small shoulder but TEM image in Figure 6.11 indicated that clay sheets were very well dispersed in the polymer matrix. For the clay loading of 1 wt %, clay sheets could not be observed in transmission electron microscopy images due to the low concentration of clay. According to the FT-IR analysis carried out in chapter 3, optimum inter-molecular association between the polymer and clay at 5 wt % loading occurs for PVPh40 and PVPh50. This results in very good dispersion of clay sheets for all the clay loadings ranging from 1-8 %. But TEM for 3% and 5% clay loadings demonstrated the presence of individual clay platelets dispersed in the polymer matrix. Presence of large number of hydroxyl groups in PVPh40 which can undergo inter-molecular hydrogen bonding with the clay provide favorable enthalpic drive and facilitate the penetration of polymeric chains between the clay galleries pushing the clay sheets apart resulting in exfoliation where clay sheets are uniformly polymer matrix. As the clay loading increases, the like-like forces of attraction between the clay sheets increase resulting in the aggregation of clay sheets. But PVPh40 has enough hydroxyl groups to
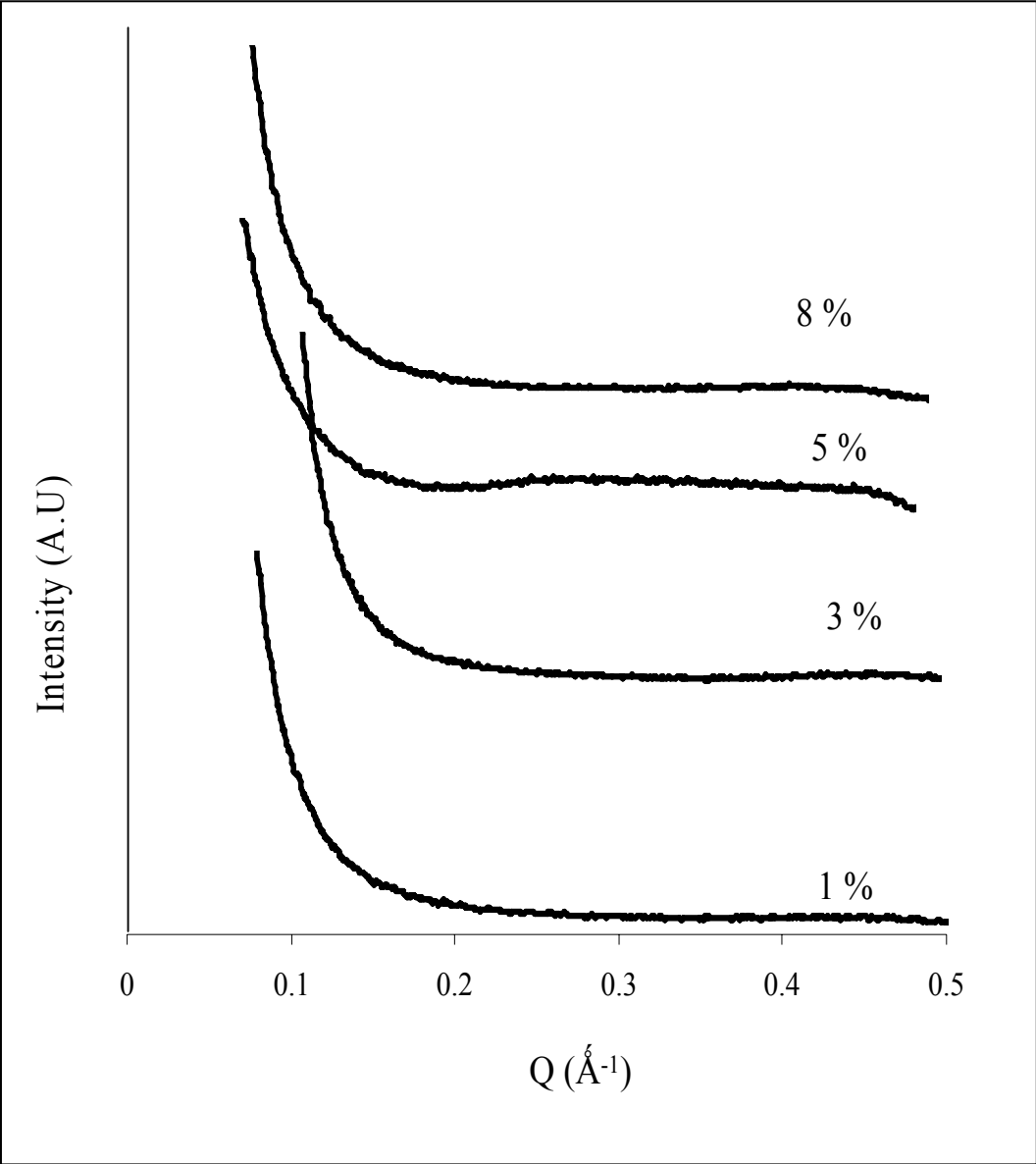
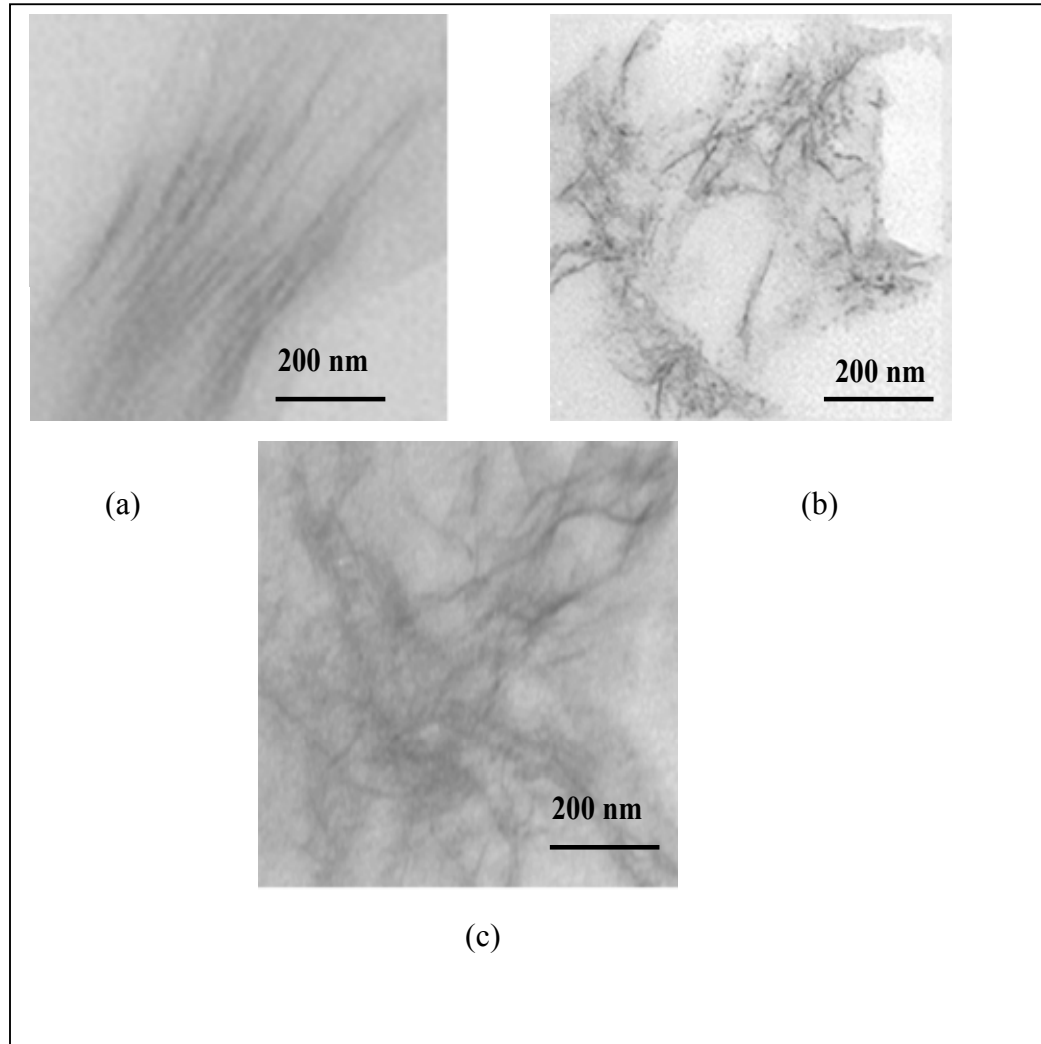**Figure 6.10 SAXS Pattern for PVPh40 Nanocomposites for different clay loadings**

Figure 6.11 TEM for PVPh40 Nanocomposites for different Clay Loadings (a) 3% clay (b) 5% clay (c) 8%clay

overpower the like-like attraction between the clay sheets even in case of 8% clay and disperse the clay sheets individually on nanoscale. A similar trend was observed for PVPh50 nanocomposites due to large number of hydroxyl groups which can hydrogen bond with the clay. Figure 6.12 shows the SAXS pattern for all the clay loadings containing PVPh50. For the clay loading ranging from 1-5 %, peak in the region of clay d-spacing completely disappeared suggesting that we have been successful in breaking up the clay agglomerates. When the clay loading was increased to 8 wt %, a small peak is observed in the region of d-spacing of the clay but the intensity is very small indicating that the clay is mostly present as exfoliated clay platelets dispersed in the polymer matrix. This is further confirmed by referring to the Figure 6.13 which represents the TEM micrographs for all the clay loadings ranging from 3-8 %.

PVPh (100% vinyl phenol) shows intercalated morphology for both 5 and 8 wt % clay loading. SAXS curves in Figure 6.14 reveal that clay peak which is observed at the d-spacing of 16.7 Å has shifted to 20 Å for both the clay loadings. It was determined in chapter 3 by the analysis of hydroxyl vibration in the nanocomposites that there is dominating tendency towards intra-molecular association of polymer chains in PVPh. Inter-molecular hydrogen bonding between the polymer and clay is dimished leading to intercalation. As explained in chapter 4, it is also expected that hydrophobic tail of the organic surfactant present in Nanomer I.24 TL shows repulsive interaction for –OH groups of the polymer resulting in some hindrance in the permeation of polymer chains in clay galleries. Only a few chains are able to permeate inside the clay galleries resulting in intercalation. TEM images in Figure 6.15 confirmed intercalated morphology for both

149

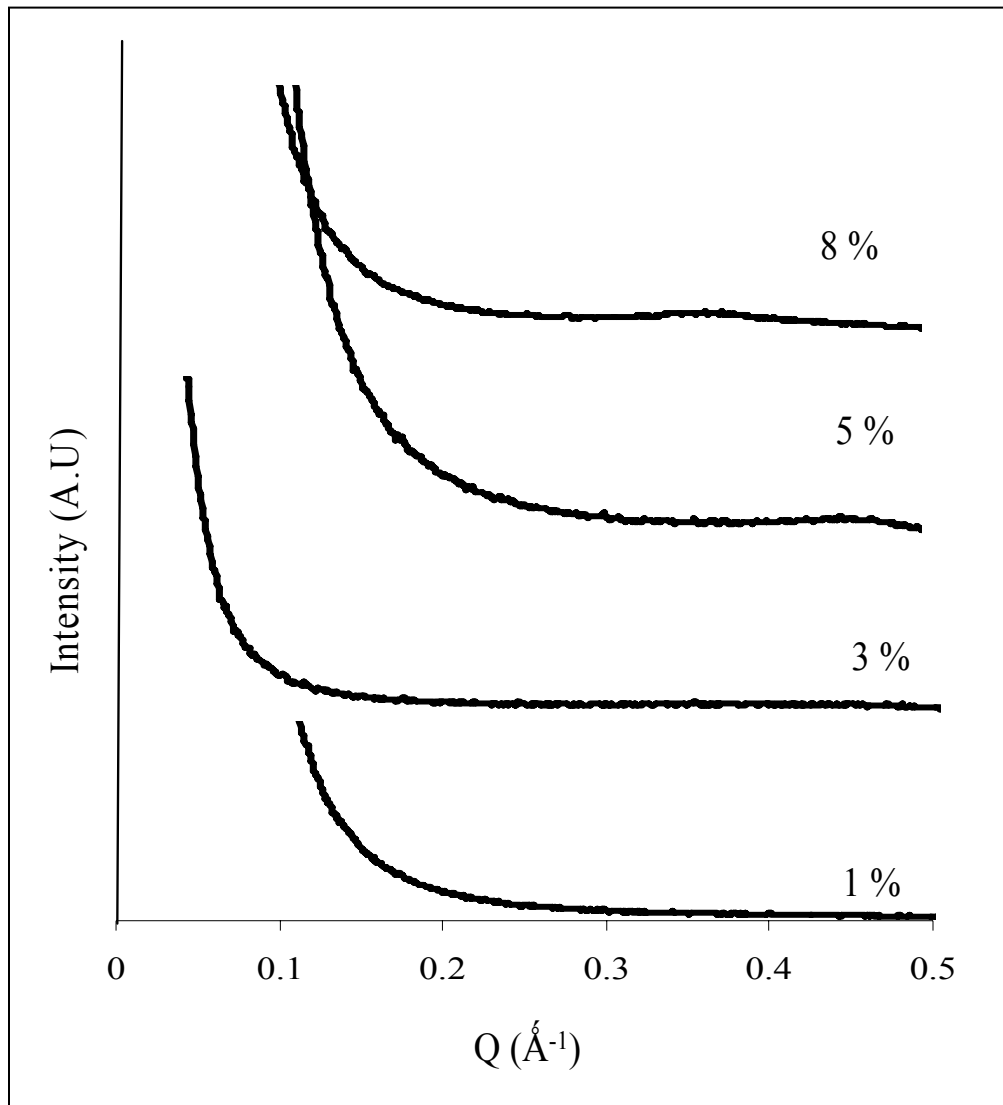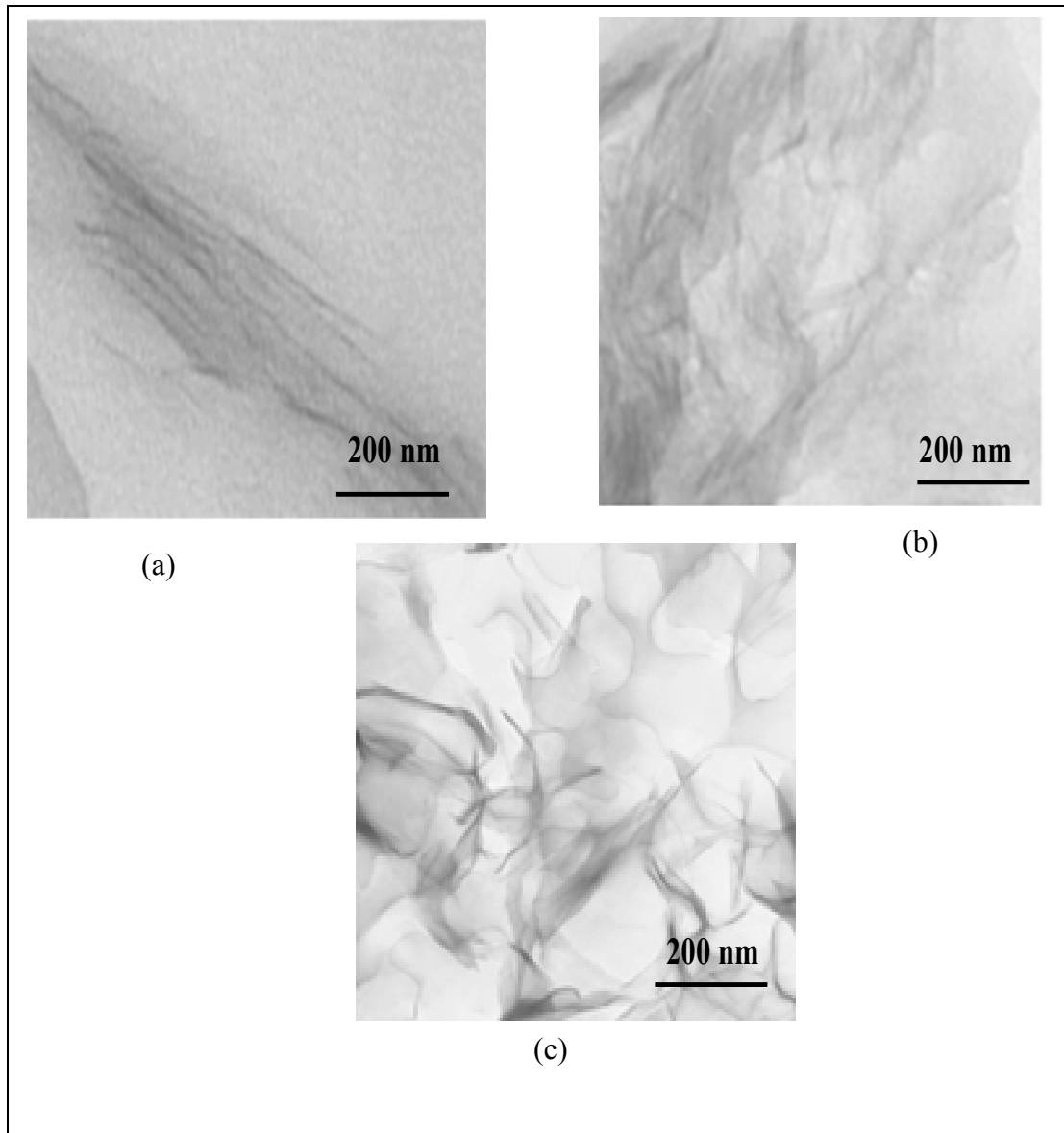**Figure 6.12 SAXS Pattern for PVPh50 Nanocomposites for different clay loadings**

Figure 6.13 TEM for PVPh50 Nanocomposites for different Clay Loadings (a) 3% clay (b) 5% clay (c) 8%clay
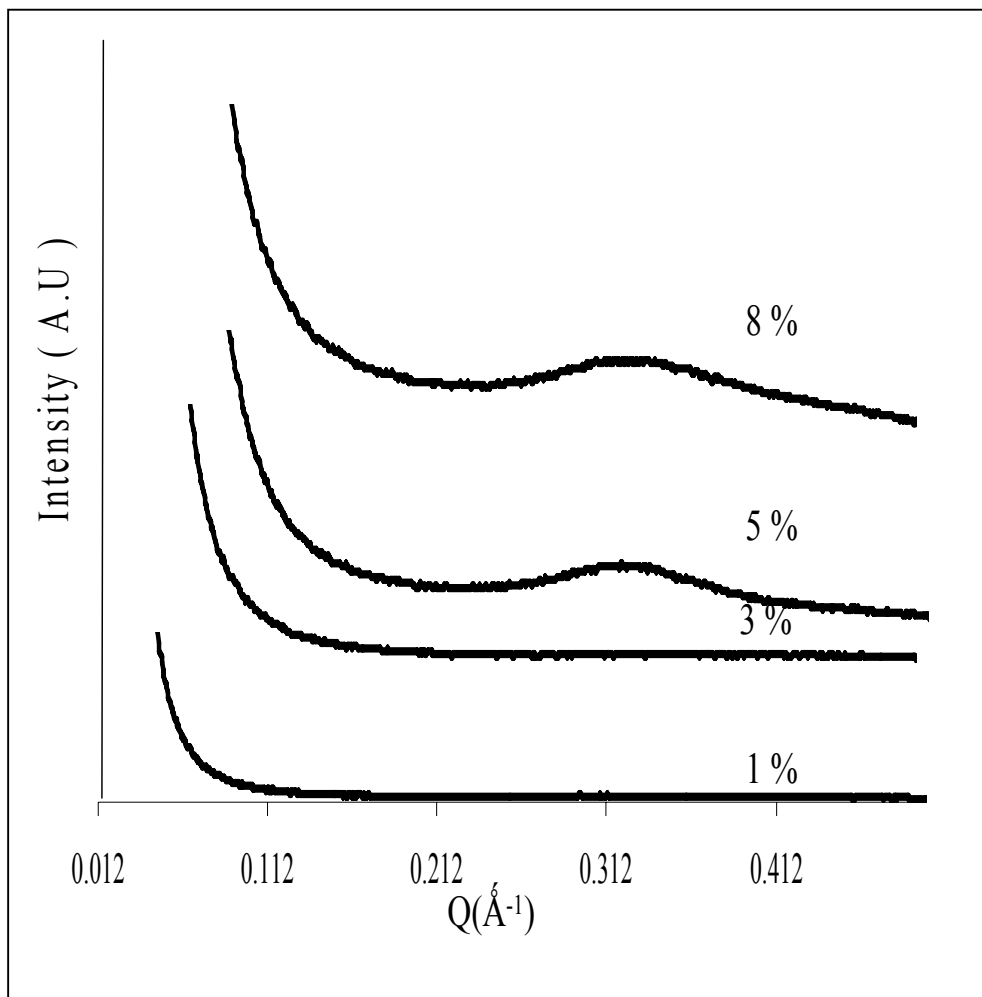
Figure 6.14 SAXS Pattern for PVPh Nanocomposites for different clay loadings
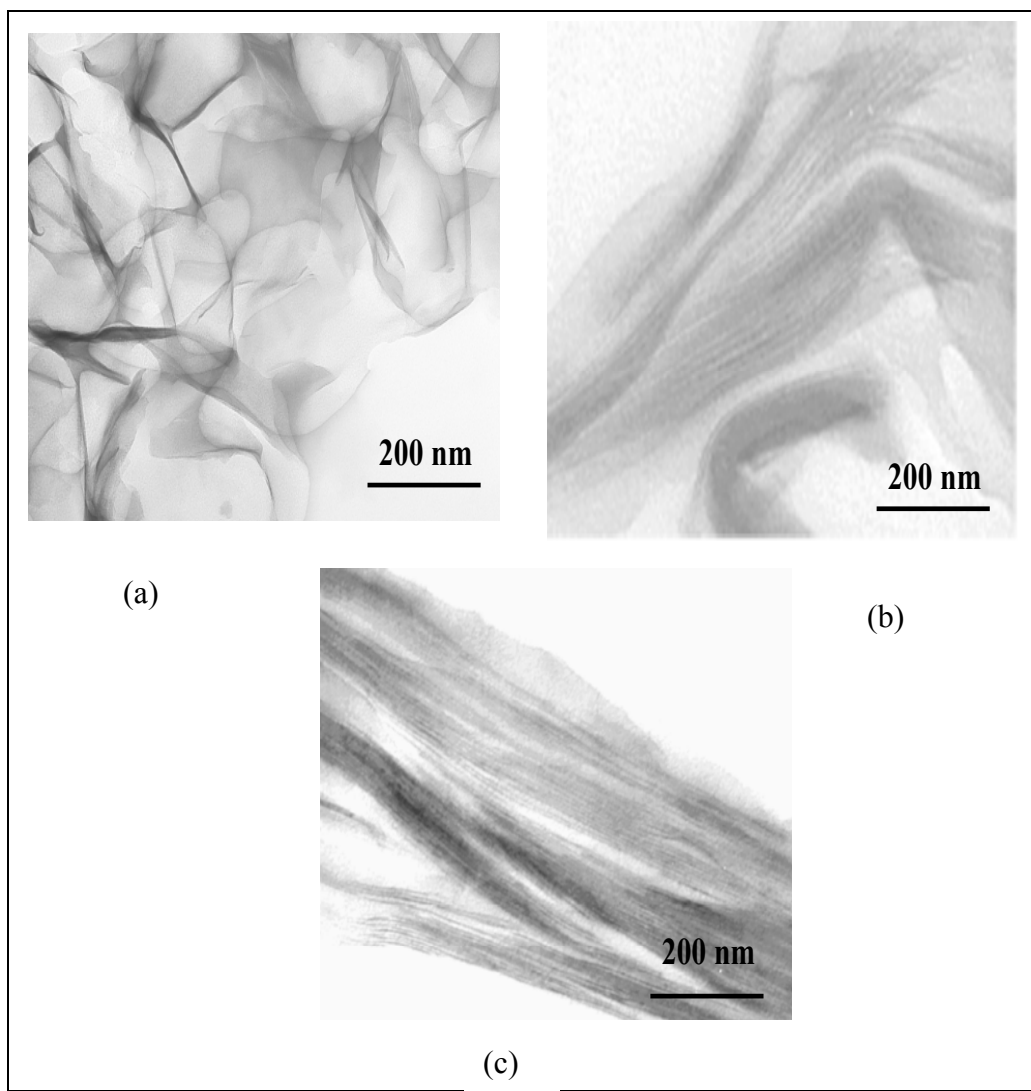
(a)

(b)

(c)

Figure 6.15 TEM for PVPh Nanocomposites for different Clay Loadings (a) 3% clay (b) 5% clay (c) 8%clay

clay loadings. On the otherhand, 3 % clay nanocomposite does not show any noticeable

peak in SAXS pattern. This indicates that it is better dispersed than 5 and 8%

This is further corroborated by TEM images where some individually dispersed clay

platelets were observed for 3 % clay loading nanocomposite.

6.3   Summary and Conclusion

Nanocomposites with 40 % and 50 % vinyl phenol display very good dispersion

with all the clay loadings (1- 8 %). SAXS and TEM data illustrate that complete

dispersion of clay sheets has taken place in the nanocomposites. PVPh40 and PVPh50 are

capable of undergoing considerable amount of inter-molecular hydrogen bonding with

the clay which impedes the propensity of clay to phase separate and result in aggregation.

As a consequence clay sheets are significantly dispersed with high interfacial interaction

between the polymer and clay in PVPh40 and PVPh50 even at 8% clay loading.

Additionally, dramatic improvement in glass transition temperature was obtained for

PVPh40 and PVPh50 nanocomposites for all the clay loadings. This has been attributed

to strong specific interactions like hydrogen bonding which play a pivotal role in

reducing the relaxation dynamics of polymer chains thus affecting the glass transition

temperature. Change in glass transition temperature for 8 % clay nanocompsites was

lower than 1-5 % clay loadings due to greater aggregation of clay platelets at higher clay

loading. PS, PSVPh10 do not show good dispersion of clay sheets irrespective of the clay

loading which is evident through presence of clay aggregates exhibited by TEM. The

copolymers have none or little hydrogen bonding sites and thus cannot undergo any

hydrogen bonding with clay resulting in poor dispersion. On increasing the vinyl phenol

content to 100 %, the propensity to engage in intra-molecular association increases giving rise to intercalation as opposed to expected "exfoliation". Inter-molecular hydrogen bonding between the polymer and clay is reduced affecting the dispersion. 5 and 8 wt % clay loading nanocomposites show intercalation but 3 wt% loading exhibits better dispersion. With the clay loading of 3 wt%, increase in T_g was 13 °C. Also SAXS data and TEM show well dispersed clay platelets in the polymer matrix for 3 wt % clay loading as opposed to 5 and 8 wt % clay loading nanocomposites.

Our findings indicate that 3 and 5 % clay loadings with PVPh40 and PVPh50 nanocomposites exhibit optimum dispersion of clay platelets with drastic improvement in glass transition temperature.

CHAPTER 7 CONCLUSIONS AND FUTURE WORK

The results observed in this study demonstrate that optimum intermolecular interactions play a pivotal role in attaining the molecular dispersion of clay sheets in the polymer matrix affecting the morphology and thermal properties of the nanocomposites. In Chapter 3, the extent of intermolecular hydrogen bonding is controlled by varying the copolymer composition of poly(styrene-co-vinyl phenol). Increase in the copolymer composition is found to enhance the energetic interactions between the polymer and clay leading to improved dispersion and thermal behavior. Nanocomposites containing 0-10 % vinyl phenol do not show any significant improvement in the morphology and glass transition temperature which is attributed to none/minimal hydrogen bonding interactions occurring between the polymer and the clay. However, on further increase of copolymer composition to 50%, completely dispersed clay platelets are observed in the polymer matrix as illustrated by TEM and SAXS with dramatic improvement in glass transition temperature. FTIR results supported the observations where optimum intermolecular hydrogen bonding was exhibited by copolymer with 50% vinyl phenol. Exceptional increase in glass transition temperature is a direct result of these interfacial interactions which affect the segmental mobility of the polymer chains. On the other hand, when copolymer composition was increased to 100%, dispersion of the clay sheets in the polymer matrix significantly reduced resulting in intercalated morphology due to diminished inter-molecular hydrogen bonding.

Additionally, three different montmorillonite clays were also investigated in their ability to affect the intermolecular interactions, where the clays had different surfactants.

The importance of the structure of the surfactant on the dispersion was evaluated. The nanocomposites of Nanomer I.24 TL, Cloisite 25A and Cloisite Na^+ showed similar morphological behavior, where the dispersion of the clay sheets is found to improve on increasing the vinyl phenol content from 10 to 50 % in the copolymer. The PVPh50 nanocomposites show optimum dispersion with all the clays as the copolymer can engage in efficient inter-molecular hydrogen bonding with the clay which results in outstanding improvement in glass transition temperature for these nanocomposites and excellent dispersion. However, the copolymer with 100% vinyl phenol showed different morphology with Cloisite Na^+ than with Nanomer I.24 TL and Cloisite 25A. PVPh/Nanomer I.TL and PVPh/Cloisite 25A nanocomposites exhibited intercalation whereas PVPh/Cloisite Na^+ showed exfoliation. Hydrophobic nature of the organic modifiers present in Cloisite 25A and Nanomer I.24 TL limits the penetration of hydrophilic PVPh chains between the clay platelets thus results in intercalation. On the other hand, Cloisite Na^+ is highly hydrophilic due to the absence of any surfactant and therefore very compatible with hydrophilic PVPh. Miscibility between Cloisite Na^+ and PVPh results in the formation of an exfoliated composite. These results are supported by FTIR spectroscopy where polymeric chains in Cloisite Na^+/PVPh nanocomposite are predominantly engaged in intermolecular hydrogen bonding. Contrarily, Nanomer I.24 TL and Cloisite 25A clays primarily engage in intra-molecular association with PVPh chains reducing the inter-molecular hydrogen bonding and as a consequence intercalation takes place in the nanocomposite.

Further support for the results was provided by solubility parameter studies on these nanocomposites. Solubility parameter difference between the polymer and clay can

157

be correlated to the interactions and the morphology in the nanocomposites. PVPh exhibited a minimum in the solubility parameter difference irrespective of the clay utilized of all the copolymer compositions. But this is contradictory to the results obtained in Chapter 4 and Chapter 3 where optimum intermolecular interactions between the polymer and clay are exhibited by PVPh50 nanocomposite. This discrepancy was resolved by accounting for intermolecular interactions and finally PVPh50 showed a minimum difference in the solubility parameter. It was also determined that PVPh50 copolymer interacts with the surfactant of the Nanomer I.24 TL clay more extensively than in Cloisite 25A clay.

Furthermore, in chapter 6, clay wt % is optimized to achieve best morphological and thermal improvements. The clay loadings are varied from 1-8 wt % which are being mixed with the various copolymers (0-100) mole percent vinyl phenol followed by characterization by TEM and SAXS. Nanocomposites with 40 % and 50 % vinyl phenol display very good dispersion with all the clay loadings (1- 8 %) with remarkable improvement in glass transition temperature. Even at 8 wt% clay, uniformly dispersed clay platelets could be observed in the polymer matrix for PVPh40 and PVPh50, due to large number of hydroxyl groups capable of undergoing hydrogen bonding with the clay thus prohibiting the clay sheets from forming the aggregates. However, PS and PVPh10 did not show any improvement in dispersion and glass transition temperature irrespective of the clay loading due to the presence of none/few hydrogen bonding sites in the polymers.

In future, mechanical properties of the nanocomposites can be studied by dynamic mechanical analysis (DMA) and determine how these results conform to the molecular

level dispersion obtained by transmission electron microscopy and small angle x-ray scattering. It will also be interesting to find their barrier properties relative to the neat copolymers which can further elucidate the nanoscale dispersion of clay platelets in the polymer matrix.

REFERENCES

References

1. Shepherd, P.D; Golemba, F. J; Maine, F.W *Adv Chem Ser* **1974**, 134, 41.

2. Yano, K; Usuki, A; Okada, A; *J. Polym. Sci., Part A: Polym. Sci* **1997**, 35, 2289-2294.

3. Giannelis E. P. *Adv Mater* **1996**, 8, 29–35.

4. Giannelis E. P; Krishnamoorti R; Manias E. *Adv Polym Sci* **1999**; 138:107–47.

5. LeBaron P. C; Wang Z; Pinnavaia T. J. *Appl Clay Sci* **1999**, *15*, 11–29.

6. Vaia R. A; Price G; Ruth P.N; Nguyen H.T; Lichtenhan J. *Appl Clay Sci* **1999,** *15*, 67–92.

7. Biswas M; Sinha R. S. *Adv Polym Sci* **2001**, *155*, 167–221.

8. Messersmith, P.; Giannelis, E. P. *Chem. Mater*. **1994**, *6*, 1719.

9. Kojima, Y.; Usuki, A.; Kawasumi, M.; Okada, A.; Kurauchi, T.; Kamigaito, O. *J. Polym. Sci., Part A: Polym Chem* **1993**, *31*, 1755.

10. Lan, T.; Pinnavaia, T. J. *Chem. Mater*. **1994**, *6*, 2216.

11. Wang, Z.; Pinnavaia, T. *Chem. Mater*. **1998**, *10*, 1820.

12. Okada, A.; Usuki, A. *Mater. Sci. Eng*. **1995**, *C3*, 109.

13. Wang, J.; Du, J.; Zhu, J.; Wilkie, C. A. *Polym. Degrad. Stab*. **2002**, *77*, 249.

14. Zhu, J.; Uhl, F. M.; Morgan, A. B.; Wilkie, C. A. *Chem. Mater*. **2001**, *13*, 4649.

15. Xu, R,; Manias, E.; Snyder A. J; Runt J. *Macromolecules* **2001**;34:337–9.

16. Bharadwaj R. K. *Macromolecules* **2001**, 34, 1989–92.

17. Messersmith P. B, Giannelis E. P. *J Polym Sci, Part A: Polym Chem* **1995**, 33, 1047–57.

18. Yano, K; Usuki, A; Okada, A; Kurauchi, T; Kamigaito, O. *J Polym Sci, Part A: Polym Chem* **1993,** 31, 2493–8.

19. Kojima, Y; Usuki, A; Kawasumi, M; Fukushima, Y; Okada, A; Kurauchi, T; Kamigaito, O *J Mater Res* **1993**, 8, 1179–84.

20. LeBaron, Peter C.; Wang, Zhen; Pinnavaia, Thomas J. *Applied Clay Science* **1999**, 15, 11–29

21. Gilman, J. W. *Appl. Clay Sci.* **1999**, 15, 31–49.

22. http://www.honeywell.com/sites/sm/aegis/aegis_hfx.htm

23. Lloyd, S. M.; Lave, L. B.; *Environ. Sci. Technol.* **2003**, 37, 3458–3466.

24. Alexandre, M.; Dubois, P. *Mater. Sci. Engng* **2000**, 28, 1–63.

25. Current Nanotechnology Applications. *Nanotechnology Now.* Accessed May 1, 2003. URL: http://nanotech-now.com/current-uses.htm

26. Buchholz, K. Nanocomposite debuts on GM vehicles. *Automotive Engineering International Online.* Accessed April 30, **2003**. URL: http://www.sae.org/automag/material/10-2001/index.htm

27. Pinnavaia,T. J.; Beall, G. W. (eds.), Polymer-Clay Nanocomposites, John Wiley & Sons, Chichester–New York **2001**.

28. Krishnamoorti, R.; Vaia, R. A. (eds.), Polymer Nanocomposites: Synthesis, Characterization, and Modeling, American Chemical Society, Washington **2001**.

29. Ji, X. L; Jing, J. K. ; Jiang, W ; Jiang, B. Z *Polym. Eng. Sci.* **2002,** 42, 983-993.

30. Fornes, T. D; Paul, D. R Polymer **2003**, 44, 4993-5013 .

31. Sheng, N; Boyce, M. C.; Parks, D. M.; Rutledge, G. C.; Abes, J. I.; Cohen, R. E. *Polymer* **2004**, 45**,** 487-506.

32. Myskova, M. Z; Zelenka, J.; Spacek, V.; Socha, F. *Mech. Compos. Mater.* **2003**, 39, 111-122.

33. Luo, J. J.; Daniel, I. M *Compos. Sci. Technol.* **2003**, 63, 1607-1616.

34. Osman, M. A; Mittal, V.; Lusti, H. R *Macromol. Rapid Commun.* **2004**, 25, 1145-1149.

35. Osman, M. A.; Mittal, V.; Morbidelli, M.; Suter, U. W. *Macromolecules* **2004**, 37, 7250-7257.

36. Nam, P. H. ; Maiti, P. ; Okamoto, M. ; Kotaka, T.; Nasegawa, N.; Usuki, A. Polymer **2001**, 42**,** 9633-9640.

37. Liu, X.; Wu, Q Polymer **2001**, 42, 10013-10019.

38. Antipov, E. M.; Barannikov, A. A.; Gerasin, V. A.; Shklyaruk, B. F.; Tsamalashvili, L. A.; Fisher, H. R.; Razumovskaya, I. V *Vysokomol. Soed.* **2003**, 45A, 1885-1899.

39. Antipov, E.; Guseva, M. A.; Gerasin, V. A.; Korolev, Yu.; Rebrov, A. V.; Fisher, H. R.; Razumovskaya, I. V. *Vysokomol. Soed.*, **2003**, 45A, 1874-1884.

40. Yano, K.; Usuki, A.; Okada, A.; Kurauchi, T.; Kamigaito, O. *J. Polym. Sci. Pt. A, Polym. Chem.* **1993**, 31, 2493-2498.

41. Lan, T.; Kaviratna, P. D.; Pinnavaia, T. J. *Chem. Mater*. **1994**, 6, 573-575.

42. Magaraphan, R.; Lilaynthalert, W.; Sirivat, A.; Schwank, J. W. *Compos. Sci. Technol.* **2001**, 61, 1253-1264.

43. Okamoto, M.; Morita, S.; Kim, Y. H.; Kotaka, T.; Tateyama, H *Polymer* **2001**, 42, 1201-1206.

44. Chen, W.; Xu, Q.; Yuan, R. Z. *Compos. Sci. Technol*. **2001**, 61, 935-939.

45. Messersmith, P. B; Giannelis, E. P.; *J. Polym. Sci. Pt. A, Polym. Chem*.**1995**, 33, 1047-1057.

46. Sheptalin, R. A.; Koverzanova, E. V.; Lomakin, S. M.; Osipchik, V. S. *Plast. Massy* **2004**, No. 4, 20-26.

47. Tutorskii, I. A.; Pokid'ko, B. V. *Kauchuk Resina* **2004**, No. 6, 33-36.

48. Kim, Y. K.; Choi, Y. S.; Wang, K. H.; Chung, I. J. *Chem. Mater.* **2002**, 14, 4990.

49. Chen, J.S.; Poliks, M. D.; Ober, C. K.; Zhang, Y.; Wiesner, U.; Giannelis, E. P. *Polymer* **2002**, *43*, 4895.

50. Ogawa, M. *Chem. Mater.* **1996**, 8, 1347.

51. Breen, C.; Rawson, J. O.; Mann, B. E.; Aston, M. *Colloids Surf., A* **1998**, *132*, 17.

52. Billingham, J.; Breen, C.; Yarwood, J. *Vib. Spectrosc.* **1997**, *14*, 19.

53. Aranda, P.; Ruiz-Hitzky, E. *Chem. Mater.* **1992**, 4, 1395.

54. Ruiz-Hitzky, E.; Aranda, P. *Adv. Mater.* **1990**, 2, 545.

55. Aranda, P.; Ruiz-Hitzky, E. *Appl. Clay Sci.* **1999**, *15*, 119.

56. Kawasumi, M.; Hasegawa, N.; Kato, M.; Usuki, A.; Okada, A. *Macromolecules* **1997**, *30*, 6333.

57. Sikka, M.; Cerini, L. N.; Ghosh, S. S.; Winey, K. I. *J. Polym. Sci., Part B: Polym. Phys.* **1996**, *34*, 1443.

58. Barber, G. D.; Calhoun, B. H.; Moore, R. M *Polymer* **2005**, 46, 6706.

59. Grim, R. E. *Clay Mineralogy* **1968**, 2nd edn; NewYork, NY.

60. Grim, R. E. *Clay Mineralogy* **1962**, 7–29 NewYork, NY.

61. Triantafillidis, C.S.; Lebaron, P.C and Pinnavaia, T. J. *J. Solid State Chem.*, **2002**, 167, 354–362.

62. Pinnavaia, T. J. *Science*, **1983**, 220, 365–371.

63. Carrado, K. A. *Appl. Clay Sci.*, **2000**, 17, 1–23.

64. Vaia, R. A.; Ishii, H.; Giannelis, E. P. *Chem. Mater.*, **1993**, 5, 1694–1696.

65. Vaia, R. A.; Giannelis, E.P. *Macromolecules* **1997,** 30, 8000–9.

66. Vaia, R.A.; Giannelis, E.P. *Macromolecules* **1997,** 30, 7990–9.

67. Yang, I-Kuan; Tsai, Ping-Hung *Polymer* **2006,** 47, 5131–5140.

68. Kojima, Y.; Usuki, A.; Kawasumi, M.; Okada A.; Fukushima, Y.; Kurauchi, T.; Kamigaito, O. *J Mater Res* **1993**, 8, 1185.

69. Barber, G.D.; Calhoun, B. H.; Moore, R. M *Polymer* **2005**, 46, 6706.

70. Pattanayak, A.; Jana, S. C *Polymer* **2005**, 46, 5183.

71. Wei, K.; Liu, Y.; Tyan, H. *Chem Mater.* **1999**, 11, 1942-1947.

72. Lee, K.M; Han, C.D *Macromolecules* **2003**, 36, 804-815.

73. Kawasumi, M.; Hasegawa, N.; Kato, M.; Usuki, A.; Okada A. *Macromolecules* **1997**, 30, 6333-6338.

74. Reichert P.; Hoffman, B.; Bock, T.; Thomann, R.; Mulhaupt, R.; Freidrich, C. *Macromol. Rapid Commun.* **2001**, 22, 519-523.

75. Kato, M.; Usuki, A.; Okada A. *J. Appl. Polym. Sci*. **1997**, 66, 1781-1785.

76. Balazs, A. C; Singh, C.; Zhulina, E.; Lyatskaya, Y. *Acc. Chem. Res.,* **1999**, 32*,* 651-657.

77. Minisini, B.; F. Tsobnang *Composites: Part A* 36 **2005**, 36, 539–544

78. Viswanathan, S.; Dadmun, M. D *Macromolecules* **2002,** 35*,* 5049-5060

79. Viswanathan, S.; Dadmun, M. D *Macromolecules* **2003,** 36*,* 3196-3205.

80. Viswanathan, S.; Dadmun, M. D *Macromolecular Rapid Communication* **2001***,* 22, 779-782.

81. Rasheed, A.; Dadmun, M. D.; Ivanov, I.; Britt, P. F.; Geohegan, D.B. *Chem. Mater*. **2006**, 18, 3513 – 3522.

82. Tang, W. L.; Coleman, M. M.; Painter, P. C. *Macromol. Symp.* **1994**, 84, 315.

83. Painter, P. C.; Tang, W. L.; Graf, J. F.; Thomson, B.; Coleman, M. M. *Macromolecules* **1991**, 24, 3929.

84. Flory, P. J. *Principles of Polymer Chemistry*; Cornell University Press: Ithaca, New York, 1953.

85. Flory, P. J. Macromolecules 1978, 11, 1138.

86. Stevens, Malcolm *Polymer Chemistry- An Introduction;* Oxford University Press, NewYork **1999.**

87. North, A. M; Postlethwaite, D *Structure and Mechanism in Vinyl Polymerization*

Chapter 4, **1969**.

88. Coleman, M. M.; Pehlert, G. J.; Painter, P.C. *Macromolecules* **1996**, 29, 6820.

89. Ledwidth, A.; Rahnema, M.; Sengupta, P. K. *J. Polym. Sci., Polym. Chem. Ed*. **1980**, 8, 2239.

90. Radmard, B. *Thesi*s, The University of Tennessee, Knoxville, Dec **1999**.

91. Coleman, M. M.; Painter, P. C. *Fundamentals of Polymer Science*, 2nd ed.; Technomic Publishing Co.: Lancaster, PA **1984**

    92. Campbell and White, *X-ray diffraction methods in polymer science*, Wiley,

NewYork **1969**

93.

94. Alexandre, M.; Dubois, P. *Materials Science and Engineering* **2000**, 28, 1-63.

94. Coleman, M. M.; Lee, K. H.; Skrovanek, D. J.; Painter, P.C. Macromolecules **1986**, 19, 2149-2157.

95. Dean, L.; Brisson, J. Polymer, **1998**, 39(4), 793-800.

96. Moskala, E. J.; Howe, S. E.; Painter, P. C.; Coleman, M. M. *Macromolecules* **1984**, 17, 1671.

97. Garton, A**.** *Polym. Eng. Sci.* **1984**, 24, 112.

98. Henniker, J. C., *Infrared Spectrometry of Industrial Polymers.* Academic Press, London, **1967**, Chap. 7.

99. Li, D.; Brisson, J. *Polymer* 1998, 39, 793-800.

100. Suneel, B.; Schiraldi, D. *Macromolecules* **2006,** *39,* 6537-6545

101. Brown, H. R.; Russell, T. P. *Macromolecules* **1996**, *29*, 798-800.

102. Paul, D. R. and Newman, S. (Eds) *Polymer Blends,* Academic Press, London, **1978**, Vols I and II

103. Kraus, S. J. *Macromol. Sci. Rev. MacromoL Chem.* 1972, C7, 251

104. Flory, P. J *Principles of polymer chemistry*, **1953** Cornell University Press, Ithaca, NY

105. Ho, D. L.; Glinka, C. J. *Chem. Mater.* **2003**, *15*, 1309-1312.

106. Olphen, O. V. *An introduction to clay colloid chemistry* **1977** Wiley, NewYork

107. Hansen C. M. *Hansen solubility parameters, a user's handbook. CRC*, Boca Raton, FL. **2000**

VITA

Deepali Pradeep Kumar was born on March 6th, 1975 in Delhi, India. She graduated with Bachelors in Chemistry from Delhi University in 1995. After graduation she went on to pursue Masters in Chemistry from Indian Institute of Tehnology, Delhi. She also obtained Masters in Polymer Science and Technology in December 1998. She worked as Software Engineer for one year after which she got admitted to graduate school at the University of Tennessee, Knoxville in 2001. After getting her Doctorate in chemistry, she joined Business school to do Masters in Business Management at the same University.